Summer 2018

# Sleep-dependent sensorimotor processing and network connectivity in the infant rat

Carlos Del Rio-Bermudez
*University of Iowa*

# SLEEP-DEPENDENT SENSORIMOTOR PROCESSING AND NETWORK CONNECTIVITY IN THE INFANT RAT

by

Carlos Del Rio-Bermudez

A thesis submitted in partial fulfillment

of the requirements for the Doctor of Philosophy

degree in Psychology in the

Graduate College of

The University of Iowa

August 2018

Thesis Supervisor: Professor Mark S. Blumberg

Graduate College
The University of Iowa
Iowa City, Iowa

CERTIFICATE OF APPROVAL

_____

PH.D. THESIS

_____

This is to certify that the Ph.D. thesis of

Carlos Del Rio-Bermudez

has been approved by the Examining Committee for
the thesis requirement for the Doctor of Philosophy degree
in Psychology at the August 2018 graduation.

Thesis Committee: _____
Mark S. Blumberg, Thesis Supervisor

_____
Jan Wessel

_____
Jason Radley

_____
Ryan LaLumiere

_____
Michelle Voss

A mi familia, por su amor incondicional y apoyo en la distancia.

*«El sueño de la razón produce monstruos»*

*«The sleep of Reason produces monsters»*

- Francisco de Goya (*Caprichos*, 1799)

## ACKNOWLEDGEMENTS

I sincerely thank Professor Mark Blumberg for being an outstanding mentor. His dedication to and passion for science will always be a source of inspiration.

None of this work would have been possible without Dr. Greta Sokoloff. I want to thank her for constant professional and personal support over the years.

I would like to thank Dr. Alex Tiriac for assuming the hard task of training me when I first joined the lab. I will never forget, amigo!

I also want to thank all current and past members of the Blumberg family: Cassandra Coleman, Alan Plumeau, Nick Sattler, Alex Yonk, Jimmy Dooley, Lex Gomez, Ryan Glanz, and Brandt Uitetmarkt. You always made me feel like home. Special thanks to the other “senior” graduate student, Didhiti Mukherjee, for being a source of support, care, and laughter.

I want to thank Dr. Jangjin Kim. Some of the work presented here would not be a reality without his valuable time and expertise.

I also would like to thank the members of my committee, Drs. John Freeman, Ryan LaLumiere, Jason Radley, and Jan Wessel, for their guidance and valuable advice throughout my graduate studies at the University of Iowa.

I finally want to thank the “other Mark,” Mr. Stastny. Life is always better when you are around.

## ABSTRACT

Early sensory experiences play a critical role in the activity-dependent development of the sensorimotor system. The sources of sensory input to the neonatal nervous system involve external stimulation (*exafference*) and sensory feedback arising from self-generated movements (*reafference*). In the perinatal period, reafference from twitches of the limbs and facial muscles during active (REM) sleep is a powerful driver of neural activity across the entire neuraxis. Thus, sleep-related twitches are thought to contribute to the activity-dependent development of sensorimotor networks. In this dissertation, we first aimed to identify a motor pathway for the generation of twitching. Using newborn rats at postnatal day (P) 8, we provide evidence that the red nucleus (RN; source of the rubrospinal tract) is involved in the production of twitching. In addition, we show that reafference from twitches drives neural activity in the RN, therefore suggesting that the RN is an important site for sensorimotor integration. Also, in the RN of P8 rats, twitch-related reafference triggers theta (4–7 Hz) oscillations. By P12, theta oscillations are expressed continuously and exclusively across bouts of active sleep. Synchronized neuronal oscillations comprise a fundamental mechanism by which distant neural structures establish and express functional connectivity. Thus, we next hypothesized that sleep-dependent theta oscillatory activity enables the expression of network connectivity between the RN and associated neural networks, such as the hippocampus. Simultaneous recordings from the hippocampus and RN at P12

show that theta oscillations in both structures are synchronized, co-modulated, and mutually interactive exclusively during active sleep. Lastly, we test the hypothesis that twitches drive synchronized oscillatory activity across functionally related sensory structures at early ages when the occurrence of oscillations largely depends on sensory input. Focusing on the cortico-hippocampal network at P8, we demonstrate that, unlike periods of wake-related movements or behavioral quiescence, twitching promotes coupled oscillatory activity at Beta2 frequency (~20-30 Hz). Altogether, the findings in this dissertation suggest that one of the functions of active sleep in early infancy is to provide a context for sensorimotor processing and for synchronizing activity within and between forebrain and brainstem structures. Consequently, any condition or manipulation that restricts active sleep can deprive the infant animal of substantial sensory experience, potentially resulting in atypical developmental trajectories.

## PUBLIC ABSTRACT

Infant animals spend the majority of their time asleep and most of that sleep time comprises active (or REM) sleep. One of the defining features of neonatal active sleep is the presence of abundant, fast, and jerky movements of the limbs and facial muscles; these movements are called *myoclonic twitches*. Why do neonates twitch so much in their sleep? It turns out that sensory feedback from twitches drive substantial neural activity throughout the sensorimotor system, thereby contributing to its development. However, the neural pathways that support the generation of twitching in early development have remained largely unknown. Here we show for the first time that the newborn rat red nucleus—a motor structure in the brainstem—is not only involved in twitch production but also processes sensory feedback from twitches. We also show that active sleep and twitches promote the generation of neuronal oscillations in the infant RN and associated networks, including the hippocampus and sensorimotor cortex. This is important because neuronal oscillations enable communication between distant but functionally related brain areas. Our findings indicate that early communication between these areas is restricted to periods of active sleep and are also promoted by twitching. Because active sleep is so important for enabling early communication between brain areas, sleep restriction or deprivation at early ages could negatively affect brain development.

## TABLE OF CONTENTS

## LIST OF FIGURES

CHAPTER 2



CHAPTER 3

CHAPTER 4



CHAPTER 5

## LIST OF TABLES

## LIST OF ABBREVIATIONS

| | |
|---|---|
| **Ach** | Acetylcholine |
| **AS** | Active Sleep |
| **AW** | Active Wake |
| **Baclofen** | β-(4-chlorophenyl)-γ-aminobutyric acid |
| **BQ** | Behavioral Quiescence |
| **CA** | Cornu Ammonis (Hippocampus) |
| **EMG** | Electromyography |
| **GABA** | Gamma-Aminobutyric Acid |
| **Hipp** | Hippocampus |
| **LFP** | Local Field Potential |
| **MS** | Medial Septum |
| **MUA** | Multi-Unit Activity |
| **P** | Postnatal Day |
| **PL** | Phase Locking |
| **REM** | Rapid Eye Movement |
| **RN** | Red Nucleus |
| **S1-BF** | Somatosensory Cortex (Barrel Field) |
| **SFC** | Spike-Field Coherence |
| **β-Alanine** | Beta-Alanine |

# CHAPTER 1: INTRODUCTION

A notable feature of sleep across the animal kingdom is its disproportionate abundance in early development. The newborns of all species studied thus far – from humans to fruit flies—sleep more than adults [1–6]. Why do neonates sleep so much? The observation that human infants spend 50% of their sleep time in active sleep (AS, or REM sleep) inspired the so-called *ontogenetic hypothesis* [1,7]. The ontogenetic hypothesis argues that early in development—when sleep is the predominant behavioral state—vigorous activity arising from brainstem structures during AS ensures that the developing brain receives substantial neural stimulation. The ontogenetic hypothesis rests on the notion that such stimulation during AS plays a fundamental role in the early activity-dependent development of the nervous system, as primarily demonstrated thus far in the visual system of kittens [8,9]. The hypothesized role of AS in brain development, however, likely extends beyond the visual system.

## Active sleep, twitching, and the development of the sensorimotor system

The functional and anatomical development of the sensorimotor system heavily relies on early sensory experiences [10–12]. In the perinatal period, sensory stimulation can arise from both external sensory stimulation (i.e., *exafference*) and from sensory feedback from self-generated movements (i.e., *reafference*) [13]. Importantly, the opportunities for reafferent stimulation in the developing sensorimotor system are not restricted to period of wakefulness. In infant

mammals, AS is characterized by the presence of abundant, discrete, and jerky movements of the limbs and facial muscles. Traditionally, these jerky movements during sleep (also known as *myoclonic twitches*) have been largely ignored by the scientific community, or considered a mere byproduct of a dreaming brain [14]. However, research over the last ten years suggests otherwise: Sleep twitches may play a critical role in the activity-dependent development of the sensorimotor system. Specifically, in newborn rats, reafference from twitches is a potent driver of early neural activity across the entire neuraxis, including the spinal cord [15,16], thalamus [17], sensorimotor cortex [18–22], hippocampus [23,24], and cerebellum [25–27].

Twitches are ideally suited for the efficient transmission of peripheral sensory feedback [14]. First, unlike wake-related movements, which involve high-amplitude movements and recruit many muscles at once, twitches result from the activation of individual muscles and rarely occur simultaneously with other twitches [28]. The discrete nature of twitches is ideal for establishing a one-to-one relationship between the muscle and the sensory neurons that process information from a particular part of the body. Second, because they occur during AS, twitches occur against a background of low muscle tone. In this context, the signal-to-noise ratio is higher than during periods of active wakefulness (i.e., there is less sensory information reaching the brain simultaneously). Consequently, reafferent signals from twitches are easier to detect than those that arise from wake movements. Finally, the state of AS provides a neurochemical context that promotes and enables neural plasticity [29].

**A motor pathway for twitching during active sleep**

The established role of twitches in driving early neural activity contrasts with how little we know about the neural pathways that contribute to their generation. Experimental evidence in fetal and neonatal rats indicates that the generation of twitching does not rely on cortical or forebrain motor systems. Specifically, spinal transections [28], decerebrations [30], and neural recordings [31,32] indicate that twitching is first controlled by spinal generators that gradually come under the control of mesopontine circuits. The mesopontine area contains structures that generate AS [33–36], which in turn are thought to produce twitching by modulating premotor nuclei in the brainstem. Early work in adult cats [37,38] and a recent study in adult mice [39] have identified the red nucleus (RN) as a premotor nucleus involved in twitch production.

The RN, located in the ventromedial mesencephalon and a source of the rubrospinal tract (RST), contains a large number of primarily glutamatergic neurons [40]. The RN supports a variety of motor abilities, including the regulation of muscle tone [41], skilled limb movements [42], and over-ground locomotion [43]. The role of the RN in motor control is particularly important in early infancy before corticospinal connections have fully developed [44].

Electrophysiological recordings in adult cats during AS revealed phasic increases of RN activity that correlated with twitches of the eye muscles (i.e., rapid eye movements, or REMs) [37,38]. In addition, pharmacological inactivation of the

adult cat RN markedly decreased twitching rates [38], and electrical stimulation of these neurons produced twitch-like contractions of the muscles in the contralateral limbs and facial muscles [45]. In adult mice, chemogenetic stimulation of glutamatergic neurons in the RN during AS increased twitching rates [39].

In Chapter 2, we tested the hypothesis that the RN contributes to the generation of twitching in early development. To tackle this question, we first recorded spontaneous extracellular activity in the RN of week-old rats during sleep and wake states. In support of a role of the RN in the generation of twitches, we found that RN neurons fire phasically before the onset of twitches. Interestingly, we also found that a subpopulation of neurons in the RN fires exclusively after twitch onset, suggesting processing of twitch-related sensory feedback. In addition, pharmacological inactivation of the RN caused a marked decrease in the occurrence of twitching during active sleep. Altogether, the data presented in Chapter 2 not only indicate that twitching in early development is generated by the RN, but also that the RN is an important site for sensorimotor integration in the developing brain.

**The red nucleus as a hub for sensorimotor integration**

The RN has been traditionally studied in the context of motor control [42–44,46]. However, the RN of rats [47], cats [48,49], monkeys [50,51], turtles [52], and humans [53] also responds to peripheral sensory stimuli. This observation has led to the hypothesis that RN neurons use sensory feedback from self-generated movements to modulate ongoing motor commands [54].

The rat RN is well integrated with a variety of sensorimotor networks that span both cortical and subcortical structures, including the spinal cord [40,55], midbrain\ and brainstem nuclei [37,41], hypothalamus [56], cerebellum [57], somatosensory cortex [58], motor cortex [59], and hippocampus [60]. Indeed, functional communication between the RN and the aforementioned structures assists in a variety of motor and cognitive skills. For example, the projections from the deep cerebellar nuclei to the RN support the execution of cerebellar-dependent learned motor responses [61]. In addition, connectivity between motor cortex and RN supports the initiation and control of skilled movements, especially those involving the forelimbs [62,63]. Lastly, it has been proposed that functional communication between the RN and hippocampus contributes to spatial navigation in adult rats [54,60].

In light of the results described in Chapter 2, the production of twitching by the RN and the processing of twitch-related feedback in the hippocampus and related structures may contribute to the early activity-dependent development of functionally connected neural networks that support such important functions as skilled motor behavior, spatial navigation, and motor learning.

**Wiring the sensorimotor system during sleep: A role for AS-dependent neural oscillations in promoting early network connectivity**

As discussed above, sensory feedback from twitches during AS drives substantial neural activity in developing sensorimotor structures. Twitch-related sensory responses are expressed in the form of increased neuronal firing rates or increased

oscillatory activity. Neural oscillations are the result of synchronized dendritic activity within large populations of neurons and exhibit specific spatiotemporal features depending on brain area, behavioral state, and age. In early development, neural oscillations contribute to a variety of neurodevelopmental processes, including synapse formation, neuronal differentiation and migration, apoptosis, and the refinement of topographic maps [64–70]. Importantly, coupled (or synchronized) oscillatory activity across neuronal structures is also a hallmark of long-range functional connectivity in both infants and adults [71–75].

As described in Chapter 3, we discovered that the infant RN exhibits state- and twitch-dependent oscillatory activity in the theta frequency band (~4-7 Hz). The expression of brief theta bursts by the end of the first postnatal week was associated with twitching during AS. By the end of the second postnatal week, theta oscillations were continuously expressed throughout AS bouts. At both ages, the expression of theta activity was markedly reduced or suppressed during periods of quiescence and during wake-related movements. This finding was surprising for several reasons. First, to our knowledge, this was the first demonstration of state-dependent oscillatory activity in a brainstem motor nucleus like the RN. Second, the developmental trajectory of theta oscillations between the first and second postnatal week mimics previous findings from our laboratory in the developing hippocampus [23]. Given the aforementioned role of coupled oscillatory activity in establishing connectivity between brain areas, we next sought to address whether theta oscillations in the developing RN and hippocampus are temporally coupled. Our results indicate that highly synchronized theta activity between these

structures is preferentially expressed during periods of AS, highlighting the role of sleep in the early expression of network connectivity between brainstem and forebrain sensorimotor structures.

In Chapter 4, we review the existing literature supporting the role of active sleep and twitching in the expression of early neural oscillations. We propose the hypothesis that twitching drives coupled oscillatory activity between developing sensorimotor structures at early ages when oscillations are highly dependent on sensory input. Finally, the experiments in Chapter 5 are aimed to test this hypothesis in the cortico-hippocampal system.

In summary, the studies described in this dissertation identify the RN as an important brain structure for the generation of twitching during AS in early development. In addition, we show that sensory feedback from twitches drives early neural oscillations in the RN and associated neural networks, including the hippocampus. Finally, our data indicate that twitching and AS provide a unique context for the emergence and expression of coupled oscillatory activity between functionally related cortical and subcortical sensorimotor networks. Altogether, our findings highlight the importance of AS for the development of the sensorimotor system. Because sensory feedback from twitching is a major source of stimulation to the neonatal brain and enables the expression of network connectivity, sleep restriction or deprivation may be an important factor driving atypical developmental trajectories in many neurodevelopmental disorders.

# CHAPTER 2: SENSORIMOTOR PROCESSING IN THE NEWBORN RAT RED NUCLEUS DURING ACTIVE SLEEP

## INTRODUCTION

The infant nervous system must adjust rapidly to changes in the biomechanical properties of limbs within the context of a continually changing body. One important contributor to this process occurs during wakefulness as infants learn about the relationship between self-generated movements and the associated sensory feedback (i.e., reafference) arising from them [76–78].

But self-generated movements are not restricted to periods of wakefulness. On the contrary, twitching of the limbs during active (or REM) sleep is among the most abundant of all newborn behaviors [1–3]. Twitches are discrete events that occur against a background of muscle atonia, thereby facilitating high-fidelity transmission of reafference related to the biomechanical properties of limbs [79]. Indeed, twitch-related reafference drives neural activity in structures across the neuraxis, including the spinal cord [16], thalamus [17], cerebellum [27], hippocampus [23], somatosensory cortex [17,20], and motor cortex [18]. Finally, reafferent signals from twitching limbs are processed differently from those associated with wake movements, further indicating that twitches are ideally suited to contribute to activity-dependent development of the sensorimotor system [18].

In contrast, we know little about the motor systems responsible for twitching. Spinal transections [28], decerebrations [30], and neural recordings [31,32] in fetal

and neonatal rats suggest that spinal generators of twitching gradually come under the control of mesopontine circuits. The mesopontine area contains nuclei that are involved in REM sleep generation [33–36] and are presumed to produce twitching via brainstem premotor nuclei. The red nucleus (RN) is one such nucleus, having been identified in adult mice and cats as a source of twitch-related motor outflow [38,39]. The RN is the source of the rubrospinal tract (RST) [40] and plays an important role in the regulation of muscle tone [41], skilled limb movements [42], and over-ground locomotion [43]. The role of the RN in motor control is particularly important in early infancy before corticospinal connections have fully developed [44].

In the present study we recorded spontaneous and evoked neural activity in the RN and selectively inhibited it in week-old rats to test the hypothesis that the RN is involved in the generation of twitches early in development. Based on findings that the RN also processes sensory information [80], we further hypothesized that RN neurons receive reafference from sleep-related twitches. The present study identifies for the first time the RN as a generator of twitching in infancy. Notably, the processing of reafferent neural signals in the RN during twitching suggests that twitches contribute to sensorimotor integration and somatotopic organization within the red nucleus and associated neural structures [60].

## METHODS

All experiments were conducted in accordance with the National Institutes of Health Guide for the Care and Use of Laboratory Animals (NIH Publication No. 80-23) and were approved by the Institutional Animal Care and Use Committee of the University of Iowa.

*Subjects*

A total of 16 7- to 8-day-old male and female Sprague-Dawley rats from 14 litters were used. If littermates were used, they were always assigned to different experimental conditions. Litters were culled to 8 pups within 3 days after birth. Mothers and their litters were housed in laboratory cages (48 x 20 x 26 cm) where food and water were available ad libitum. Animals were maintained on a 12:12 light-dark cycle (lights on 0700 h).

*Spontaneous and evoked activity in the red nucleus*

*Surgery*. Eight Pups were prepared using methods described previously [32]. Briefly, under 2-5% isoflurane anesthesia, a custom-built stainless steel head-fix apparatus was glued to the skull with cyanoacrylate adhesive gel. Bipolar EMG electrodes (50 µm diameter; California Fine Wire, Grover Beach, CA) were implanted into the nuchal muscle, the gastrocnemius muscle of the hindlimb, and the triceps brachii muscle of the forelimb contralateral to the neural recording site. After surgery, pups were transferred to an incubator and maintained at

thermoneutrality (35ºC) for 1 h to recover. After being secured in a stereotaxic apparatus (David Kopf Instruments, Tujunga, CA), the pup was briefly anesthetized again and a small hole was drilled in the skull to allow for later insertion of the electrode into the RN (coordinates in relation to bregma: AP: -4.8-5.0 mm; ML: ±0.4 mm; DV: 4.3-4.5 mm). Two additional holes were drilled at a location distant from the first one for subsequent insertion of a ground wire and a thermocouple to monitor brain temperature.

*Procedure*. As described previously [32], electrophysiological recordings were conducted in a stereotaxic apparatus with the animal's torso secured to a platform and the tail and limbs dangling freely (Figure 1A). Brain temperature was monitored using a fine-wire thermocouple (Omega Engineering, Stamford, CT) and maintained at 36-37ºC. A 90-min acclimation period allowed pups sufficient time to begin exhibiting organized sleep-wake cycles.

The EMG bipolar electrodes were connected to a differential amplifier (A-M Systems, Carlsborg, WA; amplification: 10,000x; filter setting: 300-5000 Hz). Recordings of multiunit activity (MUA) in the RN were acquired using 16-channel silicon depth electrodes (100 µm vertical separation between recording sites; NeuroNexus, Ann Arbor, MI), with impedances ranging from 1-4 MΩ, connected to a data acquisition system (Tucker-Davis Technologies, Alachua, FL) that amplified (10,000x) and filtered the signals. MUA signals were filtered using a 500-5000 Hz band-pass filter and a 60 Hz notch filter. Neural and EMG signals were recorded at sampling rates of 12.5 kHz and 1 kHz, respectively, using a digital interface and Spike2 software (Cambridge Electronic Design, Cambridge, UK). Before insertion

into the brain, the tip of the electrode was dipped in fluorescent DiI (InvitrogenLife Technologies, Carlsbad, CA) for subsequent histological confirmation of the recording sites. A Ag/AgCl ground electrode (Medwire, Mt. Vernon, NY, 0.25 mm diameter) was placed in the contralateral occipital cortex.

Before recording spontaneous activity in the RN, we determined whether stimulation of the contralateral forelimb yielded consistent RN responses in at least one recording channel; this test served to confirm electrode placement within an RN region specifically related to forelimb processing. To perform these forelimb stimulations, a fine paintbrush was used to gently flex the forelimb at the elbow [81]. When consistent evoked responses were confirmed, spontaneous RN and EMG activity during sleep and wakefulness were recorded continuously over a 30-min session. During the recording session, the experimenter scored the pup's wake movements and twitches using computer key presses that registered events in synchrony with the electrophysiological record [32].

At the end of the 30-min recording of spontaneous activity, the experimenter systematically assessed RN responses to peripheral exafferent stimulation of the forelimb. Stimulations were repeated for 10 min with interstimulus intervals of 5-10 s. The experimenter marked each stimulus event using a computer key press.

*Data analysis*. Spike2 software (Cambridge Electronic Design, Cambridge, UK) was used for spike sorting using previously described methods (Sokoloff et al., 2014). Waveforms that exceeded 3.5 standard deviations from the mean were not analyzed further. After spike sorting was complete, burst analyses were

performed using a script written for Spike2. Based on the distributions of interspike intervals (ISIs), complex spikes were defined as burst events with ISIs ≤ 8 ms (Figure 1C). All non-complex-spike events were defined as simple spikes.

Periods of sleep and wakefulness were identified using previously described methods [23,27,32,81]. Briefly, EMG records were rectified and five 1-s EMG segments each of atonia and high tone were used to calculate mean amplitude of the EMG signal. Then, the midpoint between the two was used to determine a threshold for defining behavioral state. Active wake was defined by the presence of high-amplitude limb movements against a background of high nuchal muscle tone and active sleep was defined by the presence of twitches against a background of muscle atonia [3,82]. Myoclonic twitches were defined electrographically as EMG events that exceeded at least three times the mean EMG baseline during atonia [23,27,81].

The temporal relationship between forelimb twitches and unit activity was examined as follows. First, for each individual channel with unit activity and using twitches as trigger events, we produced perievent histograms using the “event correlation” function in Spike2. These analyses were performed independently for complex and simple spikes using 10-ms bins and 1-s windows. To test for statistical significance of each event correlation, we jittered twitch events 1000 times within a 1 s window using PatternJitter [83,84] implemented in MatLab. We corrected for multiple comparisons using the method of Amarasingham and colleagues [84]. This method generates upper and lower confidence bands for each event correlation. Alpha was set at 0.01 for all tests.

To determine whether neural activity preceded or followed twitches, we identified the first time bin in each event correlation that surpassed the established 99% upper threshold for statistical significance. Next, based on this identification, we classified simple and complex spikes as twitch preceding or twitch following. Finally, we pooled data for simple and complex spikes across pups within each category and performed event correlations and statistical tests as described above.

We next determined the temporal relationship between RN activity and wake-related movements. Because there were relatively few wake movements in our records, it was not possible to perform jitter analyses on event correlations for individual units. Therefore, we analyzed wake-related unit activity using the pooled populations of twitch-preceding and twitch-following simple and complex spikes identified above. We first determined the onset of forelimb movements during wake bouts. We defined movement onset on the basis of the EMG signal surpassing an established threshold (i.e., at least 3x the value of EMG baseline during atonia for at least 1 s); movement offset occurred when the EMG signal passed below the threshold. Next, we produced wake-movement-triggered perievent histograms and performed jitter analyses on the pooled data as described above. Because wake movements are longer in duration than twitches, we used 50-ms bins and 2-s windows.

To assess RN topography, we identified those units that exhibited significant forelimb-related twitch-preceding or twitch-following activity. We then repeated the event correlation analyses described above for each of these units,

but now using nuchal or hindlimb twitches as triggers. Next, for each available unit, we used event correlations and jitter analysis to determine whether unit activity exhibited a significant relationship with forelimb, nuchal, or hindlimb twitches (defined as having #1 significant bin in its perievent histogram). We then used independent $X^2$ tests (SPSS) to assess differences in the percentage of units that were twitch-related between muscle groups. Finally, to help interpret these relationships, we performed event correlations to determine the temporal relationships between muscle groups (bin size, 10 ms; window size, 1 s). For this last analysis, we only examined those subjects for which all three EMGs were available (N = 5).

To analyze unit activity in response to forelimb stimulation, perievent histograms were constructed as described above using 10-ms bins and 1-s windows. For each unit, the first 30 stimulations were analyzed and perievent histograms were triggered on the stimulation-related onset of forelimb EMG activity. Statistical significance was again tested using the jittering method described above.

**Effect of pharmacological inactivation of the RN on motor behavior during sleep and wake**

*Surgery*. Eight head-fixed pups were used in this experiment. All surgical procedures were similar to those described for the first experiment. After recovery from surgery, they were placed in the stereotaxic apparatus in a thermoneutral

environment acclimated until they exhibited organized sleep-wake cycles. For this experiment, EMG bipolar electrodes were inserted into the nuchal muscle and both triceps brachii of the forelimbs.

*Procedure*. After the 90-min acclimation period in the stereotaxic apparatus, baseline activity was recorded for 30 min (see Figure 6A). The needle of a 0.5 µL microsyringe (Hamilton, Reno, NV) was dipped in fluorescent DiI (for subsequent histological confirmation of the infusion site) and lowered stereotaxically into the RN. Pups (N =4 per group) received a 0.1 µL unilateral infusion into the left or right RN of either a drug cocktail composed of the $GABA_A$ receptor agonist muscimol, the $GABA_B$ receptor agonist baclofen, and the glycine receptor agonist β-alanine (Sigma-Aldrich, St. Louis, MO; all drugs at 10 mM, dissolved in 0.9% physiological saline) or physiological saline (VEH; 0.9 %). (The infusion volume needed to target the RN in its entirety was determined previously in several additional pups using a microsyringe filled with either fluorescently tagged muscimol or DiI diluted in saline.) Cocktail or vehicle solutions were infused at a rate of 0.1 µL/min. A 40-min post-infusion period allowed for diffusion of the solution and acclimation of the pup prior to the final 30-min recording session. Behavior and EMG activity were monitored continuously over the entire experimental session.

Our choice of GABA and glycine agonists was based on previous studies in rats showing that the inhibitory effects of GABA in the rat RN are mediated by both $GABA_A$ and $GABA_B$ (but not $GABA_C$) receptors [85]. Additionally, glycine receptors have been found in the rat RN [86] and linked to inhibitory effects in the adult cat [87] and mouse [88]. Finally, combined pharmacological manipulation of $GABA_A$,

$GABA_B$, and glycine receptors has been used in trigeminal motoneurons to modulate twitching of the masseter muscle in adult rats [89].

*Data analysis.* Periods of active sleep for each pup were identified for pre- and post-infusion recordings. To assess the effect of the drug infusion in the time spent in active sleep, a 2 x 2 repeated-measures factorial analysis of variance (ANOVA; SPSS, IBM, Armonk, NY) with the experimental group (Cocktail or VEH) as the between-subjects factor and time (Pre- or Post-infusion) as the repeated-measures factor was performed using the time in active sleep as the dependent variable.

To calculate twitching rates, the total number of forelimb twitches for each pup was divided by the total time in active sleep (defined as the period from the first twitch within a sleep bout to the onset of the next wake bout [82]). The total number of wake-related forelimb movements in each session was also quantified using the EMG record. To assess the effect of the experimental manipulation, we performed a 2 x 2 repeated-measures factorial analysis of variance (ANOVA; SPSS, IBM, Armonk, NY) with experimental group (Cocktail or VEH) as the between-subjects factor and time (Pre- or Post-infusion) as the repeated-measures factor. Rate of twitching and number of wake-related movements were the dependent variables. To assess the temporal patterns of forelimb twitching before and after RN inactivation, we determined all inter-twitch intervals (ITIs) during active sleep and then estimated the survival function for each ITI. For the survival test, group and time were used as independent factors for both ipsilateral and contralateral forelimb activity, and a generalized Wilcoxon test (Breslow,

SPSS) was used to determine differences in the survival distribution of ITIs for the different sessions in each group. Alpha was set at 0.05.

### Histology

At the end of each experiment, pups were overdosed with sodium pentobarbital (1.5 mg/g) and perfused transcardially with phosphate-buffered saline followed by 4% paraformaldehyde. Coronal brain sections were sliced (80 µm sections) using a freezing microtome (Leica Microsystems, Buffalo Grove, IL). Electrode and microsyringe placements within the RN were verified by visualizing the DiI tract at 2.5-5X magnification using a fluorescent microscope (Leica Microsystems, Buffalo Grove, IL). Subsequent staining with cresyl violet was used for further confirmation of electrode or microsyringe placement in the RN.

## RESULTS

### Evoked and spontaneous activity in the red nucleus

Extracellular neuronal activity in the RN was recorded from 8 P7-8 pups yielding a total of 27 units (range: 2-5 units per pup). Histology confirmed that electrodes were located in the RN (Figure 1B,1C). Figure 1C illustrates the relationship between RN activity and twitching in the contralateral forelimb. In addition to single spikes of activity with ISIs >8 ms, designated here as simple spikes, RN activity was also characterized by short bursts of activity that we designated as complex spikes [90]. Complex spikes were composed of 2-11 individual action potentials

with ISIs of 2-8 ms (M = 2.4 ms; SD = 0.9 ms). It should be noted that the complex spikes described here have very similar characteristics to the bursts previously described as being well suited for efficient transmission of neural information [90].

Evoked activity in the RN. Contralateral forelimb stimulation triggered sensory responses at a minimum of one electrode site per pup, and in 19 of 27 units overall (70.3%). Figure 2A depicts, for a representative RN unit, the relationship between forelimb stimulation and neural activity. Across all units that were responsive to exafference, RN activity increased significantly shortly after stimulation ($p < 0.01$) with a mean latency of 39 ± 5 ms (N = 19; Fig. 2A, right). In contrast, stimulation of the contralateral hindlimb and ipsilateral forelimb did not trigger reliable neural activity in the units analyzed here.

Spontaneous activity in the RN. Figure 2B shows, for a representative RN unit, the relationship between spontaneous sleep–wake cycling and neural activity. During spontaneous cycling, and regardless of behavioral state, the RN neuron is phasically active during contralateral forelimb movements. Whereas short trains of activity predominated during bouts of active sleep, activity accompanying wake-related movements was longer in duration and consisted of sustained tonic firing that terminated shortly before movement offset (Fig. 2B). When the pups were not actively moving their limbs, RN activity was substantially reduced and often absent (Figs. 1C, 2B).

The temporal relationship between unit activity in the RN and contralateral forelimb twitches revealed three clear subpopulation of neurons: (1) neurons that

fired before movement onset, (2) neurons that fired after movement onset, and (3) neurons that did not show any significant relationship with contralateral forelimb movements. Unit activity from neurons in the last group (N = 5) was excluded from further analysis. Across all units that significantly increased their firing rates before twitch onset, they did so with a mean latency of 22 ± 3 ms for complex spikes (N = 16) and 30 ± 5 ms for simple spikes (N = 14; Fig. 3, top row). It should be noted that both complex and simple spike activity in this group also exhibited a significant, discrete peak of activity shortly after twitch onset. For those units that increased their firing rates only after twitch onset, they did so with a mean latency of 80 ± 16 ms for complex spikes (N = 6) and 91 ± 15 ms for simple spikes (N = 8; Fig. 3, bottom row). Across all units that consistently fired before the onset of forelimb twitches, firing rates increased significantly before contralateral forelimb wake movements with a mean latency of 50 ± 17 ms for complex spike activity (N = 16; Fig. 4, top left) and 55 # 8 ms for simple spikes (N = 14; Fig. 4, top right). The group of neurons that fired predominantly after wake movement onset showed a mean (± SEM) latency of 208 ± 46 ms for both complex spikes (N = 6; Fig. 4, bottom left) and 118 ± 35 ms for simple spikes (N = 8; Fig. 4, bottom right). Finally, as the above analyses suggest, we found that complex and simple spikes were equally likely to be associated with twitches as with wake-related movements.

**Topographic organization of the RN**

For each of the forelimb units that exhibited significant twitch-preceding or twitch-following activity (Fig. 3), we repeated the analyses using nuchal and hindlimb twitches as triggers (Fig. 5A). In general, whereas forelimb twitches were associated with substantial twitch-preceding and twitch-following activity for both complex and simple spikes, only preceding-activity for the nuchal muscle exhibited a clear twitch-related pattern. Next, across all units with available EMG records, we determined whether they exhibited significant twitch-related activity profiles. Figure 5B presents the percentage of units exhibiting significant twitch-related activity (i.e., twitch-preceding or twitch-following) for each muscle group. For both complex and simple spikes, there was a strong topographic relationship between unit activity and forelimb twitching, a weaker relationship with nuchal twitching, and an even weaker relationship with hindlimb twitching. The differences in the percentage of significant twitch-related units were statistically significant (forelimb vs nuchal: complex spikes, $X^2_{(1,54)} = 5.3$, $p < 0.03$; simple spikes, $X^2_{(1,54)} = 9.4$, $p < 0.01$; forelimb vs hindlimb: complex spikes, $X^2_{(1,45)} = 18.3$, $p < 0.001$; simple spikes, $X^2_{(1,45)} = 10.6$, $p < 0.002$). The preceding data (see Fig. 5A, B) suggest that the forelimb and nuchal muscles are more functionally integrated (or less differentiated) than the forelimb and hindlimb muscles. To examine this possibility, we cross-correlated twitch events for the forelimb, nuchal, and hindlimb muscles for those subjects with EMG records from all three muscle groups (Fig. 5C). Consistent with the above suggestion, this analysis revealed a stronger relationship between the forelimb and nuchal muscles than between the forelimb

and hindlimb muscles. Finally, in one P8 rat (Fig. 5D), we recorded from an RN unit that responded preferentially to twitches of the contralateral forelimb, and from another unit (located (200 μm ventral to the first) that responded preferentially to twitches of the contralateral hindlimb; neither unit responded strongly to twitches of the nuchal muscle.

**Effect of pharmacological inactivation of the red nucleus on motor behavior during sleep and wake**

To assess the causal role of the infant RN in the production of twitches, we selectively inactivated the RN by infusing a cocktail of $GABA_A$, $GABA_B$, and glycine receptor agonists. For all pups after the experiment, the placement of the microsyringe was histologically verified as being located within the RN.

Pups infused with vehicle continued to cycle regularly between sleep and wake (Fig. 6A). In contrast, all four pups infused with the cocktail exhibited an acute reaction characterized by elevated muscle tone and behavioral activation averaging 20.9 ± 5.3 min (Fig. 6A). During this period, isolated twitches against a background of high muscle tone were sometimes observed. After the 30 min post-infusion acclimation period, the acute response had subsided and organized sleep–wake cycles resumed. Comparisons of mean duration of active sleep (VEH Pre: 1150.5 ± 147.8 s; VEH Post: 1228.3 ± 110.6 s; Cocktail Pre: 1040.2 ± 113.6 s; Cocktail Post: 1276.5 ± 86.2 s), mean number of wake bouts (VEH Pre: 28.7 ± 3.6; VEH Post: 29.0 ± 4.2; Cocktail Pre: 25.0 ± 4.1; Cocktail Post: 21.7 ± 5.1), and

mean length of sleep–wake cycles (VEH Pre: 63.3 ± 7.7 s; VEH Post: 65.8 ± 10.3 s; Cocktail Pre: 67.9 ± 8.5 s; Cocktail Post: 75.2 ± 14.8 s) indicated no significant main effects or interactions (all $p > 0.05$).

Cocktail infusion markedly decreased twitching rates during active sleep in both the ipsilateral and contralateral forelimbs (Fig. 6B, top row). We found significant main effects of Pre/Post (ipsilateral: $F_{(1,6)} = 11.93$, $p < 0.02$, $\eta^2 = 0.30$: contralateral: $F_{(1,6)} = 6.59$, $p < 0.05$, $\eta^2 = 0.19$) as well as a Group x Pre/Post interaction (ipsilateral: $F_{(1,6)} = 6.82$, $p < 0.05$, $\eta^2 = 0.17$; contralateral: $F_{(1,6)} = 11.41$, $p < 0.02$, $\eta^2 = 0.33$; all medium-to-large effect sizes, as indicated by $\eta^2$). In contrast, rates of twitching in the vehicle-infused pups did not change after infusion for both the contralateral and ipsilateral forelimbs. Next, we determined whether the temporal patterning of twitching was altered by cocktail infusion (Fig. 6B, bottom row). Log-survivor analysis revealed that longer ITIs were more prominent after drug infusion (contralateral: $X^2_{(1,4)} = 196.96$, $p < 0.001$; ipsilateral: $X^2_{(1,4)} = 164.99$, $p < 0.001$). This effect was not present in the vehicle group, where ITIs remained constant between the preinfusion and postinfusion sessions. As expected, the total number of wake-related forelimb movements decreased over the 30 min postinfusion recording session. Specifically, the total number of forelimb wake movements during the preinfusion session (contralateral: 70 ± 11.24; ipsilateral: 61.5 ± 12.06) was less than during the postinfusion session (contralateral: 25 ± 4.05; ipsilateral: 27.75 ± 5.18). There was a significant main effect of Pre/Post (contralateral: $F_{(1,6)} = 16.54$, $p < 0.01$, $\eta^2 = 0.26$; ipsilateral: $F_{(1,6)} = 13.44$, $p < 0.02$, $\eta^2 = 0.26$), as well as a Pre/Post ! Group interaction (contralateral: $F_{(1,6)} = 9.13$, p

$< 0.03$, $\eta^2 = 0.19$; ipsilateral: $F_{(1,6)} = 11.42$, $p < 0.05$, $\eta^2 = 0.18$). It is also important to note that forelimb wake movements after inactivation were noticeably weaker and generally shorter in duration than those in the baseline or exhibited by intact pups.

## DISCUSSION

Sensory feedback arising from myoclonic twitches is thought to play an important role in driving early sensorimotor development [16,17,20,23,27,81]. With the exception of several studies in adult cats and mice [38,39], the neural pathways and mechanisms involved in the generation of twitches have remained unclear. The present findings show for the first time that the infant RN, traditionally considered a motor structure [42,43], contributes to the production of twitching and also receives sensory feedback from self-generated movements in a somatotopic manner.

### The role of the RN in the production of twitches during active sleep

Previous work in perinatal rats suggests that the spinal circuits that generate twitching progressively come under the control of supraspinal circuits [28,30,31]. In adult animals, one mesopontine nucleus, the sublaterodorsal tegmental nucleus (SLD), plays an important role in producing muscle atonia during active sleep [92]. However, because the SLD does not produce twitching, other candidate nuclei

within the mesopontine region have been postulated to be twitch generators, including the laterodorsal tegmental nucleus, the pedunculopontine tegmental nucleus, and the RN [31,92].

With regard to the RN, RN activity in adult cats increases phasically during periods of sleep-related twitching and electrolytic lesions of the RN cause a generalized impairment in twitching that lasts only for several days [38]. More recently, pharmacogenetic stimulation of the RN in adult mice was shown to increase sleep-related twitching of the masseter muscle [39]. Here, using infant rats, we also demonstrate a causal role for the RN in twitching. Specifically, we found many RN neurons that increased their activity before the onset of contralateral forelimb twitches, and pharmacological inactivation of the RN using combined $GABA_A$, $GABA_B$, and glycine receptor agonism substantially reduced the occurrence of twitching. Conversely, combined antagonism of these receptors at trigeminal motoneurons increased twitching of the masseter muscle in adult rats [89]. Importantly, RN inactivation did not abolish twitching completely, most likely due to the use of a unilateral procedure. In addition, spared twitches could reflect the contributions of other supraspinal [30,38,92] as well as spinal [79] neural circuits.

RN inactivation reduced twitching in both the contralateral and ipsilateral forelimbs. Even though the most prominent rubrospinal projections are contralateral [40], ipsilateral projections have been identified in adult cats [93,94]. Thus, the bilateral effect on twitching observed here could be due to functional bilateral rubrospinal projections.

During the period immediately following RN inactivation, we observed an acute motor response consisting of increased muscle tone and limb movements that lasted 10-20 min. We suggest that this increase in motor activity is the result of a sudden loss of RN activation of gamma motoneurons of muscle spindles [95]. With a sudden loss of this fusimotor activation, muscle spindles would contract, thus reporting an apparent loss of muscle tone and thereby triggering a compensatory motor response. We emphasize, however, that after this acute response, pups resumed organized sleep-wake cycling that were characterized by decreased rates of twitching.

**Processing reafferent feedback to the red nucleus**

The latencies for twitch-related reafference for complex and simple spikes ranged from 10 to 150 ms, suggesting more than one source of feedback from the periphery to the RN. Shorter-latency responses could be due to direct spinorubral connections, as previously reported in cats [80,96]. Regarding the longer-latency responses, twitch-related sensory feedback activates the infant rat cerebellum [27], after which it could be conveyed from the deep cerebellar nuclei (DCN) to the RN [57,97]. We have observed such direct DCN projections to the RN in week-old rats using the retrograde tracer Fluorogold (data not shown).

In previous studies when recording from such structures as hippocampus, thalamus, and motor cortex [17,23,81], we routinely failed to observe substantial neural activity in association with wake-related movements. In contrast, and as

expected given the RN's established role in motor production, we observed high levels of neural activity during wakefulness (see Figure 2B). Upon closer examination, we also found a subset of RN neurons exhibiting substantial wake-related reafferent activity, a pattern that we have not previously documented (see Figures 3 and 4). This finding suggests that corollary discharge mechanisms do not gate or cancel wake-related reafference to the RN as they appear to do in the previously studied structures [81].

**Anatomical considerations**

Despite the well-established anatomical distinction between magnocellular (RNm) and parvocellular (RNp) aspects of the RN in species including cats, monkeys, and humans [40], the boundaries between them are unclear in the rat [98]. Our histological data indicate that we recorded from anterior and posterior aspects of the RN, which are associated with the RNp and RNm, respectively. If so, then it may be that cells in both divisions drive motor-related signals to the spinal cord in infant rats, as suggested in adult cats [99]. However, the contribution of the RNp to motor outflow is controversial [100].

**Twitch-related activity in the RN as a framework for developmental investigations of sensorimotor integration**

Although the RN has been predominantly investigated with regard to its motor functions [42,43], exafferent stimulation of the limbs of adult cats and turtles

activates neurons in the RN in a somatotopic manner [49]. Here, for the first time, we demonstrate that sensory feedback arising from self-generated movements during active sleep drives RN activity in a somatotopic fashion. For example, in one P8 rat (Figure 6), we recorded from an RN unit that responded preferentially to twitches of the contralateral forelimb, and another nearby unit that responded preferentially to twitches of the contralateral hindlimb; neither unit responded strongly to twitches of the nuchal muscle. Thus, early in development, twitching provides somatotopically precise feedback to the RN that could be essential for map formation and/or refinement in this structure [44,48].

The RN is well integrated with other structures that process sensory and motor information, including the deep cerebellar nuclei [57,97], motor cortex [59], somatosensory cortex [58], and hippocampus [60]. Figure 7 provides a schematic representation of how the RN forms hierarchically organized sensorimotor loops with these structures [101]. These loops comprise descending (e.g., RST) and ascending (e.g., spinocerebellar pathway) connections. Importantly, the role of the RN in producing twitches and the substantial convergence of twitch-related feedback to the RN from multiple structures suggests that it is an important site of sensorimotor integration.

Figure 7 also suggests that the RN is a foundational structure for the development of multiple sensorimotor brain networks. As but one example, activation of the RN in adult rats drives theta oscillations in the hippocampus via the medial septum [60], in support of the sensorimotor integration model of hippocampal function [54]. Importantly, in infant rats, twitch-related feedback

drives hippocampal theta activity as soon as it emerges at P8 [23] and twitch-related feedback also drives hippocampal activity via the somatosensory cortex [24]. Thus, the production of twitching by the RN and the processing of twitch-related feedback in the hippocampus and related structures may contribute to the early development of functionally connected neural networks that support such important functions as spatial navigation [102].

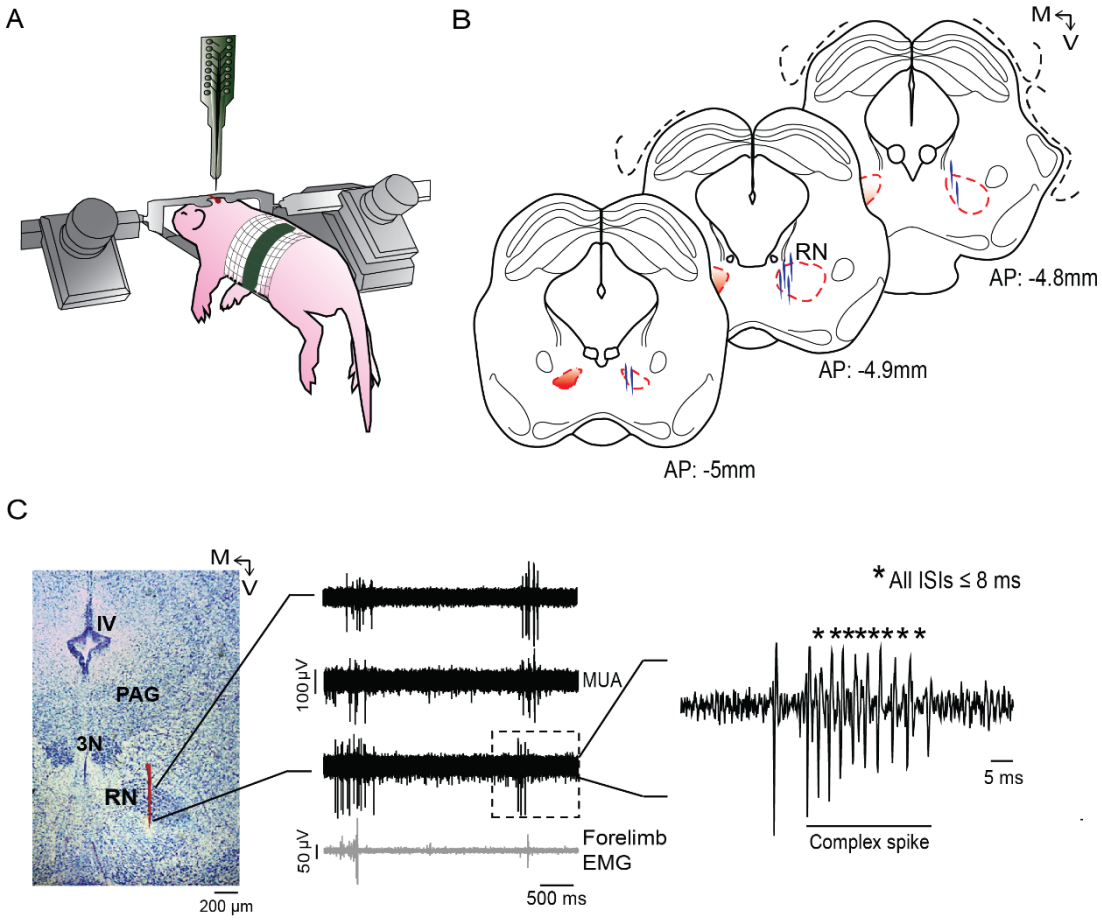


**Figure 1. Recording neural activity in the RN.** A, Illustration of a head-fixed rat pup in the recording apparatus. B, Reconstruction of electrode placements (blue vertical lines) within the RN in three successive coronal sections for all pups in the study (N = 8). C, Left, Coronal brain section stained with cresyl violet. Red vertical line is the trace of the DiI-coated electrode positioned through the RN. Middle, Representative recordings of MUA in the RN from three successive electrode sites (top traces) and EMG recordings from the contralateral forelimb (bottom trace). The unit activity contained within the dashed box is magnified at right to reveal a burst of action potentials with ISIs ≤8 ms, defined here as a complex spike. PAG, Periaqueductal gray; 3N, oculomotor nucleus; IV, fourth ventricle; M, medial; V, ventral.

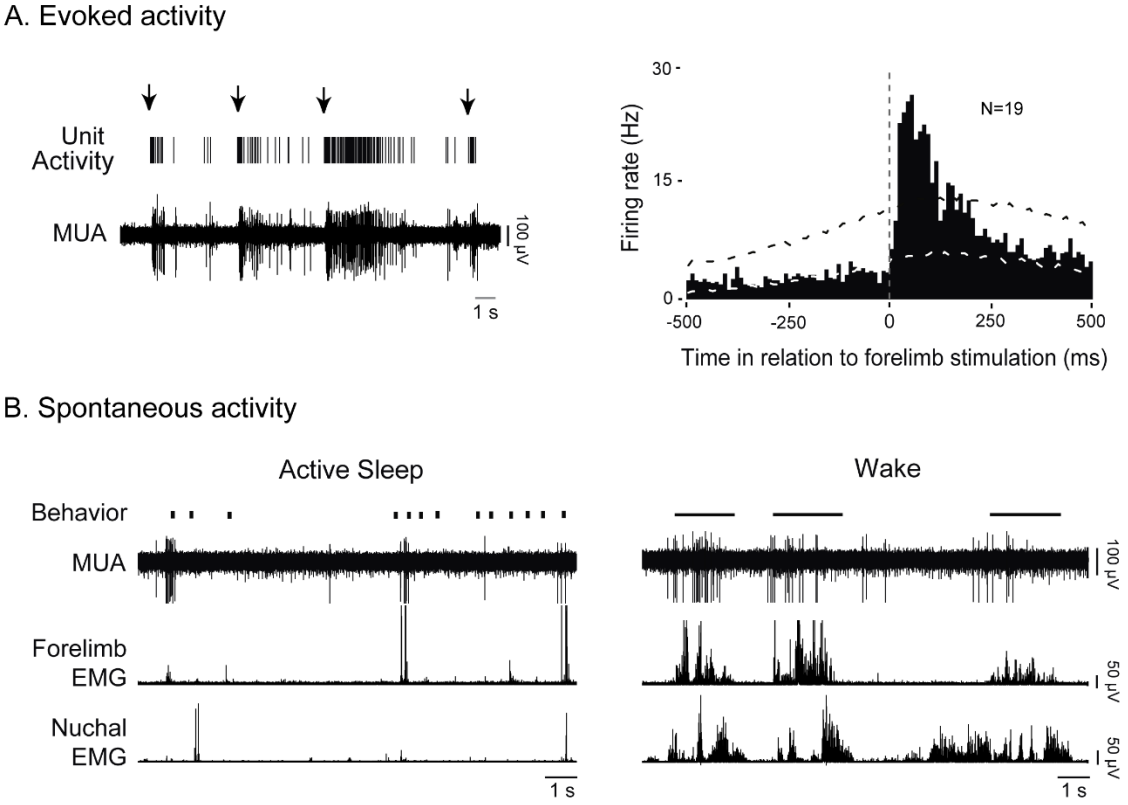


**Figure 2. Evoked and spontaneous activity in the RN during sleep and wakefulness.** A, Left, Representative recordings from the RN showing evoked sorted unit activity and MUA in response to contralateral forelimb stimulation (arrows). Right, Perievent histogram depicting mean firing rates of RN neurons in relation to contralateral forelimb stimulation. Data were pooled across all subjects (N = 8) and units (N = 19). Upper and lower confidence bands ($p < 0.01$ for each band) are indicated by the black and white dashed lines, respectively. Vertical dashed line corresponds to stimulation onset determined using forelimb EMG activity. B, Representative data depicting spontaneous behavior (vertical ticks, twitches; horizontal lines, wake movements), MUA, and contralateral forelimb and nuchal EMG activity during active sleep (left) and wake (right).

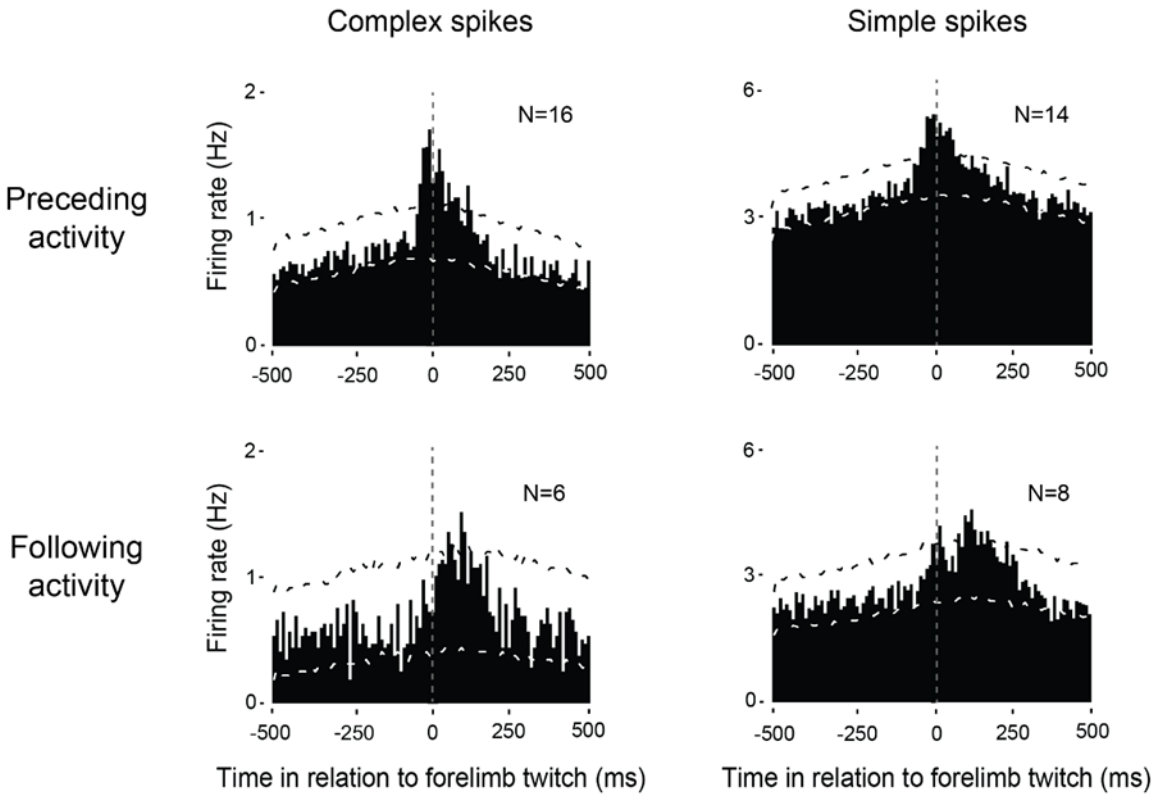


**Figure 3. Patterns of twitch-related complex and simple spike activity in the RN.** Perievent histograms for complex spikes (left) and simple spikes (right) in relation to contralateral forelimb twitches. Top row, Data pooled across all units with increases in neural activity that significantly preceded twitches. Bottom row, Data pooled across all units that significantly increased activity following twitches. Vertical dashed lines correspond to twitch onset. Number of units included in each analysis is indicated in each plot. Upper and lower confidence bands ($p < 0.01$ for each band)are indicated by the black and white dashed lines, respectively.

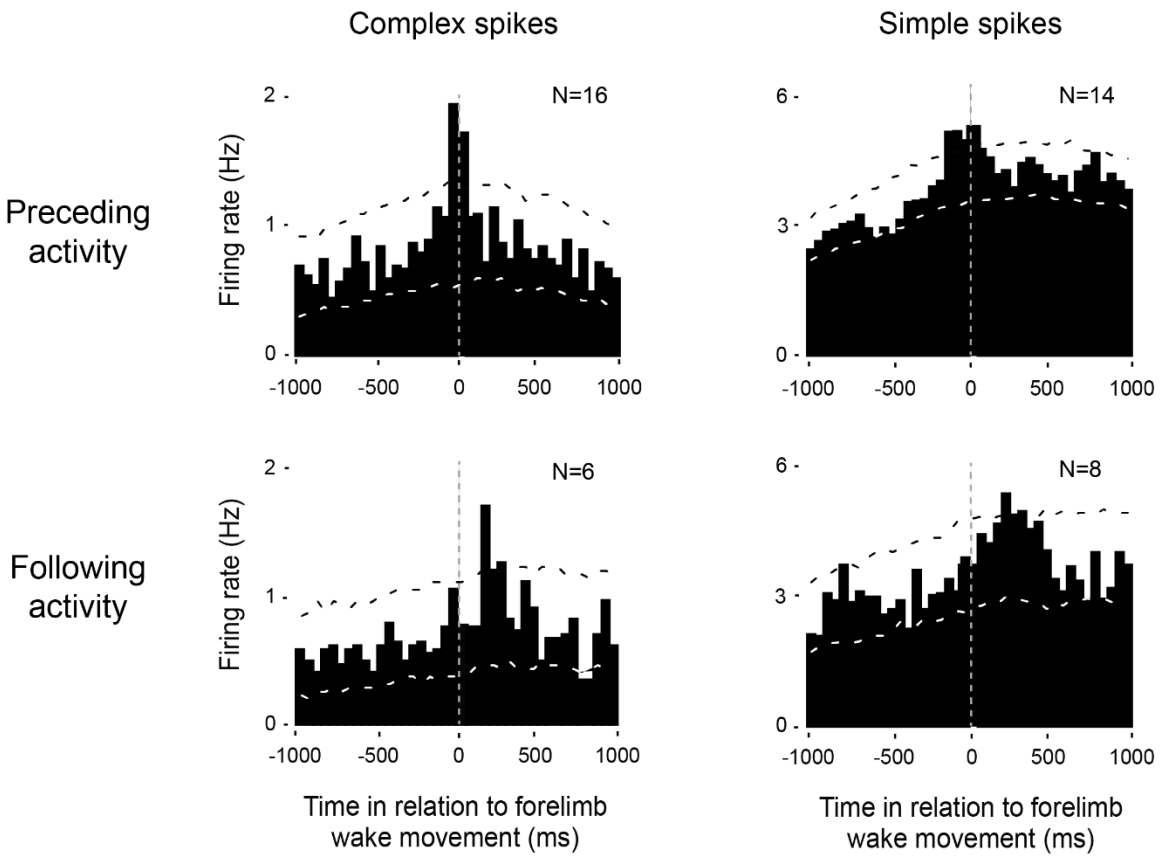


**Figure 4. Patterns of wake-movement-related complex and simple spike activity in the RN.** Perievent histograms for complex spikes (left) and simple spikes (right) in relation to the onset of the first forelimb movement during a bout of wakefulness. Top row, Data pooled across all units that significantly preceded forelimb movements. Bottom row, Data pooled across all units that significantly followed forelimb movements. Vertical dashed lines correspond to movement onset. Number of units included in each analysis is indicated in each plot. Upper and lower confidence bands ($p < 0.01$ for each band) are indicated by the black and white dashed lines, respectively.

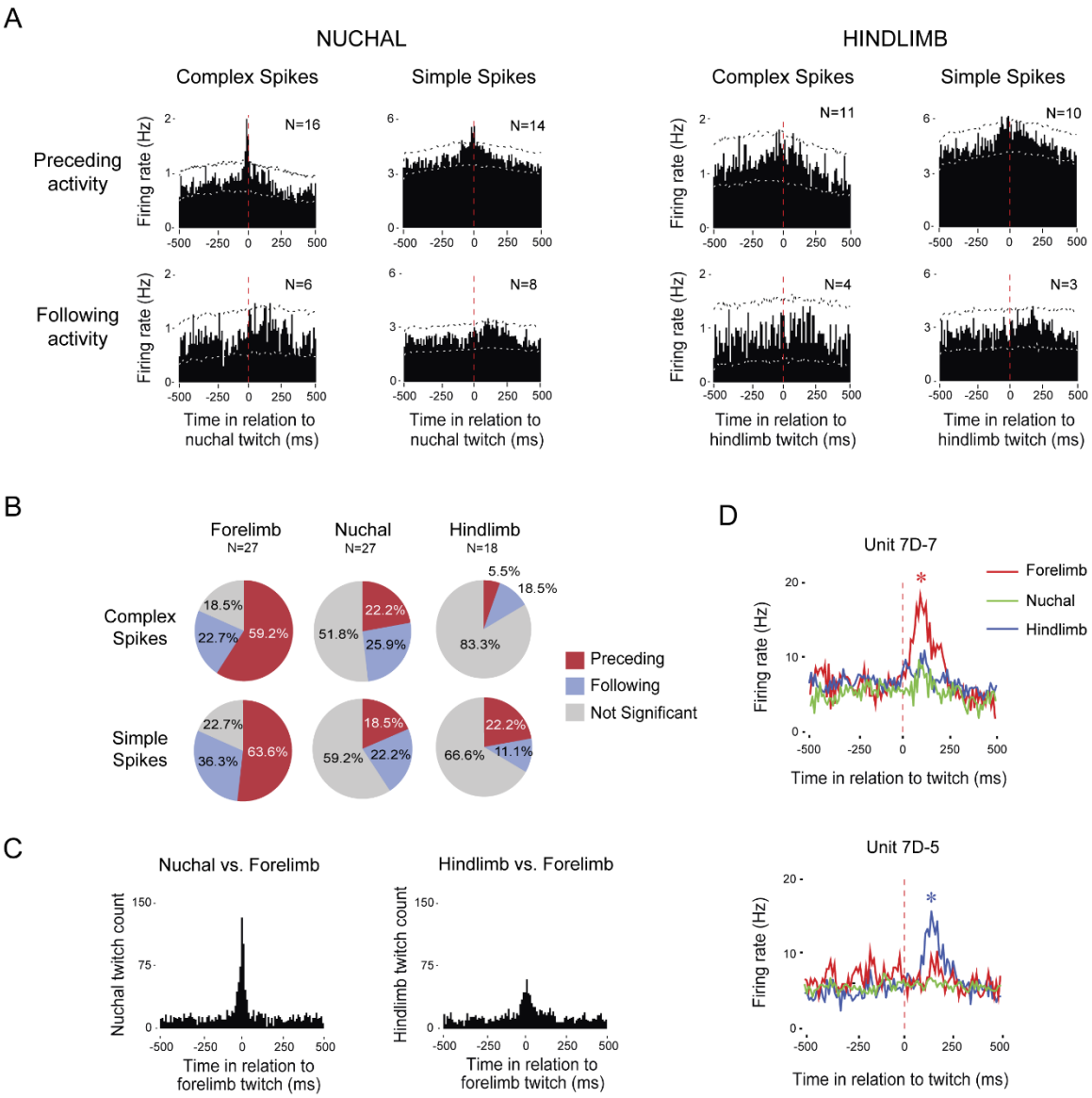


**Figure 5. Somatotopic organization of twitch-related activity in the RN.** A, Perievent histograms depicting unit activity in relation to contralateral nuchal (left) and hindlimb (right) twitches. Each histogram was created using pooled data from units that exhibited significant activity in relation to forelimb twitches (see Fig. 3). Vertical dashed lines correspond to twitch onset. Number of units included in each analysis is indicated in each plot. Upper and lower confidence bands ($p < 0.01$ for each band) are indicated by the black and white dashed lines, respectively. B, Percentage of units exhibiting significant or nonsignificant twitch-related activity for

each muscle group. C, Perievent histograms showing the number of nuchal (left) and hindlimb (right) twitches in relation to forelimb twitches for those subjects with EMG data from all three muscle groups (N = 5). D, Perievent line histograms relating activity in two adjacent units to twitches in the contralateral forelimb muscle (red), contralateral nuchal muscle (green), and hindlimb muscle (blue). Vertical dashed lines correspond to twitch onset. Asterisks indicate significant peaks in unit firing rate, $p < 0.01$.

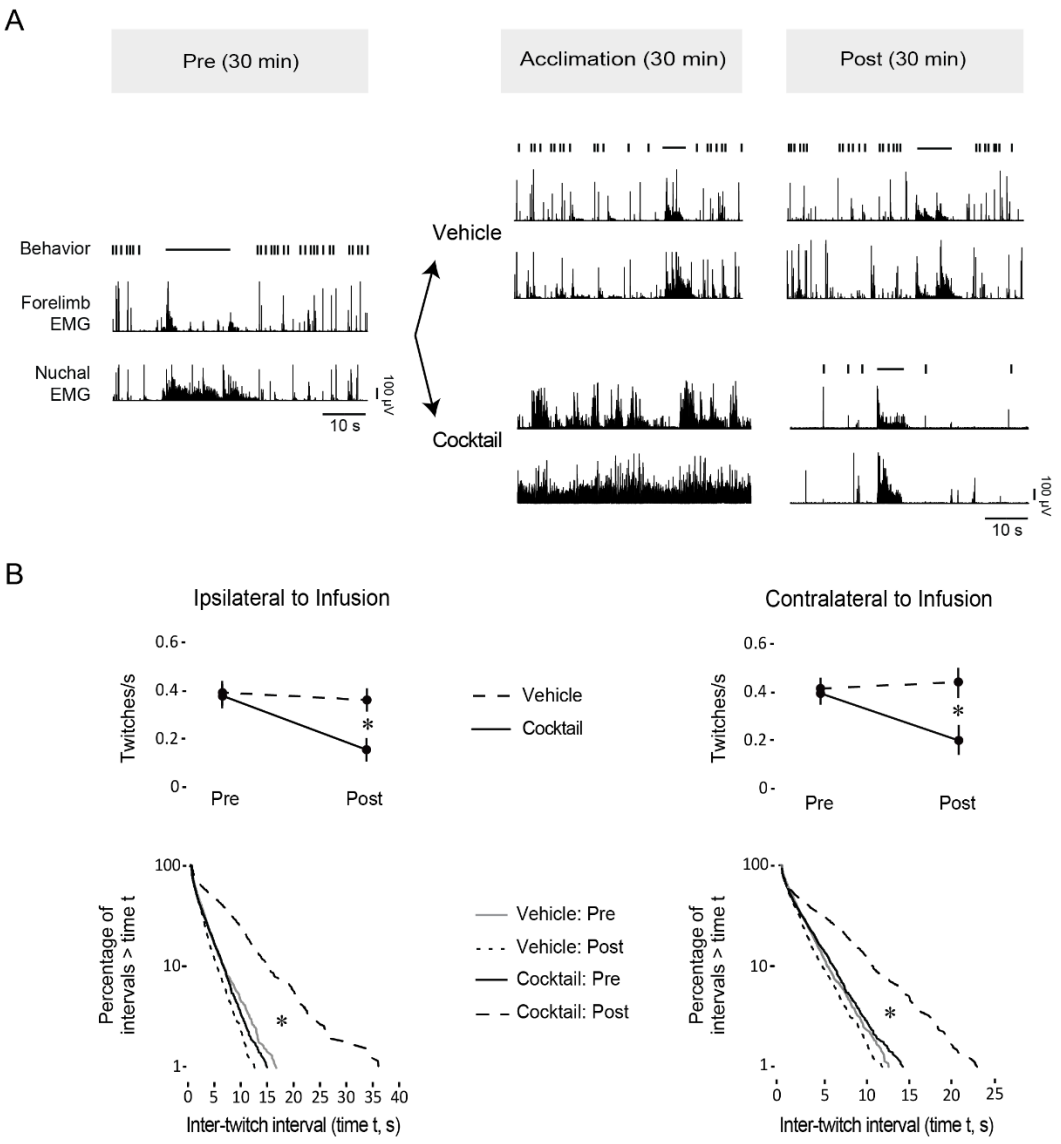


**Figure 6. Effects of pharmacological inhibition of the RN on sleep-related twitching.** A, Top, Timeline depicting the phases of the experiment before (Pre) and after (Post) infusion of a cocktail consisting of GABAA, GABAB, and glycine receptor agonists or vehicle. Bottom, Representative samples of forelimb and nuchal EMG activity and behavior (twitching, vertical ticks; wake movements, horizontal lines) during the Pre, Acclimation, and Post periods. B, Top row, Mean rate of twitching per unit time in active sleep before and after infusion of the vehicle or cocktail for the forelimb ipsilateral (left) and contralateral (right) to the infusion.

Asterisks indicate significant differences, $p < 0.05$. Bottom row, Log-survivor plots of ITIs before and after vehicle or cocktail infusions for the forelimb ipsilateral (left) and contralateral (right) to the infusion. Asterisks indicate significant Pre/Post differences for the Cocktail group, $p < 0.001$.

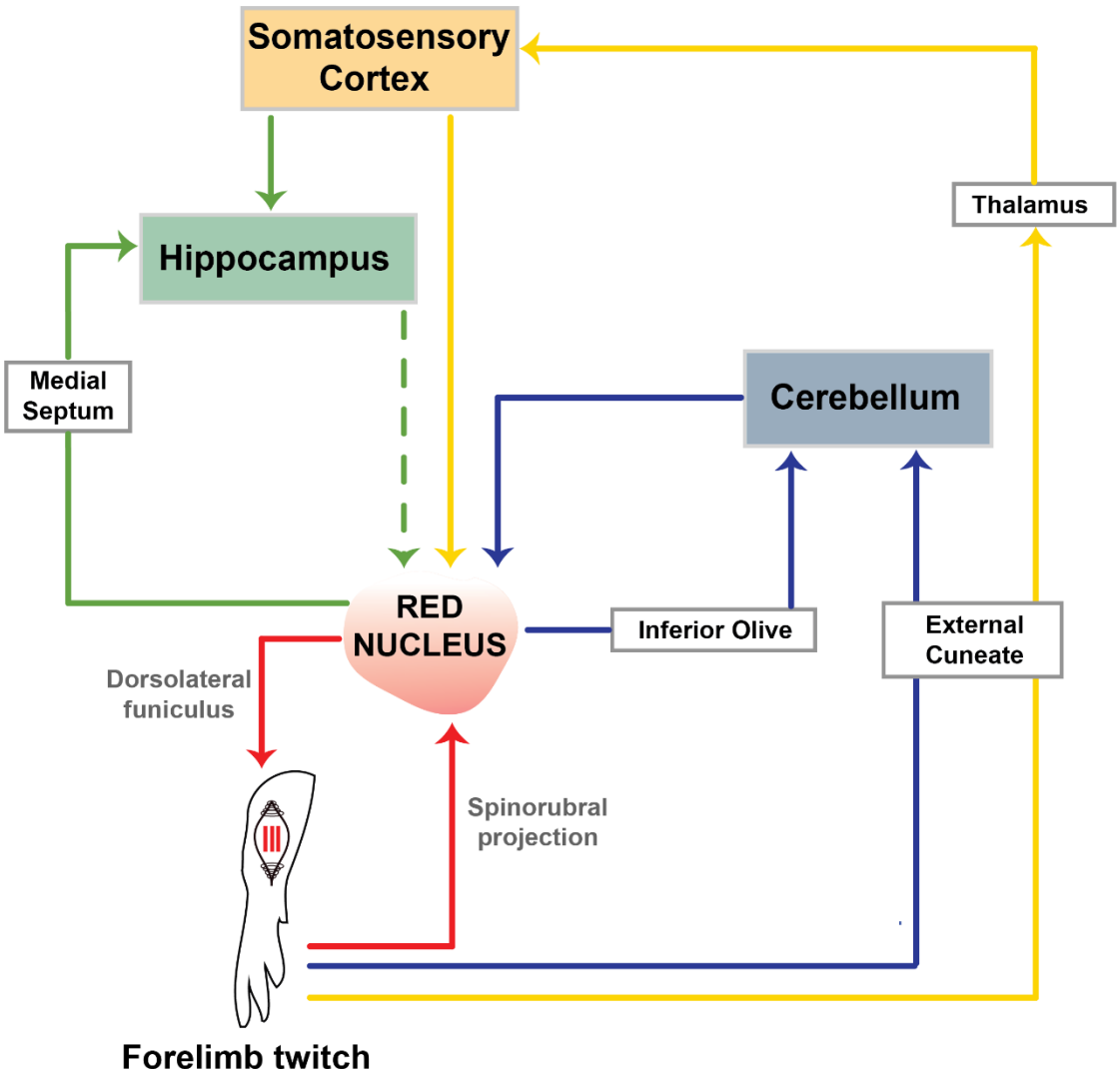


**Figure 7. Sensorimotor loops associated with twitch-related activity in the RN.** Several sensorimotor loops are illustrated, including the loop comprising the RN and its efferent and afferent connections to the spinal cord (red), as well as the loops that contain the cerebellum (blue), somatosensory cortex (yellow), and hippocampus (green). The dashed green line represents a hypothetical direct or indirect connection from the hippocampus to the RN. See text for details.

# CHAPTER 3: THETA OSCILLATIONS DURING ACTIVE SLEEP SYNCHRONIZE THE DEVELOPING RUBRO-HIPPOCAMPAL SENSORIMOTOR NETWORK

## INTRODUCTION

Sleep is the predominant behavioral state in early development [1–3,103]. Of the two primary sub-states of sleep, active sleep (AS, or REM sleep) occurs at its highest rates in the perinatal period and has long been considered a critical contributor to early brain development [8,103]. In addition, myoclonic twitching is a prominent phasic component of AS that triggers patterned neural activity throughout the neuraxis and, by doing so, can contribute to the experience-dependent development of sensorimotor networks [16,79,104,105].

In chapter 2, we showed that the newborn red nucleus (RN) is an important site for sensorimotor integration [47]. Specifically, in week-old rats, the RN is not only involved in the generation of wake movements and AS-related twitching, but also processes sensory feedback from moving limbs in a somatotopic fashion. Importantly, the RN is functionally connected with many other sensorimotor structures, including the cerebellum [25,57], sensorimotor cortex [59], and hippocampus [60,106,107]. Although the hippocampus is most typically associated with spatial memory and navigation [108], it has also long been considered a sensorimotor structure [109,110]. According to the sensorimotor integration model

of hippocampal function, the hippocampus interacts with the RN in a bidirectional manner to enable sensorimotor integration during motor performance [54,60]. The neural mechanisms that establish and maintain this long-range connectivity between hippocampus and RN have not been elucidated.

As demonstrated primarily in the adult [74,75,111] and infant [64,66,71,72] forebrain, long-range functional connectivity is maintained via synchronized neural oscillations, particularly at low frequencies including theta (4-10 Hz). In adults, oscillations in the theta band support functional connectivity in the hippocampus and associated networks during sensorimotor processing in humans [112] and rats [113]. Here we address the hypothesis that the infant hippocampus establishes long-range functional connectivity with the RN through synchronized theta oscillations. We record extracellular activity in P8 and P12 rats cycling freely between sleep and wakefulness; we chose these ages because they mark an abrupt transition in the development of hippocampal theta [23] as well as neural activity in the RN and associated structures [25]. We demonstrate for the first time that the RN exhibits robust theta activity during AS. Moreover, by P12, AS-related theta oscillations in the hippocampus and RN are coherent, comodulated, and mutually interactive. Finally, pharmacological inactivation of the medial septum (MS), an established generator of hippocampal theta, blocks AS- but not twitch-related theta in both the hippocampus and RN. These findings highlight the importance of behavioral state for the differential expression of functional connectivity in the developing nervous system. They also lay a foundation for

understanding how neural oscillations contribute to the emergence of long-range functional connectivity linking cortical and brainstem networks.

## METHODS

*Subjects*

A total of 41 male and female Sprague-Dawley Norway rats (Rattus norvegicus) at P7-9 (n = 11; hereafter designated as P8) and P11-13 (n = 30; hereafter designated as P12) were used. Whereas multiunit data from the RN-only recordings in the P8 and P12 subjects were published previously [25], the LFP data were newly analyzed for this study; all of the dual-recording data in the P12 subjects were collected for this study. With minor exceptions, the methods and equipment used in the two studies are identical. For all experiments, mothers and litters were housed in standard laboratory cages (48 x 20 x 26 cm). Animals were maintained on a 12:12 light-dark schedule with lights on at 0700 h and with water and food available ad libitum. Litters were culled to eight pups within three days of birth. Littermates were never assigned to the same experimental group. All experiments were conducted in accordance with the National Institutes of Health (NIH) Guide for the Care and Use of Laboratory Animals (NIH Publication No. 80-23) and were approved by the Institutional Animal Care and Use Committee of the University of Iowa.

*Surgery*

The surgical protocol used here is described in detail in Chapter 2. After the initial surgery, small holes were drilled in the skull for later insertion of a recording electrode into the RN (coordinates relative to bregma; P8; AP: −4.8 to -5.0 mm; ML: ±0.4 to 0.6 mm; dorsoventral (DV), 4.3 to 4.8 mm; P12; AP: −5.3 to -5.5 mm; ML: ±0.4 to 0.6 mm; DV: -5.0 to -5.5 mm) or CA1 region of hippocampus (P12; AP: −2 mm; ML: ±1.5 mm; DV: -2 to -2.5 mm; 15° lateral angle), or a microsyringe into the medial septum (P12; AP: +1.5 mm; ML: ±1.3-1.5 mm; DV: -4.5 to 5 mm; 20° lateral angle). Two additional holes were drilled, one above the visual cortex (contralateral to the hippocampal and RN recording sites) for insertion of a ground wire (which was also used as the reference electrode), and a second in frontal cortex for insertion of a thermocouple.

*General Procedure*

Following surgery, pups were transferred to a stereotaxic apparatus where the animal's torso was secured to a platform; the limbs were allowed to dangle freely. To monitor brain temperature, a fine-wire thermocouple was inserted into the cerebral cortex (Omega Engineering, Stamford, CT). Brain temperature was maintained at 36-37 °C throughout all experiments. The EMG bipolar electrodes were connected to a differential amplifier (A-M Systems, Carlsborg, WA; Tucker-Davis Technologies, Alachua, FL). A stainless steel ground electrode (0.25 mm diameter; Medwire, Mt. Vernon, NY) was inserted into the cerebral cortex. Testing

began after a 1-h acclimation period but not before organized sleep-wake cycles were observed.

*Neurophysiological Recordings*

Neural data were acquired using similar methods than those described in Chapter 2. Here we used 16-channel silicon depth electrodes or 4-channel linear probes (NeuroNexus, Ann Arbor, MI; A1x16-Poly2-5mm-50-177; A1x16-10mm-100-177; Q1x4-10mm-50-177). Neural and EMG signals were sampled at 25 kHz and 1 kHz, respectively.

*Pharmacological Inactivation of the Medial Septum*

To assess the effects of pharmacological inactivation of the medial septum on spontaneous hippocampal and RN activity at P12, we first recorded spontaneous activity in the RN and hippocampus over a baseline period of 30 min. Then, a 0.5 µl microsyringe (Hamilton, Reno, NV) was lowered stereotaxically into the medial septum (see coordinates above). Pups received a 0.1 µl infusion into the medial septum of either fluorophore-conjugated muscimol (MUS, N = 6; ThermoFisher Scientific; 1.6 mM, dissolved in 40% dimethyl sulfoxide) or 0.9% saline (SAL, N = 6) at a rate of 0.1 µl/min. After a 15-min period to allow for drug diffusion, the 30-min post-infusion recording session began [25,114]. This infusion/recording protocol is similar to that used previously to assess the effect of inactivating the deep cerebellar nuclei (DCN; coordinates for microsyringe placement at P12: AP, -3.7 mm; ML, ±3 mm; DV, -3.2 mm; 20° lateral angle) on RN activity [25].

*Histology*

Electrode location and drug diffusion were confirmed using the same methods described in Chapter 2.

*Quantification and Statistical Analysis*

All analyses and statistical tests for neural data were performed using custom-written Matlab routines (MathWorks, Natick, MA), Spike2 software (Cambridge Electronic Design), and SPSS (IBM, Armonk, NY). Alpha was set at 0.05 for all analyses, unless otherwise stated. When repeated-measures analysis of variance (ANOVA) was performed, post hoc pairwise comparisons were performed using the Bonferroni correction procedure. Reported group data are always mean ± standard error (SE).

*Behavioral State*

As described previously [115], EMG signals and behavioral scoring were used to identify behavioral states. Active wake (AW) was defined as periods characterized by high-amplitude limb movements against a background of elevated muscle tone. Active sleep (AS) was defined by the presence of myoclonic twitches against a background of muscle atonia [3,82]. Twitches were identified electrographically as spikes in the EMG record with amplitudes at least 3x larger than background atonia. Behavioral quiescence (BQ) was defined as periods of low muscle tone, an absence of spiking activity in the EMG, and behaviorally confirmed absence of

overt movement. Such periods typically occurred between bouts of AW and AS and were required to last at least 1 s [25].

*Spike Sorting*

As described in Chapter 2, spike sorting was performed using template matching and principal component analysis in Spike2. We excluded waveforms as outliers when they were larger than 3.5 SDs from the mean of a given template.

*LFP Power Spectrum and Theta Ratios*

For all LFP-related analyses, one LFP channel from each structure per pup was selected. Selection of the LFP channel was based on electrode placement within hippocampus or RN as well as maximum theta power during AS. Power spectra were calculated from the down-sampled LFP (1 kHz) using a 2-s Hanning window in Spike2. For time-normalization and subsequent statistical comparisons, the spectral power density values in each bin were divided by the total duration of the file comprising data for each behavioral state (see above). Theta ratios were calculated as follows: For each LFP channel and behavioral state, raw power values within theta frequency (4-7 Hz) were summed and divided by the summed raw power at 12-15 Hz; this method served to normalize values of theta power. State-dependent differences in theta ratios were calculated using repeated-measures ANOVA with theta ratio as the dependent variable. When data from two age groups were analyzed, state-dependent differences in theta ratio were calculated using a repeated-measures factorial ANOVA with age group (P8, P12)

as the between-subjects factor and behavioral state (AW, BQ, AS) as the repeated-measures factor.

*Twitch-Related LFP Activity*

To generate individual twitch-triggered time-frequency spectrograms, the LFP signals around forelimb twitches (peri-twitch window = 1 s) were convolved using a complex Morlet wavelet. The Morlet wavelet was created as follows: the frequency band of interest (0-20 Hz) was divided into 30 bins, and the temporal resolution of the wavelet was established using a minimum of 2 and a maximum of 3 cycles. Twitch-triggered LFP theta power was calculated as follows: First, raw neural signals were filtered using a 4-7 Hz band-pass filter (IIR, Butterworth, $2^{nd}$ order). Next, the signal was converted using root mean square (RMS; time constant = 0.1 s). Then, data from all pups within each age or experimental group were concatenated into one file. Using forelimb twitches as trigger events, waveform averages of theta activity were calculated in Spike2 (peri-twitch window = 2 s); we tested statistical significance by jittering twitch events 1000 times (jitter window = 1000 ms) using the interval jitter parameter settings within PatternJitter [83,84] in Matlab. We corrected for multiple comparisons using an established method [84]; this method produces upper acceptance bands to establish statistical significance for each waveform average. For analyses of twitch-related activity before and after inactivation of the medial septum (see below), we similarly created waveform averages and power spectra, both triggered on forelimb twitches and using a 2-s peri-twitch window.

*LFP-LFP and Spike-LFP Coherence*

LFP-LFP and Spike-LFP coherence analyses were conducted using one LFP per pup and neural structure, based on the criteria described above. Using custom-written Matlab codes, coherence analyses were calculated from cross-spectral density. Each signal was convolved using a complex Morlet wavelet. The Morlet wavelet was created as follows: the frequency band of interest (0-20 Hz) was divided into 50 bins, and the temporal resolution of the wavelet was established using a minimum of 4 and a maximum of 8 cycles. To calculate state-dependent differences in coherence, we performed repeated-measure ANOVAs with behavioral state (AW, BQ, or AS) as the repeated measure and average coherence within the theta range (4-7 Hz) as the dependent variable. Differences in spike-LFP coherence across theta conditions during AS were calculated as follows: First, we selected those spike-LFP pairs that exhibited a coherence peak within the theta frequency range (4-7 Hz) for periods of high-amplitude theta (see below). Then, we calculated statistical differences across theta amplitude conditions using repeated-measures ANOVAs, with coherence values within the theta-frequency range as the dependent variable.

*Granger Causality*

Wiener-Granger causality analyses were conducted using the same LFPs per pup and neural structure selected above. The linear regression model used in this analysis aimed to calculate, for two structures, the prediction error for a current LFP data point in one structure based on past LFP data points in the other

structure. Hipp→RN and RN→Hipp prediction errors were calculated using a function adapted from the BSMART toolbox [116,117]. The LFP data across the entire session for each pup were divided into sequential 2-s segments to provide a sufficient number of samples for Granger analysis. Statistical significance for Granger causality was assessed against a null-hypothesis baseline distribution [71,118] generated using a bootstrap-shuffle (n = 100 shuffles) in which the 2-s segments of hippocampal and RN LFP data were randomly paired. The same calculation was conducted with 3-s temporal segments to confirm that the obtained results were not sensitive to the chosen segment size. For those pups that exhibited significant Granger values (hippocampus→RN or RN→hippocampus) during AS, we performed related-samples t tests using peak Granger value as the dependent variable to assess differences in strength between the two directions.

*LFP Cross-Correlation*

The amount of temporal synchrony between hippocampal and RN theta oscillations (4-7 Hz) was measured by cross-correlating the two band-pass-filtered LFP signals (bin resolution = 1 ms). Cross-correlation analyses were conducted using the same LFPs per pup and neural structure selected above. The hippocampal signal was always the driving signal. For this analysis, entire bouts of AS were divided into 2-s segments to compute average theta power. The correlation coefficient in each calculation was compared with the value produced using a bootstrap-shuffle method (n = 1000) applied to the hippocampal LFP; for this method, in each iteration we selected a random point on the LFP and switched

the 2-s segments on either side of that point. To verify that the current results were not obtained by chance, the same calculations were performed using different segment sizes (1-s and 5-s segments); the results with different temporal segments were not quantitatively or qualitatively different. Differences between original and shuffled data were calculated using independent-samples t tests with the cross-correlation coefficient as the dependent variable.

*Phase Locking*

Theta phases were calculated by applying the Hilbert transform to the band-pass-filtered theta rhythms in the hippocampus or RN [119]. Rayleigh's tests were used to determine whether MUA signals were significantly phase-locked to the theta (4-7 Hz) oscillation [120,121]. For this test, a phase estimate was first assigned to each spike time and a phase histogram (20 degree/bin) was generated for each MUA signal. Next, the phase-locking value (PLV) was calculated to quantify the amount of phase-locking [122,123]. Z-transformed PLVs were calculated by using a bootstrap-shuffle method (n = 1000); for this method, in each iteration we selected a random point on the LFP and switched the segments on either side of that point. If both Rayleigh's test and the Z-transformed PLV were statistically significant for a given MUA signal, the MUA signal was regarded as significantly phase-locked to the theta rhythm for that structure. We calculated statistical differences across theta amplitude conditions using repeated-measures ANOVA, with PLVs within the theta-frequency range as the dependent variable.

*Inactivation of the Medial Septum*

To assess the effect of medial septum inactivation on sleep measures, we calculated mean time spent in AS and mean twitching rates during the pre- and post-infusion recording periods. Twitching rates were calculated by dividing the total number of twitches in each muscle group (forelimb, nuchal) by total time spent in AS. To assess statistical differences in these sleep measures, we performed independent pairwise comparisons (pre- vs. post-inactivation) using the Wilcoxon matched-pairs signed-ranks tests. Effects of medial septum inactivation on theta activity during AS were statistically evaluated using a 2 x 2 repeated-measures factorial ANOVA with experimental group (MUS or SAL) as the between-subjects factor and time (Pre or Post) as the repeated-measures factor. For this analysis, theta ratios in each structure (see above) were used as the dependent variables. The same analytical approach was adopted to evaluate the effects of inactivation of the deep cerebellar nuclei (DCN) on oscillatory activity in the RN; this last analysis was performed using data from a previously published study [25].

## RESULTS

### The infant RN exhibits state- and twitch-dependent theta oscillations

We first characterized developmental patterns of oscillatory activity in the RN using data from a previous study [25]. At P8 (n = 11), the local field potential (LFP) in the RN exhibited short, discontinuous bursts of oscillatory activity (Figure 8A). These bursts occurred predominantly at theta frequency (4-7 Hz) and within periods of

AS. In contrast, theta activity at P12 (n = 11) was continuous during periods of AS (Figure 8B). This rapid developmental transition from discontinuous to continuous oscillatory activity in the RN is similar to that observed in forebrain areas such as prefrontal cortex [71], sensorimotor cortex [81], and hippocampus [23,71]. Quantitative analyses of theta power revealed a significant main effect of Behavioral State ($F_{(2, 40)} = 4.9$, $p < 0.02$) as well as an Age x Behavioral State interaction ($F_{(2, 40)} = 14.6$, $p < 0.001$); theta power at P12 was significantly higher during AS in relation to the other behavioral states (post hoc pairwise comparisons, $ps < 0.002$; Figure 8C, D).

Sensory feedback (i.e., reafference) from myoclonic twitches is a potent driver of RN activity at P8 and P12 [25,47]. Thus, we next asked whether the brief theta oscillations observed during AS at P8 were attributable to twitch-related reafference. Individual twitch-triggered spectrograms and LFP waveforms of theta activity, pooled across all pups (n = 11), indicate that twitch-related reafference triggered brief theta oscillations ($p < .01$; Figure 9A). Surprisingly, at P12 and against a background of continuous theta oscillations (n = 11), twitch-related reafference continued to trigger increased theta power ($p < .01$; Figure 9B). This transition between P8 and P12 from brief, twitch-related theta bursts to continuous, AS-related oscillations in the RN mirrors previous findings in the hippocampus [23].

**Theta oscillations in the hippocampus and RN are tightly coupled during AS at P12**

We next asked whether the continuous theta oscillations in the hippocampus and RN, first observed at P12, are temporally coupled, thus indicating functional connectivity between these two structures. To address this question, we performed simultaneous extracellular recordings in the RN and hippocampal CA1 (n = 19; Figure 10A). As expected, continuous theta oscillations in the hippocampus and RN were most prominently expressed during AS (Figure 10B). Theta power was higher for periods of AS in both the hippocampus (Figure 10C, $F_{(1.4,25.9)} = 31.3$, $p < 0.001$, correction: Greenhouse-Geisser) and RN (Figure 10D; $F_{(1.4,26.1)} = 19.8$, $p < 0.001$, correction: Greenhouse-Geisser) in relation to active wake (AW) and behavioral quiescence (BQ; post hoc pairwise comparisons, ps < 0.001). It should be noted that the theta-frequency peak observed here at P12 (5 Hz) is lower than that reported in the hippocampus of adult rats during AS (typically 8 Hz; Montgomery et al., 2008). The frequency peak found here at P12 is consistent with the finding of a progressive increase in theta frequency across age from ~5.5 Hz at P16 to ~7.5 Hz by P28 [125].

We next assessed the coherence of hippocampal and RN theta oscillations across the three behavioral states (Figure 11A). Coherence spectra revealed that coupling in the theta-frequency range was significantly greater during AS (Figure 11B; $F_{(2,36)} = 47.2$, $p < 0.001$) than during AW or BQ (ps < 0.001). To characterize the strength and directionality of information flow between the hippocampus and RN during AS, we next performed Granger causality analysis [117,126] (Figure

11C). This analysis was performed on LFP pairs from all 19 pups, from which we identified 9 pups that exhibited (i) significant Granger values (ps < 0.01) and (ii) clear Granger value peaks within theta frequency. From these pups, the average pattern comprised a substantial hippocampus→RN peak and a smaller RN→hippocampal peak. These results are consistent with the sensorimotor integration model of hippocampal function [54,60], which posits bidirectional communication between the hippocampus and RN.

Having established functional connectivity in the theta band between the hippocampus and RN, we next assessed whether theta oscillations are temporally associated with spiking activity in the two structures. Hippocampal spiking activity was highly coherent with hippocampal LFP in the theta-frequency range during AS ($F_{(1.1,39.4)} = 17.2$, $p < 0.004$, correction: Greenhouse-Geisser) as compared with AW and BQ (post hoc pairwise comparisons, ps < 0.004; Figure S1A). In contrast, theta-related spike-LFP coherence in the RN was negligible (Figure S1B). Visual examination of the RN data, however, suggested that spiking activity increases substantially during periods of increased theta amplitude (e.g., see Figure S2B). Therefore, we next examined the temporal fluctuations in theta amplitude before testing the hypothesis that spike-LFP coherence in the RN is enhanced during periods of high-amplitude theta.

**Comodulation of theta amplitude in the hippocampus and RN at P12**

We defined high-amplitude theta as continuous theta oscillations with at least three cycles that exceeded the baseline amplitude by 1.5 SDs; all other periods were

designated as low-amplitude theta (Figure 12A). As expected, this method yielded two distinct categories of AS-related theta in the hippocampus ($F_{(1,18)} = 32.1$, $p < 0.001$) and RN ($F_{(1,18)} = 84.7$, $p < 0.001$; Figure 12B). High-amplitude theta during AS was often closely associated with periods of abundant myoclonic twitching (Figure 12A); indeed, rates of twitching in the forelimb were significantly higher during periods of high-amplitude theta in both the hippocampus ($F_{(1,18)} = 16.5$, $p < 0.002$) and RN ($F_{(1,18)} = 26.2$, $p < 0.001$; Figure 12C). Cross-correlations between theta-filtered LFPs in the hippocampus and RN during AS indicated robust synchrony and coherent amplitude modulation (i.e., comodulation; Figure 12D, left; mean lag for pooled data: 10 $\pm$ 9 ms); cross-correlations coefficients were significantly higher in relation to shuffled data ($t_{(18)} = 10.1$, $p < 0.001$; Figure 12D, right).

**Theta oscillations modulate spiking activity in the hippocampus and RN at P12**

Having characterized fluctuations in theta amplitude across AS, we next returned to the hypothesis that spike-LFP coherence is specifically enhanced during periods of high-amplitude theta. To test this hypothesis, we produced spike-LFP coherence spectra restricted to periods of high-amplitude theta and selected those units showing clear peaks within the theta-frequency range (see Methods). For these pairs, and in comparison to entire bouts of AS, spike-LFP coherence was significantly greater during periods of high-amplitude theta in the hippocampus ($F_{(1,23)} = 10.8$, $p < 0.004$; Figure 12E) and RN ($F_{(1,23)} = 29.5$, $p < 0.001$; Figure 12F).

In addition to spike-LFP coherence, hippocampal and RN units were phase-locked to local theta oscillations during periods of high-amplitude theta. Examples of phase-locked spiking activity are shown for the hippocampus (Figure 12G, left) and RN (Figure 12H, left). In total, significant phase-locking was found in 79% of the hippocampal neurons and 61% of the RN neurons (ps < 0.01). Moreover, phase locking was significantly higher during periods of high-amplitude theta in both the hippocampus ($F_{(1,25)} = 9.8$, $p < 0.005$, Figure 12G, right) and RN ($F_{(1,35)} = 14.9$, $p < 0.001$; Figure 12H, right). These results suggest that theta oscillations in the developing hippocampus and RN modulate neuronal activity during AS, especially during periods of high-amplitude theta.

Spike-LFP coherence and phase locking within the RN suggest that theta oscillations are locally expressed rather than being volume conducted from a nearby structure. We further addressed this issue of local generation in a subset of P12 subjects (n = 5) by retracting the electrode to locations dorsal to the RN and performing additional recordings (Figure S2A). As shown for a representative subject (Figure S2B), theta power during AS was equally high in the two sites within the RN—where spiking activity was also present—and decreased at sites approximately 2 mm dorsal to the RN. This pattern of decrease in theta power was found in the theta ratios averaged across all five subjects (Figure S2C). Interestingly, the retention of high theta ratios in the region immediately dorsal to the RN could reflect RN-like activity in nearby premotor nuclei within the so-called mesodiencephalic junction [127].

**Inactivation of the medial septum blocks theta in the hippocampus and RN at P12**

The findings presented thus far suggest that theta oscillations in the hippocampus and RN share a common neural generator. The medial septal area, including medial septum (MS) and diagonal band of Broca (DBB), is known to generate hippocampal theta in adult [128] and neonatal [71] rats. To determine whether it also generates theta in the RN, we compared hippocampal and RN activity at P12 before and after pharmacological inactivation of the MS (Figure 13A,B). These inactivations were performed in a subset of the subjects described above (n = 6 in each group) by infusing 0.1 µl of the $GABA_A$ receptor agonist muscimol (1.6 mM) or saline [129].

The LFPs and time-frequency spectrograms for one representative subject are shown in Figure 13C; in both the hippocampus and RN, theta oscillations during AS were markedly reduced after MS inactivation. These reductions are equally clear in the averaged power spectra in Figure 13D. With respect to theta power across the two structures, there was a significant main effect of Pre/Post (Hipp: $F_{(1,10)} = 9.3$, $p < 0.02$; RN: $F_{(1,10)} = 9.9$, $p = 0.01$) as well as a significant Group x Pre/Post interaction (Hipp: $F_{(1,10)} = 13.4$, $p < 0.005$; RN: $F_{(1,10)} = 8.7$, $p < 0.02$). Post hoc tests revealed significant decreases in theta power after MS inactivation for the hippocampus ($p < 0.02$; Figure 13D, top) and RN ($p = 0.01$; Figure 13D, bottom). Importantly, MS inactivation had no effect on the expression of AS or twitching (Table 1). Thus, the MS specifically modulates the expression of AS-related theta in both the hippocampus and RN without affecting the

expression of sleep or twitching.

In addition to inputs from the forebrain, the RN receives a prominent input from the deep cerebellar nuclei (DCN) [57,97]. In a previous study that used similar methods in P12 rats (Figure S3A), we found that inactivation of the DCN reduced firing rates in the RN during AS by 40-50% [25]. We returned to these data to ask whether DCN inactivation had any effect on the expression of theta in the RN. We found that it did not (Figure S3B), thus providing further evidence that RN theta is specifically tied to the septo-hippocampal system.

Finally, spiking activity in both the hippocampus and RN [23,25,47] increases in response to twitching; in the hippocampus, twitch-related reafference is conveyed from the sensorimotor cortex [24]. This raises the possibility that twitch-triggered activation of theta bursts within the hippocampus and RN occur independently of septal influence. Indeed, inactivation of the MS at P12 blocked AS-related—but not twitch-related—theta in both the hippocampus and RN (all $p < 0.05$; Figure 14). Moreover, in the absence of septal input, twitch-triggered theta activity at P12 now mirrored the discontinuous theta-burst pattern observed here at P8 in the RN (see Figure 9A) and previously in the hippocampus [23].

## DISCUSSION

We have discovered in infant rats the presence of continuous theta oscillations in the RN, a premotor brainstem structure that plays an outsized role in controlling

newborn behavior [44,47]. These theta oscillations emerged rapidly toward the end of the second postnatal week and were expressed predominantly during AS. By recording simultaneously from the RN and hippocampus at P12, we found that theta in the two structures was coherent and comodulated during AS, indicating close functional and state-dependent coupling between them. Finally, by inactivating the MS—a structure known to generate hippocampal theta—we found that theta is lost in both the hippocampus and RN. Although it has been proposed that theta oscillations in the hippocampus contribute to its functional connectivity with brainstem motor nuclei [54], the possibility of oscillatory coupling among these structures had not been considered.

**The transition from discontinuous to continuous oscillatory activity**

During AS, theta oscillations in the RN are expressed at P8 as discontinuous bursts and transition to continuous oscillations by P12; this transition from discontinuous to continuous theta is identical to that observed in the hippocampus [23]. Similar oscillatory transitions have been reported in the rat cerebral cortex at the beginning of the second postnatal week [23,64,71,81,104] and in human infants toward the end of the third trimester [64,130,131]. In rats, these transitions coincide with abrupt increases in single-unit firing rates in the RN [25], cerebellum [25,26], sensorimotor cortex [81], and hippocampus [23]. Moreover, the rapidity with which these transitions occur suggest that these ages define a sensitive period for brain development [26].

The emergence of hippocampal theta bursts at P8 [23] coincides with the rapid proliferation of perisomatic interneuronal synapses [132] and the emergence of parvalbumin-immunoreactive GABAergic neurons in the MS and hippocampus [133,134]; both contribute to theta production [135,136]. Like the hippocampus, the rodent RN contains a well-characterized subpopulation of GABAergic interneurons, including parvalbumin-immunoreactive cells [137,138]. In addition, the density of GABAergic receptors in the rat RN peaks around P10 [139], just before the emergence of continuous theta. The similarities in the developmental timing of theta in the RN and hippocampus, as well as similarities in the emergence of GABAergic networks, suggest that theta in both structures is generated through similar mechanisms.

As illustrated in Figure S4, continuous theta in the RN could arise through a number of different pathways. Specifically, RN theta could arise independently of the hippocampus through direct or indirect input from the septal area, including the MS and the DBB [56], or through an indirect projections from the hippocampus, perhaps through the zona incerta [56,140] or the lateral septum and hypothalamus [56,141].

**Reafference from twitches triggers a third type of theta activity**

At P8, discontinuous theta bursts in the RN were predominantly expressed immediately after forelimb twitches, suggesting reafferent activation. Bursts of oscillatory activity can contribute to a variety of developmental processes,

including synapse formation, cell differentiation and migration [64], and map formation and refinement [66]. Importantly, the close temporal association between twitching and brief bursts of cortical [81,104] and hippocampal [23] activity inspired the hypothesis that twitch-related reafference contributes to the development of these forebrain networks [79,104,105]. The present findings extend these ideas to brainstem structures like the RN [47]. To the extent that increases in LFP power reflect enhanced neuronal synchrony [142], twitch-triggered increases in theta power may reflect greater network synchronization in the rubro-hippocampal system.

In the adult hippocampus, two types of theta oscillations have been identified, based in part on their behavioral correlates [143]: Type 1 or movement-related, theta, and type 2 or immobility-related theta. Moreover, whereas type 1 theta occurs during periods of “phasic AS” (defined by the presence of phasic events, including twitches), and type 2 theta occurs during “tonic AS” [144]. At P12 during AS, hippocampal theta exhibited characteristics that correspond with types 1 and 2, and inactivation of the MS suppressed both of them, as occurs in adults [145]. Strikingly, we found the same pattern of results in the P12 RN.

During AS, Type 1 theta is identified only with *periods* surrounding phasic activity and has not been specifically associated with reafference from twitches. In contrast, as noted above, inactivation of the MS at P12 suppressed both types of theta while sparing the expression of twitch-triggered theta bursts; this suggests that reafferent theta is conveyed via non-septal pathways (see Figure S4). This finding raises the possibility that twitch-reafferent theta in adults is present but

masked, as previously proposed in relation to twitch-reafferent spindle-burst activity in sensorimotor cortex [146]. Accordingly, we propose that twitch-reafferent theta constitutes a distinct—type 3—category of theta. The pathways conveying twitch-related reafference to the RN likely bypass the cerebellum [25] and involve direct spinorubral projections [147]; on the other hand, the pathway to the hippocampus likely passes first through somatosensory cortex [24].

**The rubro-hippocampal network and its role in sensorimotor integration**

In adults, functional connectivity between the hippocampus and RN is thought to enable motor behavior that adjusts adaptively to sensory input [54,60]. For example, both the hippocampus and RN are necessary for the acquisition and expression of trace eyeblink conditioning [107,148], and theta oscillations appear important for synchronizing the hippocampus and cerebellum to enhance this learning [149]; this opens the possibility that theta oscillations in the RN also participate in this system-wide synchronization within learning contexts. In addition, the role of hippocampal theta in modulating locomotor speed in mice [150] may be mediated by subcortical premotor structures such as the RN. Theta-dependent functional connectivity could also contribute to the acquisition and consolidation of skilled forelimb movements, which are highly dependent on the RN [46].

**Functional connectivity in developing networks: Beyond the "resting state"**

Although AS is a relatively prominent behavioral state in early infancy [1–3,103], investigations of functional connectivity in infants have largely focused on the so-called "resting state," on periods of slow-wave sleep, or under anesthetic conditions that suppress normal sleep-wake cycles [151]. Given the hypothesized role of AS in brain development [1,8,79,103], one might expect network interactions to be very different during this sleep state; indeed, in adults, AS specifically enhances theta-dependent synchrony in hippocampal networks [124,152] and, moreover, AS-related theta appears to be causally related to hippocampal-dependent memory consolidation [153]. Here, using infant rats, we found that the state of AS permits the expression of theta-dependent functional connectivity between the hippocampus and RN, perhaps driving activity-dependent developmental plasticity at ages when wake-related expression of hippocampal-dependent learning has yet to emerge [121]. Importantly, given that theta oscillations in the developing hippocampal system are preferentially expressed during AS, we suggest that—under normal conditions—the state of AS promotes maximal theta-dependent coupling among structures within the hippocampal network (including the prefrontal cortex, [71]).

We did not see evidence of prominent theta during periods of wake-related movements, as occurs in the adult hippocampus [143]. Although it is possible that wake-related theta develops later, our head-fix method is incompatible with the expression of the kinds of wake behaviors (e.g., running, rearing, jumping) that

accompany theta in adults. However, even in unrestrained rats, these wake behaviors are relatively infrequent at P12 [154], especially compared with AS.

**Disrupted functional connectivity in neurodevelopmental disorders**

Aberrant long-range connectivity occurs in such neurodevelopmental disorders as schizophrenia [155], autism [156], and ADHD [157]. Although investigations in these domains have focused largely on the cortical networks that subserve cognitive and social functions [72], it is important to acknowledge that many neurodevelopmental disorders also entail substantial sensorimotor deficits. For example, autism not only comprises cognitive and social deficits, but also deficits in motor control [158] and sensorimotor integration [159]. In addition, autism entails aberrant functional connectivity between cerebral cortex and subcortical networks involved in sensorimotor processing, including the cerebellum [160] and striatum [161]. Moreover, in children with autism, functional connectivity is specifically affected in the theta band [162].

As recently shown in the hippocampal-prefrontal system in a mouse model of schizophrenia, abnormal connectivity was detected very early in development before cognitive deficits were apparent [163]. In a similar vein, the current findings suggest that impaired functional connectivity in the rubro-hippocampal network may predict and contribute to sensorimotor deficits; such impairments could be caused by a number of factors, including sleep disruption. Accordingly, further research into the oscillatory dynamics and state-dependent modulation of

forebrain-brainstem networks has the potential to reveal common neural processes underlying the emergence of the cognitive and sensorimotor deficits of neurodevelopmental disorders.

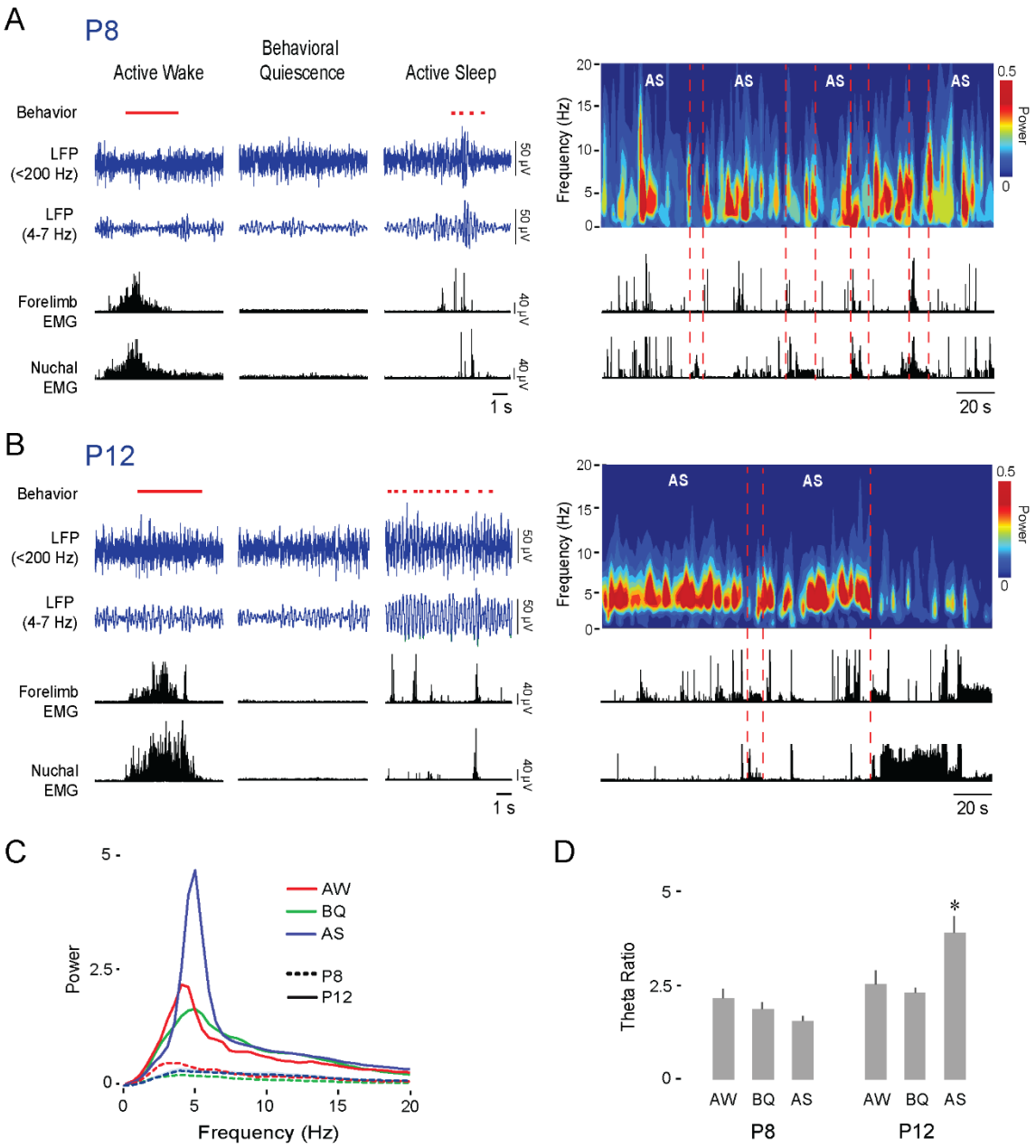


**Figure 8. The infant RN exhibits AS-dependent theta oscillations.** (A) Left: Representative data in a P8 rat depicting sleep and wake behavior (wake movements: horizontal red line; twitches: red ticks; manually scored), RN LFP (blue traces), and forelimb and nuchal EMGs (black traces) across behavioral states. Right: Representative time-frequency spectrogram and associated EMG

activity at P8 as pup cycles in and out of AS. (B) Same as in (A) but at P12. (C) Mean power spectra of LFP activity in the RN of P8 (11 pups, dashed lines) and P12 (n = 11 pups, continuous lines) rats during AW (red), BQ (green), and AS (blue). (D) Mean (+ SE) theta ratio for P8 and P12 rats during AW, BQ, and AS. Asterisk indicates significant difference from other behavioral states at P12, $p < 0.002$.

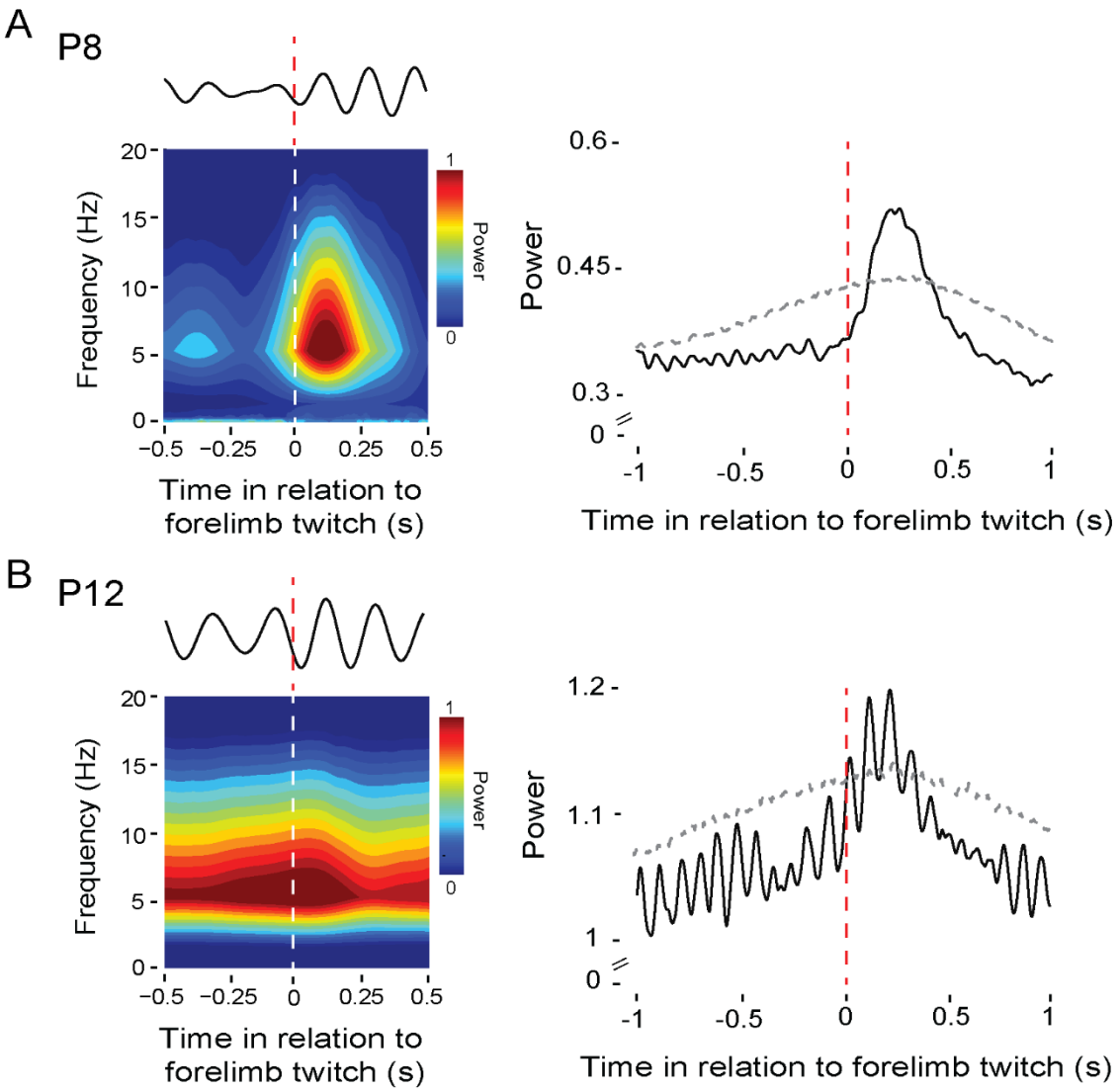


**Figure 9. Myoclonic twitches trigger theta oscillations in the RN.** (A) Left: Twitch-triggered time-frequency spectrogram for a representative P8 rat (108 forelimb twitches). Above the spectrogram is a representative LFP signal (4-7 Hz) from the same pup in response to a single forelimb twitch. Right: Mean twitch-triggered LFP power (4-7 Hz, root mean square) pooled across subjects (11 pups; 2,292 forelimb twitches). Horizontal dashed line denotes upper acceptance band, $p < 0.01$. (B) Left: Same as in (A) but at P12 (147 forelimb twitches). Right: Same as in (A) but at P12 (11 pups; 1,054 forelimb twitches).

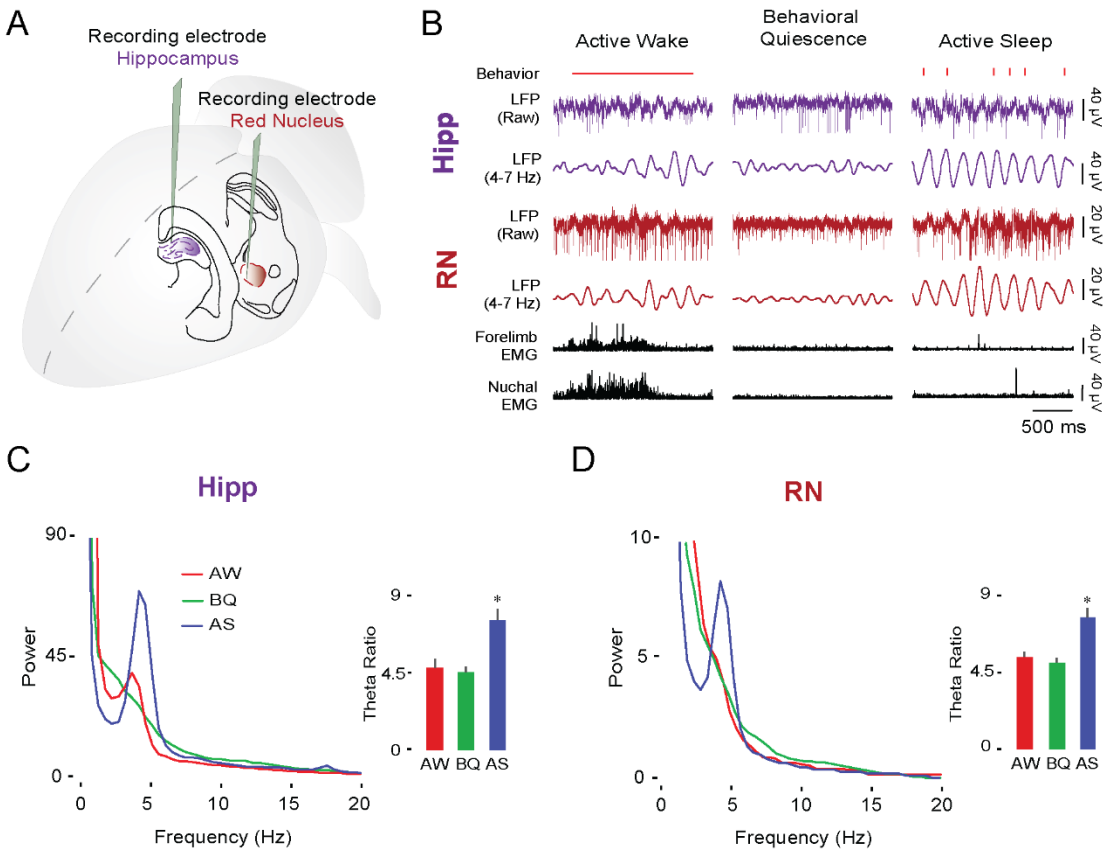


**Figure 10. The hippocampus and RN exhibit similar state-dependent theta activity at P12.** (A) Illustration depicting electrode placements in the dorsal hippocampus and RN. (B) Representative data from a P12 rat showing sleep and wake behavior (wake movements: horizontal red line; twitches: red ticks; manually scored), simultaneously recorded LFP activity in the hippocampus (purple traces) and RN (red traces), and forelimb and nuchal EMGs (black traces) across behavioral states. (C) Mean LFP power spectra and mean (+ SE) theta ratios in the hippocampus at P12 (19 pups) during AW (red), BQ (green), and AS (blue). * significant difference from other behavioral states, $p < 0.001$. (D) Same as in (C) but for RN. See also Figure S2 and Figure S3.

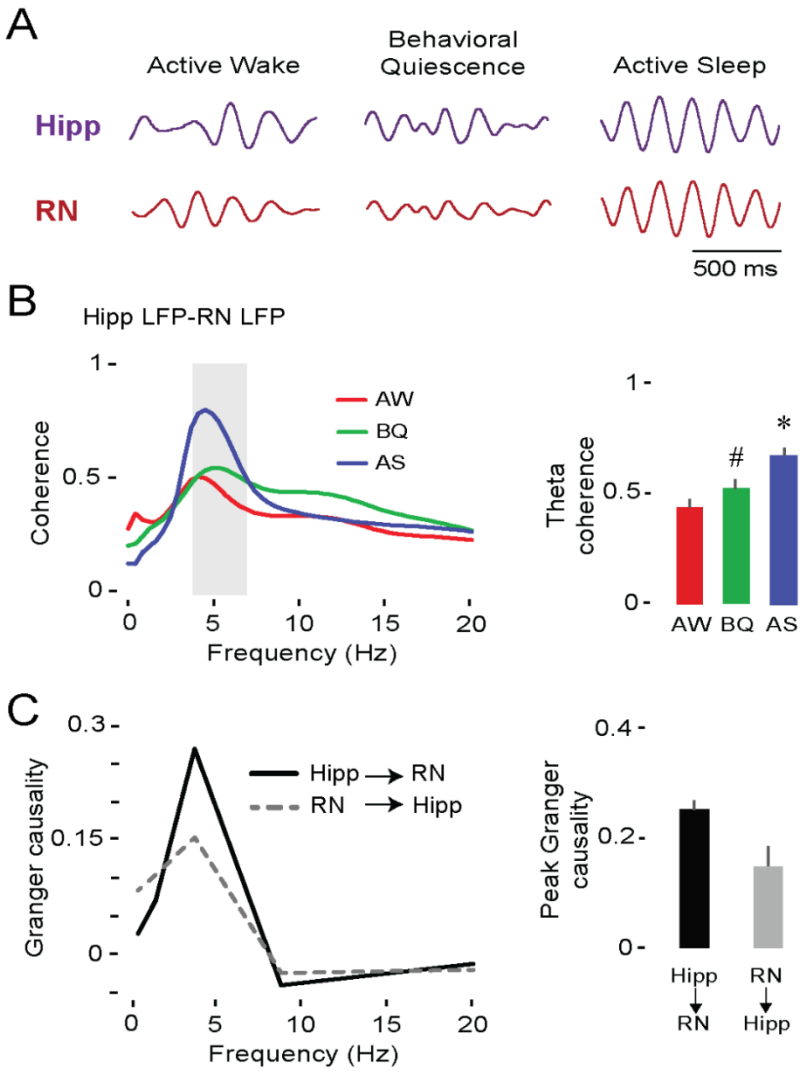


**Figure 11. Theta oscillations in the hippocampus and RN at P12 are coherent and mutually interactive during AS.** (A) Representative theta-filtered LFPs (4-7 Hz) in the hippocampus (purple trace) and RN (red trace) in a P12 rat across behavioral states. (B) Left: Mean LFP-LFP coherence spectra between hippocampus and RN (19 pups, 19 LFP pairs) during AW (red), BQ (green), and AS (blue). Shaded gray area indicates theta-frequency range. Right: Mean (+ SE) theta coherence across behavioral states. * significant difference from AW and BQ, $p < 0.001$. Hashtag indicates significant difference from AW, $p < 0.05$. (C) Left: Mean Granger causality spectra for pups exhibiting significant bidirectional interactions between hippocampus and RN ($p < 0.01$; 9 pups, 9 LFP pairs). Right: Mean (+ SE) peak Granger causality value within theta-frequency range (9 pups, 9 LFP pairs). See also Figure S4.

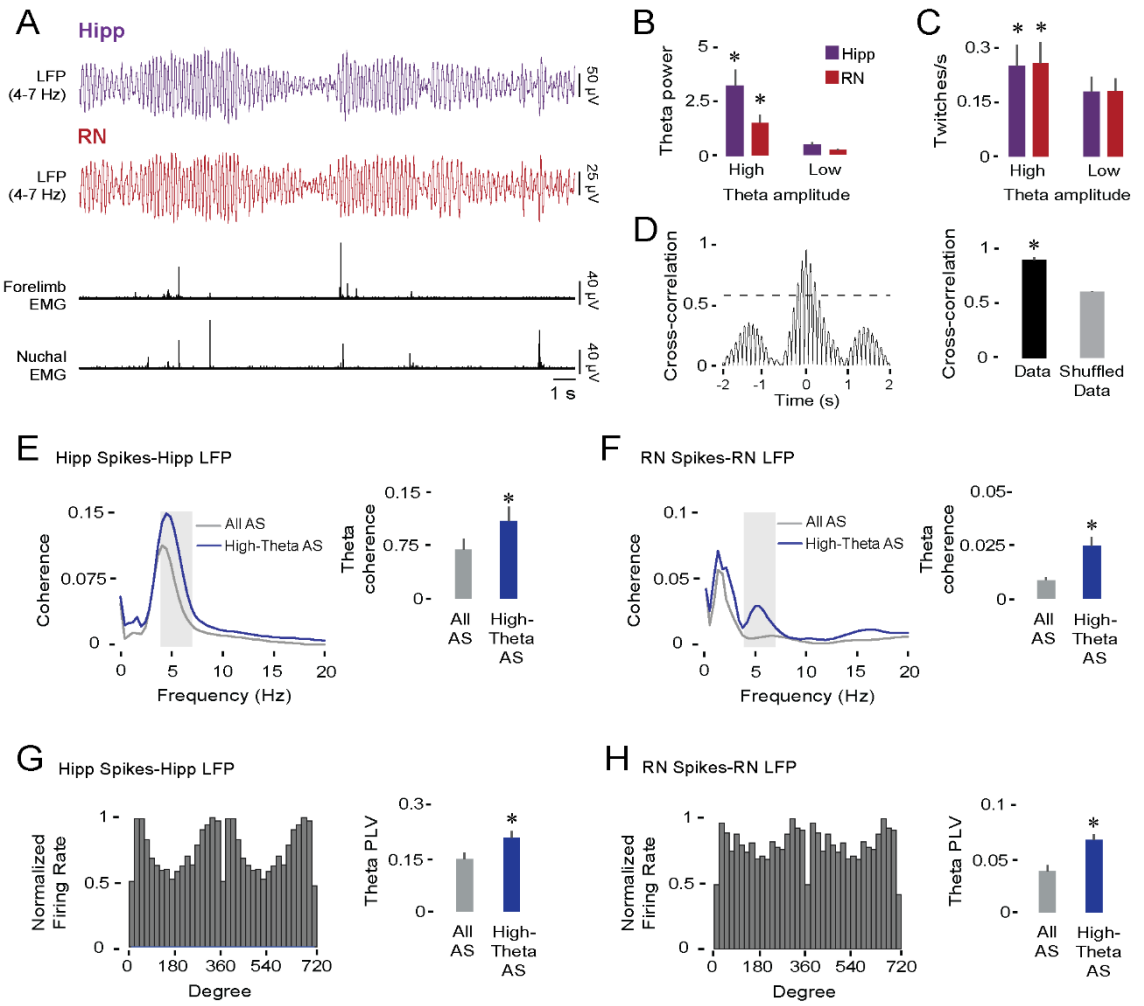


**Figure 12. Comodulation of theta in the hippocampus and RN during AS at P12.** (A) Representative data in a P12 rat depicting simultaneously recorded theta-filtered LFPs (4-7 Hz) in the hippocampus (purple trace) and RN (red trace), and forelimb and nuchal EMGs (black traces). (B) Mean (+ SE) theta power in the hippocampus (purple bars) and RN (red bars) during periods of high- and low-amplitude theta (19 pups). * significant difference from low-amplitude theta values, $p < 0.001$. (C) Same as in (B) but for twitching rate. (D) Left: Representative cross-correlogram between theta-filtered LFPs in the hippocampus and RN of a P12 rat. Dashed line denotes threshold for statistical significance, $p < .01$. Right: Mean (+

SE) LFP cross-correlation coefficients between hippocampus and RN for actual and shuffled data (19 pups, 19 LFP pairs). * significant difference, $p < 0.001$. (E) Left: Averaged hippocampal spike-LFP coherence spectra during entire periods of AS (gray line) and periods of AS with high-amplitude theta (blue line; 27 spike-LFP pairs). Shaded gray area indicates theta-frequency range. Right: Mean (+ SE) spike-LFP coherence within the theta-frequency range. * significant difference, $p < 0.004$. (F) Same as in (E) but for RN spike-LFP coherence (27 spike-LFP pairs). (G) Left: Representative example of significant phase-locked spiking activity in the hippocampus. Right: Mean phase-locking values within the theta-frequency range during entire periods of AS (gray bar) and periods of AS with high-amplitude theta (blue bar; 27 spike-LFP pairs). * significant difference, $p < 0.005$. (H) Same as in (G) but for RN phase-locking (36 spike-LFP pairs). See also Figure S1 and Figure S4.

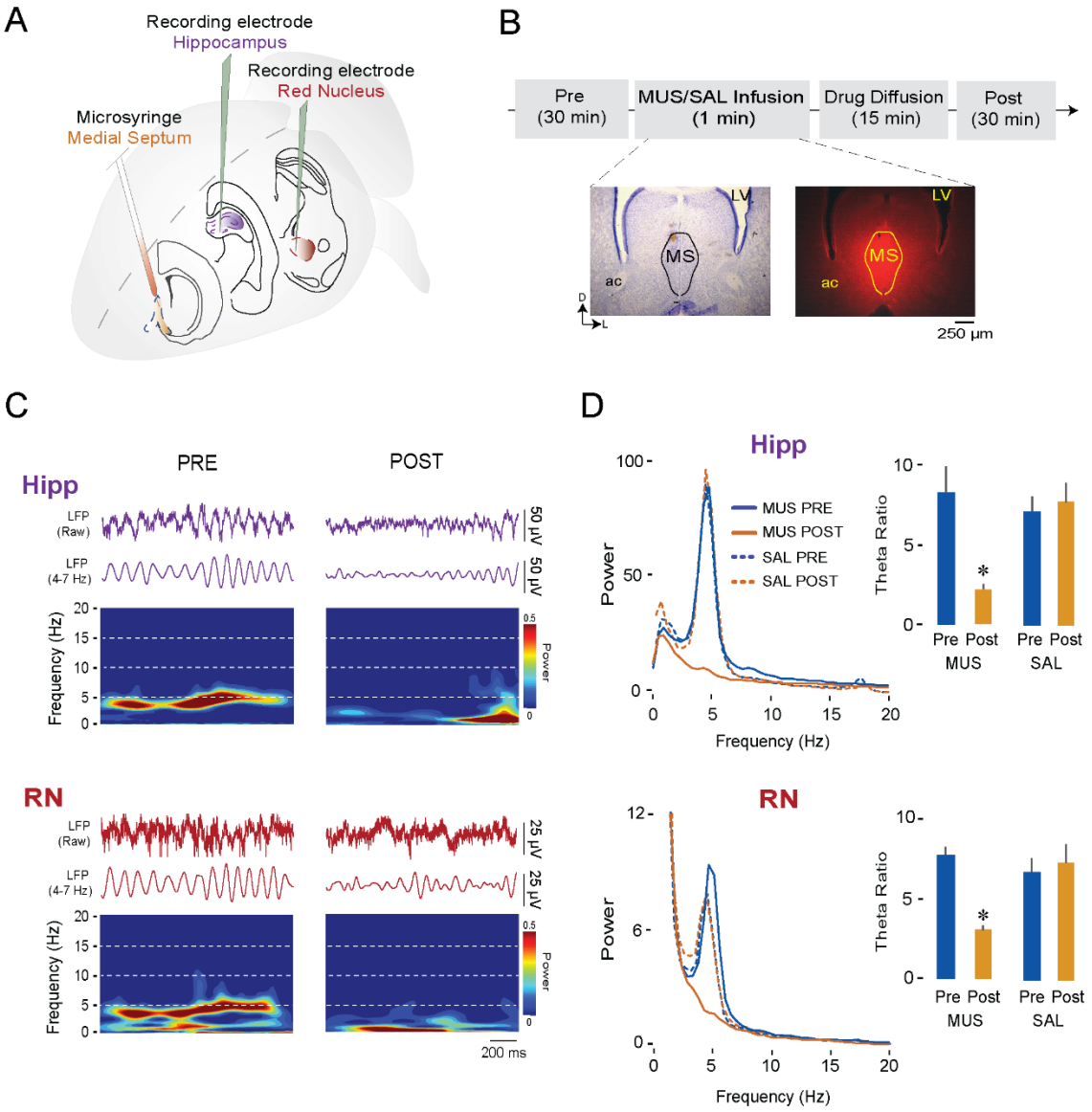


**Figure 13. Pharmacological inactivation of the medial septum (MS) blocks theta oscillations in both the hippocampus and RN at P12.** (A) Illustration depicting electrode placements in the hippocampus and RN and microsyringe placement in the MS. (B) Experimental timeline and representative coronal Nissl-stained brain section (left) and corresponding section showing diffusion of fluorescent muscimol in the MS (right). LV = lateral ventricle; ac = anterior commissure. (C) Representative dual LFP recordings during AS in a P12 rat from the hippocampus (purple traces) and RN (red traces) and corresponding time-frequency spectrograms. (D) Left: Averaged LFP power spectra during AS in the

hippocampus (top) and RN (bottom) before (Pre) and after (Post) infusion of either muscimol (MUS; 6 pups) or saline (SAL; 6 pups) into the MS. Right: Mean (+ SE) theta ratios during AS in the hippocampus (top) and RN (bottom) before and after infusion of muscimol or saline into the MS. Asterisks indicate significant difference from Pre, $p < 0.02$. See also Figure S3, Figure S4, and Table 1.

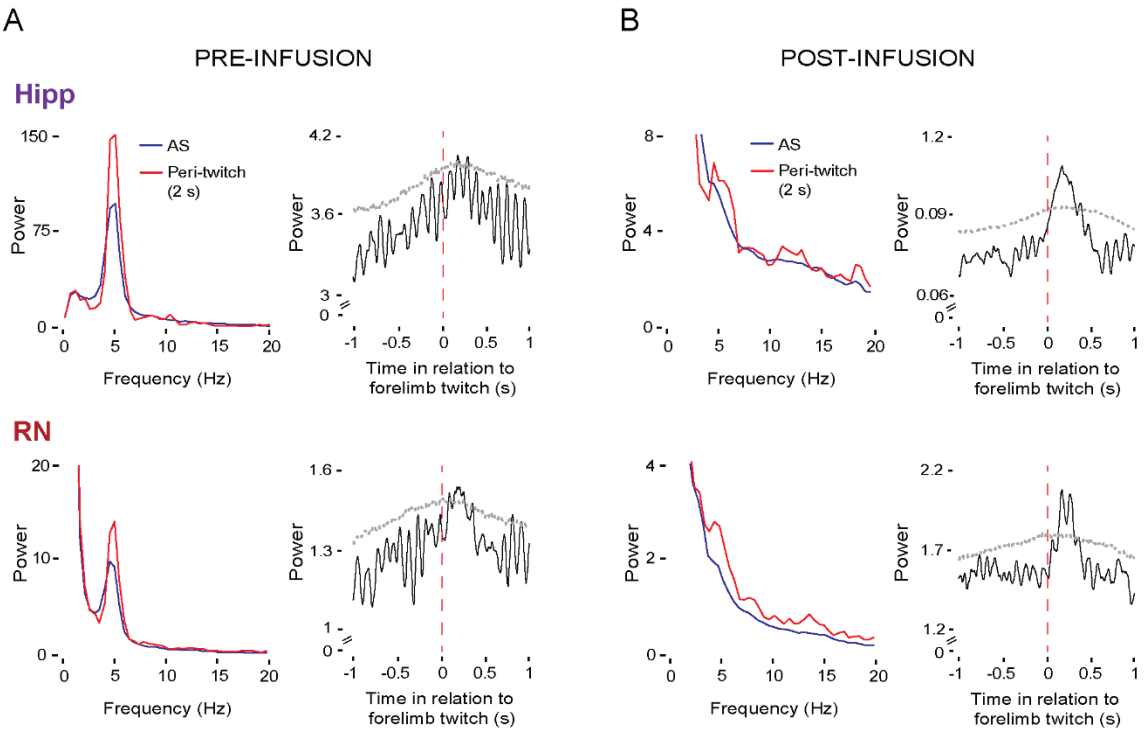


**Figure 14. Twitch-triggered theta oscillations are preserved in the hippocampus and RN after pharmacological inactivation of the medial septum (MS) at P12.** (A) Left: Averaged LFP power spectra in the hippocampus (top) and RN (bottom) across periods of AS (blue lines) and periods around twitches (red lines) across P12 subjects (6 pups) before infusion of muscimol into the MS. Right: Mean twitch-triggered LFP power (4-7 Hz, root mean square) for the hippocampus (top) and RN (bottom) pooled across subjects (6 pups; 256 forelimb twitches). Horizontal dashed lines denote upper acceptance bands, $p < 0.05$. (B) Same as in (A) but after infusion of muscimol into the MS. Data for mean twitch-triggered LFP power are from 305 forelimb twitches pooled across six pups. See also Figure S4.

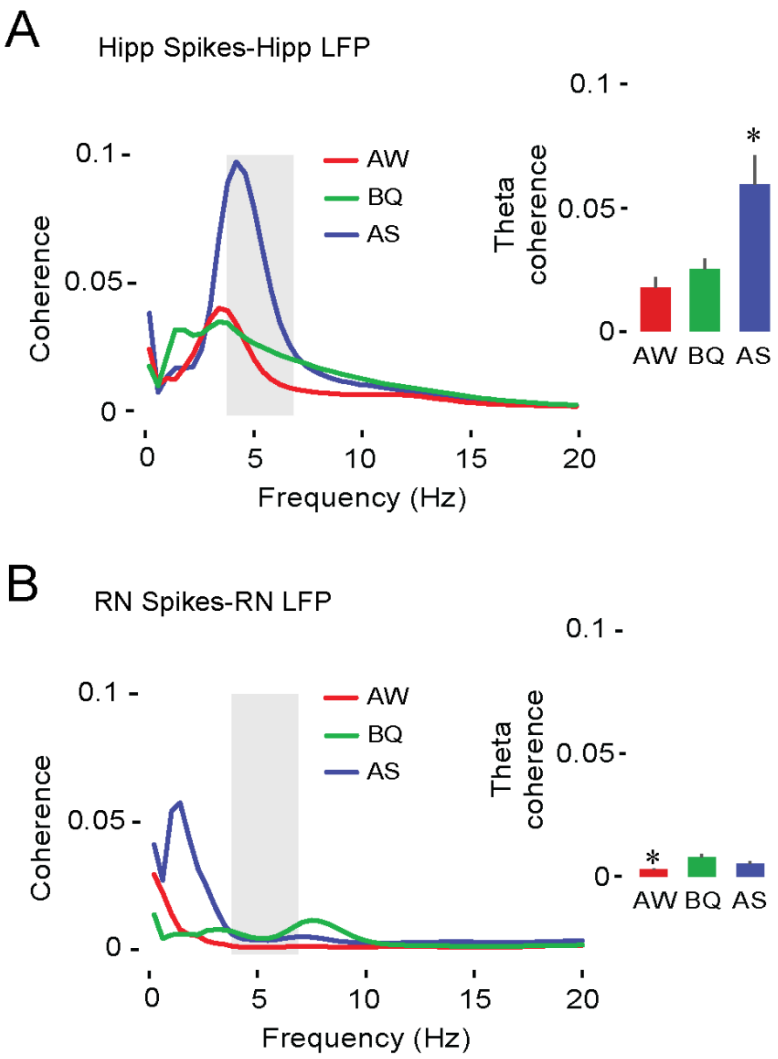


**Figure S1. State-dependent spike-LFP coherence in the hippocampus and RN at P12.** (A) Left: Averaged hippocampal spike-LFP coherence spectra during periods of AW (red), BQ (green), and AS (blue; 34 spike-LFP pairs). Shaded gray area denotes the theta-frequency range (4-7 Hz). Right: Mean (+ SE) spike-LFP coherence within the theta-frequency range. * significant difference from other behavioral states, $p < 0.004$. (B) Same as in (A) but for RN spike-LFP coherence spectra (59 spike-LFP pairs). * significant difference from other behavioral states, $p < 0.05$.

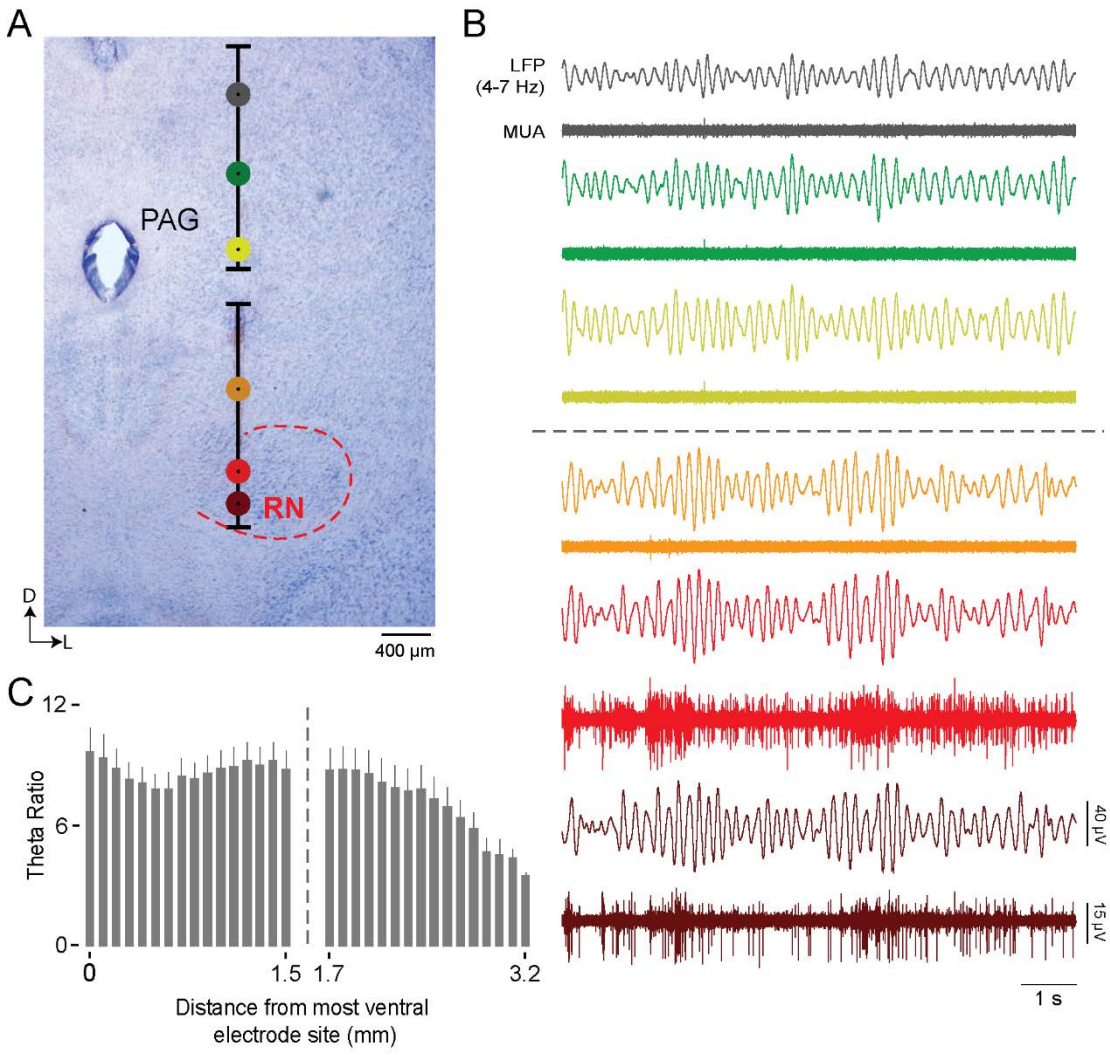


**Figure S2. Theta power during AS decreases with distance from the RN.** (A) Nissl-stained coronal section depicting reconstruction of two placements of the same electrode (black bars) within a single recording session in a P12 rat. Recording sites are color-coded. (B) Representative theta-filtered LFPs (4-7 Hz) and MUA (500-5000 Hz) associated by color with the electrode placements in (A). Dashed line separates two independent recordings in the same pup. (C) Mean theta ratios (n=5 subjects) calculated across AS periods for each of 16 recording sites at two adjacent electrode locations within and dorsal to the RN.

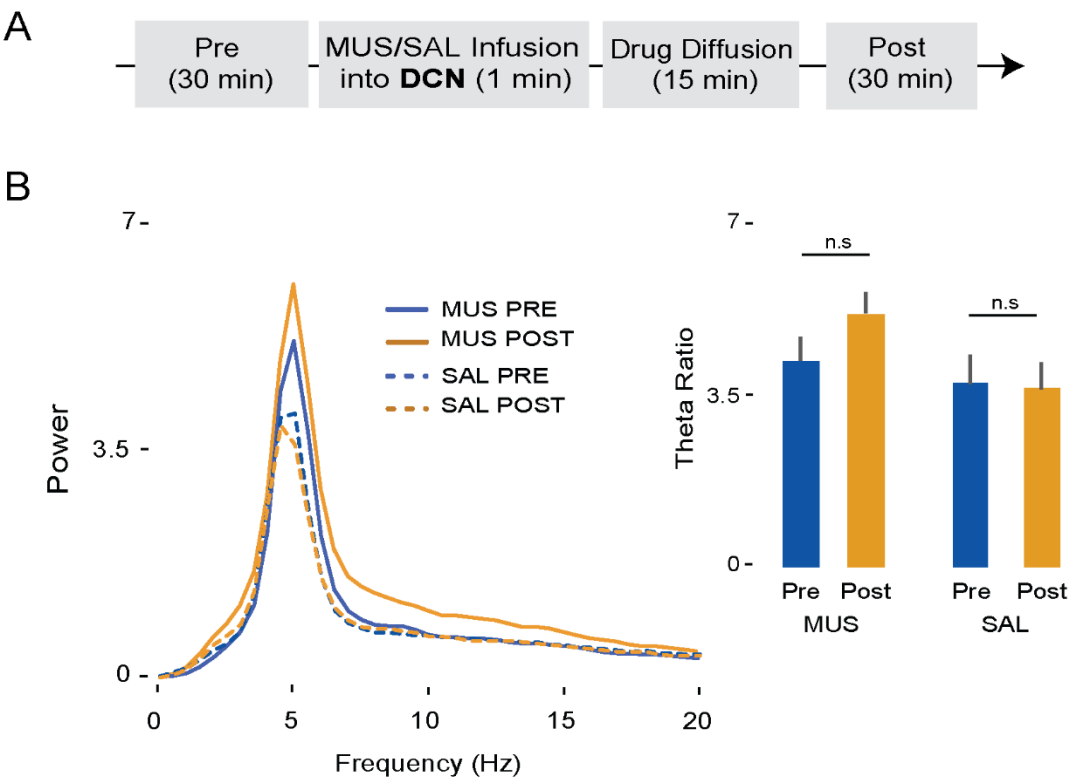


**Figure S3. Pharmacological inactivation of the deep cerebellar nuclei (DCN) does not affect theta oscillations in the RN at P12**. (A) Experimental timeline for the infusion of muscimol (MUS) or saline (SAL) into the DCN and subsequent RN recording. (B) Left: Averaged LFP power spectra during AS in the RN before (Pre) and after (Post) infusion of either muscimol (6 pups) or saline (6 pups) into the DCN. Right: Mean (+ SE) theta ratios during AS before and after infusion of muscimol or saline into the DCN. n.s = not significant.

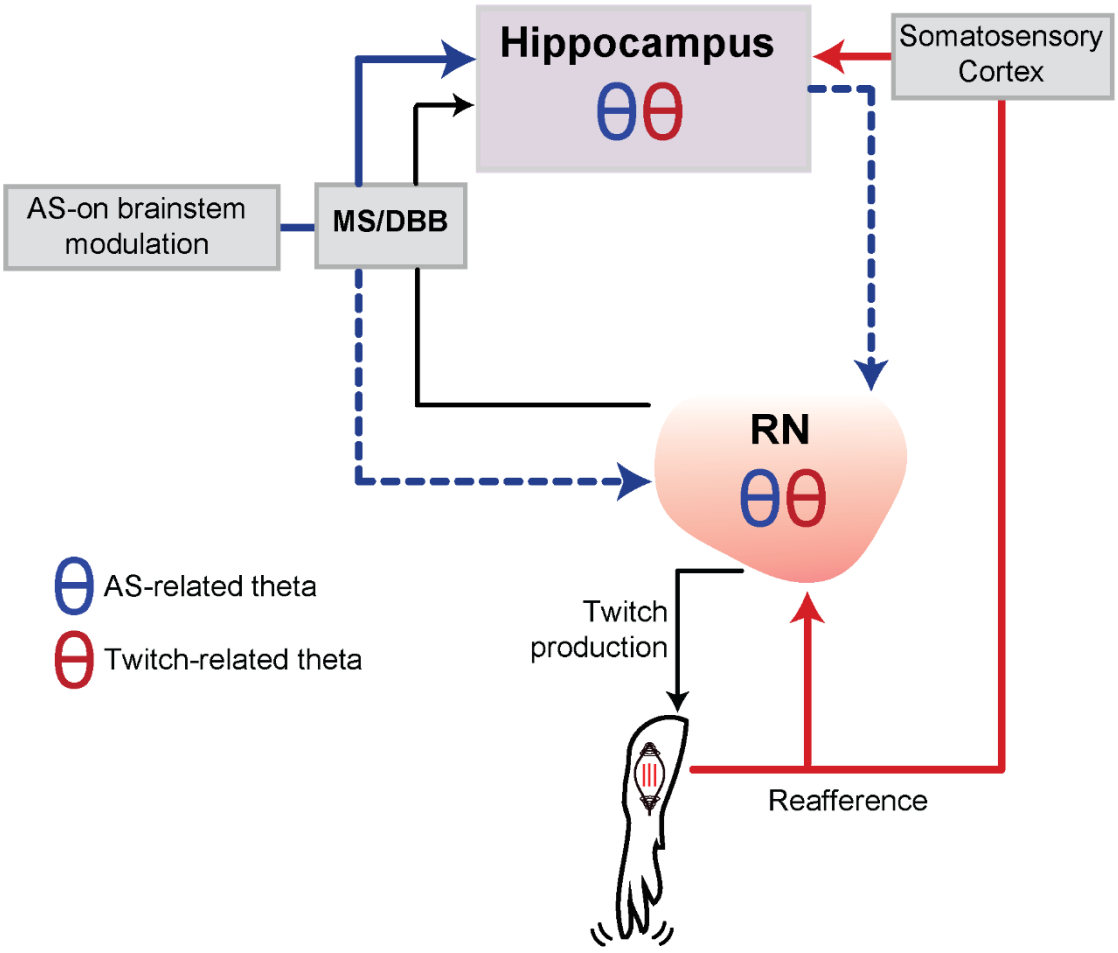


**Figure S4. Diagram illustrating possible pathways involved in the production of AS- and twitch-related theta oscillations in the hippocampus and RN.** The figure distinguishes between continuous AS-related theta (blue) and discontinuous twitch-triggered theta (red). Dotted lines denote more complex pathways that have yet to be fully characterized. See text for discussion.

| | MUSCIMOL | | SALINE | |
|---|---|---|---|---|
| | **Pre** | **Post** | **Pre** | **Post** |
| **Time (s) in active sleep** | | | | |
| | 360 (±78) | 463.9 (±68) | 376 (±127) | 433.6 (±175) |
| **Twitching rates (twitches/s)** | | | | |
| **Nuchal** | 0.2 (±0.04) | 0.15 (±0.02) | 0.16 (±0.01) | 0.18 (±0.02) |
| **Forelimb** | 0.1 (±0.02) | 0.11 (±0.01) | 0.1 (±0.02) | 0.1 (±0.03) |

**Table 1. Medial septum inactivation does not affect active sleep times or twitching rates in P12 rats.** Mean total time spent in active sleep and twitching rates in the forelimb and nuchal muscles before (Pre) and after (Post) infusion of muscimol or saline into the medial septum in P12 rats. Each recording session lasted 30 min. Values are mean (±SE).

# CHAPTER 4: ACTIVE SLEEP PROMOTES FUNCTIONAL CONNECTIVITY IN DEVELOPING SENSORIMOTOR NETWORKS

Complex behavioral and cognitive skills are supported by precisely timed interactions between distant neural networks. These long-range interactions depend on the temporal coupling of neural oscillations, or brain rhythms [75,142]. Neural oscillations are the result of synchronized activity within large populations of neurons and exhibit specific spatiotemporal features depending on brain area, behavioral state, and age.

The functional roles of neural oscillations have been predominantly examined in the adult forebrain, although brain rhythms are present throughout the neuraxis and emerge in early development [15,23,64,71–73,81,104,164–170]. In the cerebral cortex of humans and rodents, the earliest neural activity is characterized by the presence of brief oscillatory bursts interposed with periods of silence; this pattern of fragmented activity is referred to as *discontinuous*. Although different from the continuous oscillatory patterns of adults, these early oscillations appear to have important functions for the development of the nervous system [64–67]. In addition, temporal coupling or coactivation of brief oscillatory events is indicative of connectivity among functionally related neural structures [64,71–73,171].

Early oscillatory dynamics in rats have often been described using *in vitro* preparations or under anesthetic conditions *in vivo* that preclude the normal expression of sleep-wake cycles. Based on such studies, one might conclude that

the expression of brain rhythms is independent of experience or behavioral state. Within the developing sensorimotor system, however, early neural oscillations are largely triggered by sensory input arising from external stimulation (*exafference*) or sensory feedback arising from self-generated movements (*reafference*) [13,73].

The opportunities for reafferent stimulation in the developing sensorimotor system are not restricted to periods of wakefulness. In the perinatal period when sleep is the predominant behavioral state, myoclonic twitching during active sleep is one of the most abundant of all behaviors [1–3]. Twitches are brief, discrete jerky movements that occur against a background of muscle atonia and are generated by brainstem motor structures, including the red nucleus [38,47]. Unlike wake-related movements, twitches are ideally suited for the efficient transmission of peripheral sensory feedback and provide a major source of neural activation to the infant's plastic brain (for review, see [79,102]). Moreover, sensory feedback from twitches reliably triggers synchronized neural oscillations across the neuraxis, suggesting that these oscillations also contribute to the development of long-range network connectivity. More broadly, independently of twitching, active sleep may provide a context that promotes functional connectivity in the sensorimotor system including, as shown in Chapter 3 in 12-day-old rats, highly synchronized oscillatory activity between the hippocampus and red nucleus [73].

These and other findings regarding active sleep and the early expression of coupled oscillatory activity have important methodological and clinical implications. From a methodological perspective, any testing condition (e.g., anesthesia) that interferes with the normal expression of sleep-wake cycles will also interfere with

the normal expression of oscillatory activity. From a clinical standpoint, disruption or deprivation of active sleep in early infancy is likely to interfere with the typical development of network interactions in the sensorimotor system; indeed, prolonged disruptions of perinatal sleep may help to explain the sensorimotor deficits that characterize such neurodevelopmental disorders as autism and schizophrenia.

**Synchronized oscillations orchestrate the development of neuronal networks**

Early oscillatory activity *in vivo* has been most extensively—but not exclusively [15,73]—described in the cortex and hippocampus [23,64,71,72,81,131,164,166–168,170,172,173]. In these forebrain structures, fragmented oscillatory activity is thought to assist in the development of local neuronal networks, with effects on synapse formation, neuronal differentiation and migration, programmed cell death (apoptosis), and formation and refinement of topographic maps [64–70].

During the first postnatal week in rats, sensory feedback from whiskers drives two distinct oscillatory patterns of activity in the whisker “barrel” cortex: spindle bursts (5-30 Hz with components in the theta, alpha, and beta bands) and early gamma oscillations (EGOs; 30-50 Hz) [167,174]. Both spindle bursts and EGOs originate in cortical layer 4 and are highly dependent on thalamic input. Between birth and 3 days of age, spindle bursts and EGOs are both enabled by gap junctions; by the end of the first postnatal week, such oscillatory patterns are primarily generated by glutamatergic currents and involve the recruitment of

cortical interneurons. In the hippocampus by the end of the first postnatal week, brief oscillatory events at theta (4-14 Hz) and gamma (~20-100 Hz) frequencies become apparent [23,168], likely reflecting the proliferation of hippocampal interneurons [132]. In addition, the emergence of theta oscillations reflects the strengthening of cholinergic and GABAergic projections from the medial septum[133].

Perhaps the most direct, causal evidence for a role of oscillations in brain development comes from studies assessing their involvement in apoptosis [65,69]. Apoptosis is the physiological process through which neurons and other cells die. This death is a normal process that complements the over-production of neurons that characterizes early development; accordingly, apoptosis is a key contributor to the anatomical and functional development of the nervous system [175]. Notably, in rat pups, oscillatory activity appears to determine the rate of apoptosis in sensorimotor cortex [65]. Specifically, area-specific levels of neuronal activity inversely correlate with the number of apoptotic neurons detected in local networks. Importantly, selective manipulation of neuronal activity affects the rate of apoptosis in sensory and motor cortices. In support of this finding, the amount of alcohol-induced suppression of early oscillatory bursts correlates with the amount of apoptosis detected in somatosensory cortex [69]. These findings demonstrate that alteration of oscillatory activity in early development is detrimental to typical cortical development and can mediate the detrimental effects associated with early exposure to teratogens. These findings may have translational value: In premature human infants, the amount of early oscillatory

cortical activity correlates with subsequent brain growth [176] and later mental development [177].

As noted above, most of our knowledge about early brain oscillations *in vivo* comes from studies that have not examined oscillatory dynamics across the sleep-wake cycle. When behavioral state is taken into consideration, it is evident that neural oscillations in the developing sensorimotor system are predominantly expressed during active sleep [23,73,81,173].

**Spontaneous motor activity during active sleep drives early oscillatory activity within local cortical and subcortical sensorimotor networks**

Rodents rely heavily on the whisker system to navigate and explore their world [178]. For this reason, the whisker system has proven extremely valuable for understanding how complex sensorimotor systems develop [17,179]. In rat pups, deprivation of whisker-related sensory experience during sensitive periods—including the first postnatal week—disrupts anatomical and functional development of whisker-related brain areas, including somatosensory cortex [10–12]. Such studies demonstrate how typical development of this system relies heavily on sensory experience.

In developing brain areas that process whisker-related sensory information (such as the ventral posterolateral thalamus and barrel cortex), twitching of the whiskers during active sleep is a prominent source of sensory experience [17]. Sensory feedback from twitching elsewhere in the body, such as the limbs, drives

neural activity in somatotopically related brain areas (i.e., areas that specifically map to parts of the body; see Table 2 and Figure 1). In rat pups through the first two postnatal weeks, twitches drive oscillatory events with distinct spatiotemporal features depending on the brain area. For example, in the newborn rat sensorimotor cortex, twitch-related reafference triggers spindle bursts [19,81,104]. Spindle bursts are thought to contribute to the anatomical and functional development of the cortex [68,174,180,181]. Although spindle bursts can be generated endogenously, their occurrence decreases threefold (i.e., only ~30% of spindles remain) in the absence of peripheral sensory input [104]. Moreover, the occurrence of spindle bursts in intact rat pups is markedly higher during periods of twitching in relation to wakefulness [19,81]. In the neonatal rat hippocampus, periods of twitching are also associated with the emergence and maximal expression of two prominent rhythms that synchronize hippocampal networks: theta and gamma [23,73,173]. All together, these results highlight the contribution of active sleep and twitch-related sensory feedback to the generation of early oscillatory activity within local circuits in the neonatal cortex and hippocampus.

As illustrated in Table 2, the role of twitch-related sensory feedback in the generation of brain rhythms is not restricted to cortical and hippocampal circuits. Using rat pups, we showed that the red nucleus, a brainstem structure that plays an important role in the production of infant motor behavior [47], exhibits theta oscillations predominantly during active sleep [73]. Indeed, in 8-day-old rats, brief, discontinuous theta oscillations were most prominently associated with twitches. Just four days later, theta oscillations in the red nucleus were expressed

continuously during active sleep while also exhibiting enhanced amplitude during periods of twitching. The discovery of state-dependent theta oscillations in the developing brainstem raises a host of new questions. For example, do oscillations play a similar developmental role in the brainstem as they do in the forebrain? What are the mechanisms that promote sleep-dependent oscillations in the brainstem? What cognitive and behavioral functions are supported by oscillatory coupling between brainstem and forebrain areas? These and other questions can be answered now that we have overcome the technical barriers to recording brain activity in the neonatal brainstem [115].

**Oscillations during active sleep promote neuronal synchrony across distant sensorimotor structures in early development**

So far, we have discussed the role of twitching during active sleep in the generation of early oscillatory activity *within* local sensorimotor networks. In addition, coupled oscillatory activity *across* neuronal structures is a hallmark of long-range functional connectivity in both the infant and adult nervous system [71–75]. In the developing prefrontal-hippocampal network, for instance, synchronized oscillatory activity in the ventral hippocampus drives oscillatory activity in prefrontal cortex [71]. Because twitches drive precisely timed oscillatory activity across the neuraxis, including the hippocampus (Figure 1), twitching may optimize the probability of early synchronization of sensorimotor networks during active sleep. Indeed, even within the neonatal spinal cord, reafference from spontaneous self-generated movements (including wake-related movements and twitches) coordinates

neuronal activity between motor and sensory zones [15,16]. Dorsal rhizotomy, which prevents sensory input to the spinal cord, uncouples this neural activity, thus demonstrating a role for early sensory feedback in neuronal synchrony in intrasegmental spinal circuits [15]. Such disruptions of spinal processing can have functional consequences; for example, genetically altered newborn mice that lack muscle spindles—which provide proprioceptive input to the spinal cord—fail to develop the monosynaptic stretch reflex [182].

Future research will assess the relative role of twitch-related sensory feedback in the coupling of oscillatory activity in higher-order sensorimotor networks. For example, twitch-related activation of hippocampal circuits depends on sensory input from somatosensory cortex via entorhinal pathways [24]. In support of a role for twitching in promoting such cortico-hippocampal communication, twitching of the whiskers during active sleep specifically promotes oscillatory coupling between barrel cortex and dorsal CA1 in hippocampus [183]. Figure 2 provides a representative example of the oscillatory dynamics in the barrel field and hippocampus of an 8-day-old rat following whisker twitches during active sleep. As shown in Figure 2A, sensory feedback from whisker twitches reliably triggers 20-30 Hz oscillations in both structures. Spectral coherence (a measure of synchrony) across behavioral states reveals enhanced cortico-hippocampal synchrony at 20-30 Hz following twitches but not during active wake (AW) or behavioral quiescence (BQ; Figure 2B).

Independent of twitching, the state of active sleep facilitates the emergence and expression of early functional connectivity in the sensorimotor system. Using

P11-13 rats, we addressed this question by characterizing state-dependent oscillatory coupling between the red nucleus and the hippocampus [73]. When continuous theta oscillations in the red nucleus emerged around P11, they were coherent (i.e., synchronous) and co-modulated (i.e., their amplitudes vary in lockstep) with theta oscillations in the hippocampus. Crucially, synchronization of theta rhythms between the hippocampus and red nucleus occurred almost exclusively during periods of active sleep; twitching enhanced the amplitude of these oscillations. Whereas pharmacological inactivation of the medial septum abolished sleep-dependent theta activity in both structures, twitch-dependent theta was still preserved, suggesting that these two forms of theta arise from two independent pathways. Altogether, these results indicate that active sleep is necessary for the expression of functional connectivity upon the emergence of continuous oscillatory activity in networks involving both forebrain and brainstem structures.

**State-dependent functional connectivity and the origins of neurodevelopmental disorders**

Aberrant network connectivity can be detected very early in development and appears to presage cognitive and sensorimotor impairments [184]. In humans, atypical connectivity patterns are present in individuals diagnosed with ADHD [157], autism [156], and schizophrenia [155].

Importantly, connectivity and neural synchrony in healthy infants and adults varies across the sleep-wake cycle [73,124,185,186]. Unfortunately, the majority of studies assessing early functional connectivity in neurodevelopmental disorders have not examined state-dependent network interactions. When behavioral state is taken into account, however, it becomes clear that sleep affects the expression of synchronized oscillatory activity in young and adult individuals diagnosed with autism [187,188]. Thus, analyses of state-dependent connectivity may provide novel insights into the etiology and mechanisms underlying a variety of neurocognitive symptoms, and could be used as an early marker for atypical development [189].

**A causal role of active-sleep disruption in atypical development**

Early perturbations to the sensorimotor system, specifically during sensitive periods, can trigger irreversible developmental consequences [10–12]. Given the role of active sleep in brain development, early active-sleep disruption or deprivation can be one such perturbation. Consistent with this idea, sleep deprivation affects synaptic plasticity in such sensorimotor structures as motor cortex [190], hippocampus [29], and cerebellum [191]. In addition, because sensory feedback from twitching is a major source of stimulation to the neonatal brain, active sleep restriction or deprivation can be also conceptualized as a form of sensory deprivation during critical periods for brain development. If active sleep indeed contributes to the early expression of coupled oscillatory activity between distant sensorimotor structures, active-sleep restriction may underlie the

sensorimotor deficits present in a variety of neurodevelopmental disorders. Indeed, decreased active sleep is a prevalent symptom in neurodevelopmental disorders characterized by sensorimotor deficits, including autism, Rett Syndrome, Fragile X Syndrome, Angelman Syndrome, Williams Syndrome, and Down Syndrome [192].

**Conclusions and future directions**

Synchronized neural oscillations are a hallmark of coordinated activity in developing and adult cortical and subcortical networks [64,66,71–75,166]. We have reviewed evidence here that one of the functions of active sleep in early infancy is to facilitate the expression of neuronal oscillations and oscillatory coupling in the sensorimotor system. Specifically, the evidence thus far indicates that sensory feedback from sleep-related twitches drives precisely timed oscillatory activity across the sensorimotor system, thereby contributing to that system's activity-dependent development.

Until now, the importance of active sleep in development and plasticity has been supported by showing the negative impact of sleep deprivation [8,103]. The methods used to deprive animals of sleep, however, often entail nonspecific side-effects that make it difficult to identify the specific contributions of sleep to developmental outcomes. Also, the motor centers that generate twitching in early development also support wake-related movements [47]; because methods that disable these motor structures affect all motor activity, they cannot distinguish the relative contributions of twitching to brain development. Recent methodological

advances with optogenetics, however, now enable the rapid expression of opsins during the first two postnatal weeks, which allows direct manipulation of neonatal networks with high temporal precision and cell specificity [193,194]. In addition, as recently demonstrated in adult mice [153], optogenetics can be used to selectively manipulate active-sleep-dependent oscillations and assess their specific roles in behavior and cognition. Accordingly, it may soon be possible to selectively enhance or block sensory input and motor output to evaluate the role of twitch-related reafference in the activity-dependent development of sensorimotor structures.

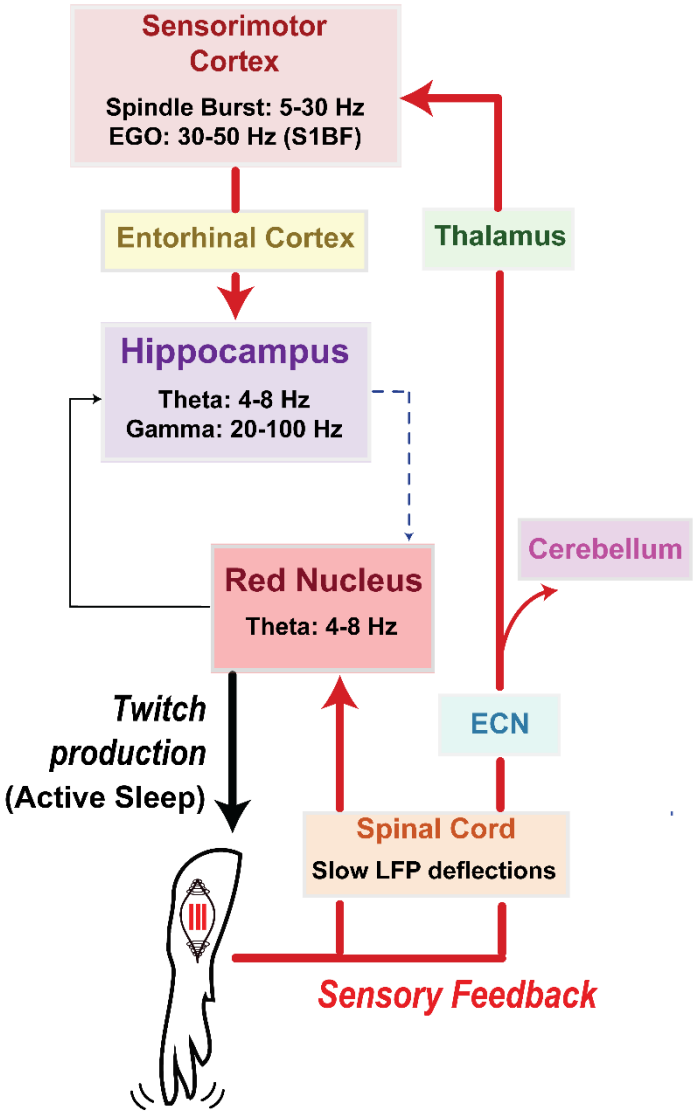


**Figure 15. Diagram illustrating anatomical pathways conveying twitch-related sensory feedback in neonatal rats.** A twitch of the forelimb is generated in the red nucleus during active sleep. Sensory feedback (or reafference) from the twitch causes a cascade of precisely timed neural responses in sensorimotor structures across the neuraxis, including spinal cord, red nucleus, sensorimotor cortex, and hippocampus. Through repeated activation of these structures, twitches provide a unique opportunity for the synchronization of oscillatory activity. See text for further discussion.

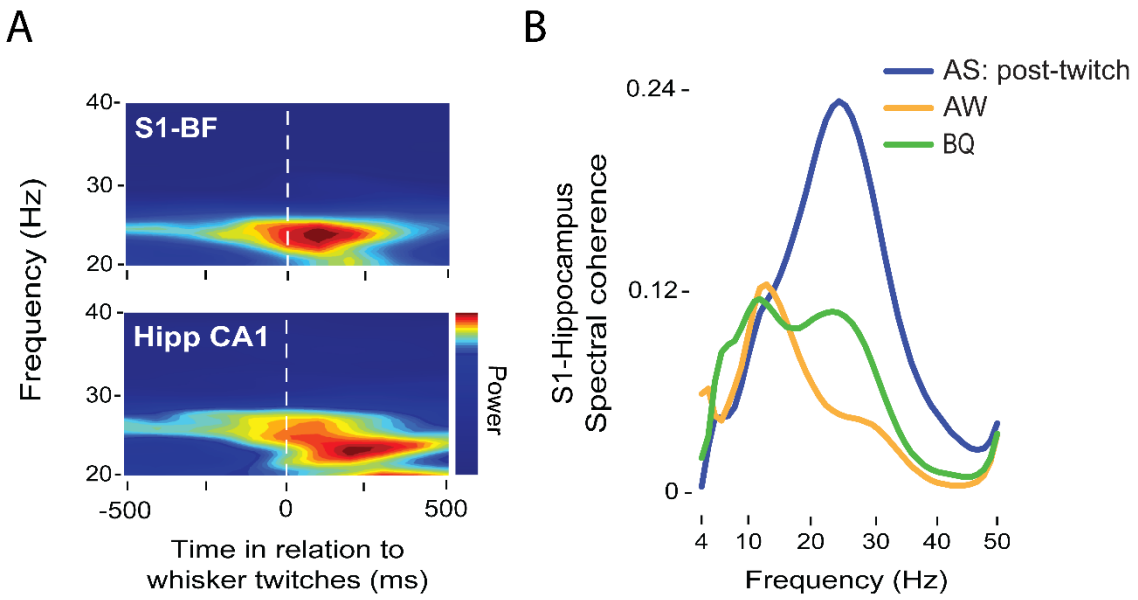


**Figure 16. Twitches during active sleep promote coherent oscillations in developing sensorimotor networks.** A: Representative twitch-triggered time-frequency spectrogram in the barrel field of somatosensory cortex (S1-BF, top) and hippocampal CA1 (Hipp CA1, bottom) of an 8-day-old rat. Note the increase in power at ~25 Hz in both structures after twitch onset. B: Representative coherence spectra between S1-BF and Hipp CA1 following twitches during active sleep (restricted to the 500-ms period after twitch onset; blue), active wake (AW; orange), and behavioral quiescence (BQ; green).

| Area | Species | Age | MUA | Oscillatory Events (LFP/EEG) | | Refs. |
|---|---|---|---|---|---|---|
| | | | | Event Features | Description | |
| ***Cortex*** | | | | | | |
| **Somatosensory cortex** | Rat | P1-12 | Twitch-following Somatotopic | Spindle Burst ~5-30 Hz 0.1-3 s. | Twitch-following Somatotopic | [19–22,24,81,169] |
| | Human | PCA 29-31 | N/A | Delta Brush ~8-25 Hz 1-2 s. | Twitch-following Somatotopic | [195] |
| **Primary motor cortex** | Rat | P4-12 | Twitch-following Somatotopic AS-On | Spindle Burst ~5-30 Hz | Twitch-following Somatotopic AS-On | [81,196] |
| | | | | Gamma oscillation ~30-40 Hz 0.1-0.3 s. | Twitch-following | [196] |
| ***Hippocampus*** | | | | | | |
| **CA1** | Rat | P1-9 | Twitch-following Twitch-active AS-On | Theta oscillation (>P7) ~4-14 Hz | Twitch-following Twitch-active | [23,24] |
| | | | | Gamma oscillation ~ 20-100 Hz | Twitch-active | |
| | | P11-13 | | Theta (continuous) ~4-14 Hz; 4-7 Hz | Twitch-following Twitch-active AS-On | [23,73] |
| **DG** | Rat | P1-12 | Twitch-following Twitch-active AS-On | Theta oscillation ~4-14 Hz | Twitch-following Twitch-active | [23] |
| | | | | Gamma oscillation ~20-100 Hz | Twitch-following Twitch-active | |
| ***Cerebellum*** | | | | | | |
| **Cortex (Purkinje Cell)** | Rat | P4-P12 | Twitch-following AS-On | ? | N/A | [26,27] |
| **Interposed Nucleus** | Rat | P8-13 | Twitch-following Somatotopic | ? | N/A | [25] |
| ***Thalamus*** | | | | | | |
| **Somatosensory** | Rat | P1-8 | Twitch-following Somatotopic | ? | N/A | [81,104] |
| ***Midbrain/Brainstem*** | | | | | | |
| **Red Nucleus** | Rat | P7-9 | Twitch-following Twitch-preceding Somatotopic | Theta oscillation ~4-7 Hz | Twitch-following | [25,47,73] |
| | | P11-13 | " " | Theta (continuous) ~4-7 Hz | Twitch-active Twitch-following AS-On | [73] |
| **External cuneate** | Rat | | Twitch-following Somatotopic AS-On | ? | N/A | [19] |
| **Medulla (Gi, LC)** | Rat | P6-10 | Twitch-active AS-On | ? | N/A | |
| ***Spinal Cord*** | | | | | | |
| | Rat | P5-17 | Twitch-following Twitch-preceding Somatotopic | Negative deflection <1 Hz | Twitch-following Somatotopic | [15,16] |

**Table 2. Twitch-related neural activity in the developing nervous system.** MUA = multi-unit activity; LFP = local field potential; EEG = electroencephalogram; P = postnatal day; PCA = post-conceptional age (in weeks); CA = cornus amonius; DG = dentate gyrus; Gi: nucleus gigantocellularis; LC: locus coeruleus. * this study

also uses voltage-sensitive dye imaging. Twitch-following: neural activity increases immediately after twitch events. Twitch-active: neural activity increases during periods of twitching. Twitch-preceding: neural activity increases immediately before twitch events. AS-On: Neural activity increases during active sleep in relation to other behavioral states. N/A = not applicable.

# CHAPTER 5: SENSORY AND STATE-DEPENDENT CORTICO-HIPPOCAMPAL COMMUNICATION IN NEONATAL RATS

## INTRODUCTION

In Chapter 4, we reviewed the existing evidence supporting the role of twitch-related reafference in the generation of neural oscillations in cortical and subcortical developing networks. Neural oscillations assist in such neurodevelopmental processes as neuronal differentiation and migration, apoptosis, and somatotopic map formation [66–72]. In addition, early functional connectivity is expressed via coupled or synchronized oscillatory activity [64,71–73,171]. Thus, we hypothesized that twitch-related oscillatory activity is not only important for the development of local ensembles, but also affords the opportunity for oscillatory coupling across distant sensorimotor structures, thereby promoting early functional connectivity [197].

In the present study, we test this hypothesis in sensory “barrel” cortex and hippocampus. Previous investigations in rat pups already demonstrated that both sensory cortex (including the barrel cortex) [17,20,198] and hippocampus [23,24,73] exhibit twitch-related responses. Importantly, twitch-related activity in the hippocampus is largely driven by the sensorimotor cortex via entorhinal pathways [24]. These findings indicate that in early development, the cortico-hippocampal ensemble is anatomically connected, and twitches promote the early flow of information within this network. However, the state-dependent oscillatory

dynamics between the developing cortex and hippocampus have remained unknown.

Here we show in week-old rats that, unlike periods of active wakefulness or behavioral quiescence, whisker twitches during active sleep drive oscillatory coupling between barrel cortex and the CA1 area in the hippocampus; this coupling was specifically supported by beta2 (20-30 Hz) oscillations. These findings indicate that twitching during active sleep enables cortico-hippocampal communication in early postnatal development.

## METHODS

*Subjects*

A total of 16 male and female Sprague-Dawley Norway rats (Rattus norvegicus) at P7-9 (hereafter designated as P8) were used. Mothers and litters were housed in standard laboratory cages (48 x 20 x 26 cm). Animals were maintained on a 12:12 light-dark schedule with lights on at 0700 h and with water and food available ad libitum. Litters were culled to eight pups at P3. Littermates were never assigned to the same experimental group. All experiments were conducted in accordance with the National Institutes of Health (NIH) Guide for the Care and Use of Laboratory Animals (NIH Publication No. 80-23) and were approved by the Institutional Animal Care and Use Committee of the University of Iowa.

*Surgery*

The details for the surgical procedures used here were described in Chapter 2. After the initial surgery, small holes were drilled in the skull for later insertion of a recording electrode into the "barrel field" of somatosensory cortex (S1BF; coordinates relative to bregma: AP: −1.5 mm; ML: ±4.5 mm; DV: -0.5 to -0.9 mm; 15° lateral angle) and CA1 region of hippocampus (AP: −2 mm; ML: ±1.5 mm; DV: -2 to -2.5 mm; 15° laterofrontal angle). Two additional holes were drilled, one above the visual cortex (contralateral to the recording sites) for insertion of a ground wire (which was also used as the reference electrode) and a second in frontal cortex for insertion of a thermocouple.

*General Procedure and Neurophysiological Recordings*

The general procedure for neurophysiological recording used here was described in detail in Chapter 3. Neural data were acquired using 16-channel silicon depth electrodes (NeuroNexus, Ann Arbor, MI; A4x4-3mm-100-177) connected to a data acquisition system (Tucker-Davis Technologies). Neural and EMG signals were sampled at 25 kHz and 1 kHz, respectively.

*Spontaneous and Evoked Activity in S1BF and Hippocampus*

Before recording spontaneous activity in S1BF and hippocampus and to confirm electrode placement, we determined whether stimulation of the whiskers yielded consistent S1BF responses. Stimuli consisted of brief 50-ms air puffs (with pressure of 10-15 psi) delivered to the vibrissa contralateral to the neural recording

sites. Air puffs were delivered through a flat-end needle attached to a plastic tube. Stimulus duration and pressure we controlled using a solenoid valve controlled by a pulse stimulator (A-M Systems; Sequim, WA). After sensory responses were confirmed, spontaneous activity in S1BF and hippocampus were recorded for at least 30 min.

*Histology*

After testing, the pup was overdosed with ketamine/xylazine (0.08 mg/g i.p.) and perfused transcardially with phosphate-buffered saline and 4% paraformaldehyde. The brain was sliced coronally at 80 µm using a freezing microtome (Leica Microsystems, Buffalo Grove, IL). Electrode locations and drug diffusion were visualized at 2.5–5X magnification using a fluorescent microscope and digital camera (Leica Microsystems). Following fluorescent photography, cortical sections were stained for cytochrome oxidase (CO), which has been shown in developing rats as young as P5 to reliably delineate primary sensory areas [199]. Briefly, cytochrome c (3mg per 10mL solution), catalase (2 mg per 10mL solution; Sigma-Aldrich) and 3,3'-diaminobenzidine tetrahydrochloride (DAB; 5 mg per 10mL solution; Spectrum) were dissolved in a 1:1 dilution of PB-H2O and distilled water. Sections were developed in well plates on a shaker table at 35-40° C for 3-6 hours. Sections were then washed and mounted.

*Quantification and Statistical Analysis*

All analyses and statistical tests of neural data were performed using custom-written Matlab routines (MathWorks, Natick, MA), Spike2 software (Cambridge Electronic Design), and SPSS (IBM, Armonk, NY). Alpha was set at 0.05 for all analyses, unless otherwise stated. When repeated-measures analysis of variance (ANOVA) was performed, post hoc pairwise comparisons were performed and the Bonferroni correction procedure was applied. Group data are always presented as mean ± standard error (SE).

*Behavioral State*

The assessment of behavioral state was conducted using methods describe in Chapter 3.

*Spike Sorting*

Spike sorting was conducting using the methods already described in Chapter 2.

*State-dependent firing rates*

For each recorded neuron in S1BF or CA1, we determined mean firing rates across behavioral states (AW, AS, BQ). On rare occasions, units were excluded when firing rates exceeded 2.5 times the standard deviation within a behavioral state. Average firing rates for each behavioral state within either structure were pooled across units in all pups. Statistical significance was calculated using repeated-measures ANOVAs with behavioral state as the repeated measure.

*State-Dependent LFP Power Spectrum*

For all LFP-related analyses, one LFP channel from each structure per pup was selected. For all subsequent analyses, LFP signals were down-sampled to 500 kHz and a DC-remove filter (time constant: 1 s) was applied. Selection of the LFP channel was based on electrode placement within S1BF or hippocampus CA1. Power spectra were calculated using a 500-ms Hanning window in Spike2. For time-normalization and subsequent statistical comparisons, the spectral power density values in each bin were divided by the total duration of the file comprising data for each behavioral state. LFP power within each structure was normalized to the maximal power within the 4-50-Hz frequency range across behavioral states. State-dependent differences in LFP power were calculated using repeated-measures ANOVA with power in each frequency range (theta: 4-8 Hz; alpha: 8-13 Hz; beta2: 20-30 Hz; slow gamma: 30-50 Hz) across behavioral states as the repeated measure.

*Twitch-Related Neural Activity*

*Spikes*. For each individual unit recorded from either S1BF or hippocampus, using whisker twitches as trigger events, we generated perievent histograms (10-ms bins, 1-s windows). To test for statistical significance, we jittered twitch events 1,000 times within a 500-ms window using PatternJitter [83,84]. To correct for multiple comparisons, we generated upper and lower acceptance bands for each correlation ($p < 0.01$ for each band; [84]). Units in each structure that crossed the established threshold were pooled for further analysis. Next, firing rates around

twitch events for each unit were normalized to the bin exhibiting the highest firing rate and averaged across all units. For visualization purposes, histograms were smoothed (time constant: 10 ms).

*LFP*. To generate individual twitch-triggered time-frequency spectrograms, we used the methods described in Chapter 3. Twitch-triggered LFP waveforms within the Beta2 range were calculated as follows: First, raw neural signals were filtered using a 20-30 Hz FIR band-pass filter. Next, the signal was converted using root mean square (RMS; time constant = 0.1 s). Using whisker twitches as trigger events, waveform averages of beta2 activity for both structures within the same pup were calculated using a peri-twitch window of 1 s. To assess the temporal relation between twitch-triggered Beta2 oscillations in barrel cortex and hippocampus, we first calculated the latency between twitch onset and peak in the beta2 oscillation for each structure. Average latencies for each structure were averaged across pups. To calculate statistical differences between peak latencies, we used a paired t-test.

*Coherence*

LFP-LFP coherence analyses were conducted using one LFP per pup and neural structure, based on histological confirmation of recording sites. Using custom-written Matlab codes, coherence analyses were calculated from cross-spectral density. Each signal was convolved using a complex Morlet wavelet. The Morlet wavelet was created as follows: The frequency band of interest was divided into

50 bins, and the temporal resolution of the wavelet was established using a minimum of 4 and a maximum of 8 cycles. To calculate state-dependent differences in coherence, we performed repeated-measure ANOVAs with average coherence within each frequency range (theta: 4-8 Hz; alpha: 8-13 Hz; beta2: 20-30 Hz; slow gamma: 30-50 Hz) across behavioral states as the repeated measure.

## RESULTS

### Barrel cortex and hippocampus exhibit state- and twitch-dependent activity

We first recorded extracellular neuronal activity simultaneously in S1BF (n = 119 units) and Hipp CA1 (n = 83 units) from P7-9 pups (hereafter designated as P8; n = 16). Histology confirmed electrode placement in both structures (Figure 1A). Recordings began after confirming that exafferent stimulation of the whiskers (see Methods) evoked consistent neural responses in at least one electrode channel in S1BF.

Figure 1B illustrates, for a representative pup, LFP and single-unit activity across behavioral states in S1BF and Hipp CA1. We observed state-dependent modulation of single-unit and oscillatory activity in both structures. In S1BF, firing rates were significantly higher during AS than AW, which was in turn higher than BQ (Figure 2A, top; $F_{(2,\ 236)} = 56.8$, ps < 0.001). In Hipp CA1, neurons also increased their firing rates during AS in relation to AW and BQ (Figure 2A, bottom;

$F_{(2, 164)} = 44.5$, ps < 0.001); unlike S1BF, firing rates in Hipp CA1 were higher for BQ than AW (ps < 0.001).

Next, we asked whether sensory feedback from whisker twitches drove unit activity during AS in both structures. We first determined whether individual neurons in S1BF and Hipp CA1 exhibited statistically significant responses to whisker twitches. Figure 2B (left) shows, for representative neurons in S1BF (top) and Hipp CA1 (bottom) from the same pup, increased firing rates following whisker twitches during AS. Next, we averaged twitch-related activity in all neurons that significantly increased their firing rates after twitch onset in S1BF (n = 33; 27.7% of units, p < 0.01) or Hipp CA1 (n = 10; 12.04%, p < 0.01). As shown in Figure 2B (right), twitch-related activity in S1BF exhibited shorter latencies (76 ± 10 ms) than those in Hipp CA1 (178 ± 30 ms). Unlike twitch-related response curves in S1BF, which were precisely timed and tuned, twitch-related response curves in Hipp CA1 were broader and more variable in their timing.

As with unit activity, we also found that oscillatory activity in both structures was predominantly expressed during periods of twitching during AS. Figure 2C shows, for a representative pup, twitch-related LFP activity in S1BF (top) and Hipp CA1 (bottom). Power spectra averaged across pups (n = 16) in both structures revealed that the temporal window immediately following twitches of the whiskers during AS was associated with an increase in the theta (4-8 Hz; S1BF: $F_{(2, 27.4)} = 16.63$, p < 0.001; Hipp CA1: $F_{(2, 30)} = 8.42$, p < 0.01), alpha (8-13 Hz; S1BF: $F_{(2, 26.5)} = 19.34$, p < 0.001; Hipp CA1: $F_{(2, 23.9)} = 15.50$, p < 0.001), beta2 (20-30 Hz; S1BF:

$F_{(2, 26.4)}$ = 65.23, p < 0.001; Hipp CA1: $F_{(2, 30)}$ = 43.75, p < 0.001), and sgamma (30-50 Hz; S1BF: $F_{(2, 27.2)}$ = 34.7, p < 0.001; Hipp CA1: $F_{(2, 30)}$ = 44.89) frequencies in relation to AW and BQ (Figure 2D; all ps < 0.01). Thus, twitching during AS drives oscillatory activity in the neonatal barrel cortex and hippocampus.

**Sensory feedback from whisker twitches drives oscillatory coherence between barrel cortex and hippocampus**

To test whether twitches promote the expression of coupled oscillatory activity between S1BF and Hipp CA1, we performed spectral coherence analyses [71,73,184]. As shown in Figure 3A, periods of twitching were associated with the highest levels of coherence between S1BF and Hipp CA1 (Figure 3A; $F_{(2, 30)}$ = 4.16, p < 0.05) as compared with AW or BQ (ps < 0.05). Specifically, even though whisker twitches triggered oscillatory responses across frequency bands in both structures, twitch-related coherence was promoted at beta2 (20-30 Hz) frequency (Figure 3B, p < 0.05). Taking coherence as a measure of functional connectivity, our results indicate that twitching during AS facilitates early connectivity between sensory cortex and hippocampus.

We next sought to determine the directionality of information carried by beta2 oscillations between S1BF and Hipp CA1. Twitch-evoked LFP waveforms of beta2 activity revealed that LFP responses in S1BF were shorter in latency (mean latency: 66.6 ± 10 ms) and exhibited a more tuned, narrower peak than LFP responses in the hippocampus (mean latency: 98.1 ± 10.1 ms; Figure 3D; $t_{(15)}$ = 2.8, p < 0.13; Figure 3D). In agreement with previous findings in the developing

cortico-hippocampal network [24], this finding suggests that twitches drive hippocampal activity via cortical circuits, most likely involving projections from the somatosensory cortex to the entorhinal and perirhinal cortices [24].

## DISCUSSION

The temporal synchronization or coupling of neural oscillations supports important cognitive and behavioral abilities in adult animals [75,111,142,152,200] and indicates early functional connectivity in infancy [64,71–73,171] . Because twitches during AS drive precisely timed oscillatory activity in developing sensorimotor structures [197], we hypothesized that twitching enables oscillatory coupling in early development. Here we tested this hypothesis in the network comprising barrel cortex (S1BF) and CA1 area of hippocampus (Hipp CA1). Our results indicate that sensory feedback from whisker twitches during AS drives oscillatory activity in both networks. Importantly, oscillatory synchrony between barrel cortex and hippocampus in the beta2 frequency band (20-30 Hz) was higher for periods immediately following twitches compared with AW or BQ. Thus, twitching and AS appear to promote network connectivity within the newborn cortico-hippocampal network.

**Whisker twitches during AS drive neural activity in the newborn barrel cortex and hippocampus**

Bidirectional communication between the adult cortex and hippocampus support important behavioral and cognitive abilities, including memory formation and consolidation [201], processing of temporal and spatial information [202,203], and navigation [202,204]. In rats and mice, interactions between barrel cortex and hippocampus are of special interest because rodents use tactile information from whiskers to form spatial representations and efficiently navigate their environment [205]. Consequently, sensory feedback from whiskers reliably triggers neural activity in the adult barrel cortex, which is further conveyed to the hippocampus via entorhinal pathways [206,207].

The nature and functions of cortico-hippocampal interactions in the early postnatal period are less understood. In early development, sensory feedback from twitches during AS is a prominent driver of neuronal activity in both barrel cortex [17,22,24] and hippocampus [23,24,73]. Importantly, twitch-related activity in the hippocampus is largely dependent on projections from the somatosensory cortex, indicating that twitches promote the flow of information between these two structures [24]. These findings further suggest that sensory feedback from twitches contribute to the early activity-dependent development of these local networks and enable the earliest form of cortico-hippocampal connectivity.

Consistent with previous results, we found that firing rates in both S1BF and Hipp CA1 were higher during AS than AW or BQ. A subpopulation of neurons in

both S1BF and Hipp CA1 increased their firing rates in response to twitches of the whiskers during AS. Twitch-related response curves for unit activity in S1BF were more tuned and had less variability in latencies than those in Hipp CA1, where we observed a much broader response with variable latencies across pups. Unlike S1BF, which exhibits very specific somatotopy and exclusively processes sensory feedback from whiskers, the broadness and high variability of twitch-related responses in Hipp CA1 can be attributed to its lack of somatotopic organization. Indeed, activity in the neonatal hippocampus can be driven by twitches elsewhere in the body, including nuchal muscle and limbs [23,24,73].

Sensory feedback from twitches triggered oscillatory activity in the theta, alpha, beta2, and sgamma frequency bands in both S1BF and Hipp CA1. This result indicates that AS and twitching provide an unique context for the expression of early oscillations and suggests that AS plays a key role in those neurodevelopmental processes that rely on early oscillatory activity, such as programmed cell death [181].

**Twitch-dependent oscillatory synchrony between barrel cortex and hippocampus**

Far from being an epiphenomenon of “immature” neural activity, the temporal coupling of neural oscillations in the early postnatal period is thought to enable early network communication [64,71–73,171]; and can presage cognitive and behavioral deficits at later stages in development [184]. Here we found that oscillatory coupling between S1BF and Hipp CA1 reached maximal levels after

whisker twitches during AS, as compared with periods of AW or BQ. Even though we observed significant increases in LFP power across frequency bands following whisker twitches in both structures, twitch-dependent oscillatory coherence was specifically enhanced in the beta2 band. However, this coherence resembled that occurring after passive stimulation of the whiskers (data not shown). Nonetheless, although reafference and exafference trigger similar patterns of oscillatory coupling between cortex and hippocampus, the predominance of active sleep and twitching in early infancy ensures that this coupling will occur on a regular basis.

Previous findings in the adult [206] and neonatal [24] cortico-hippocampal system demonstrated that reafferent and exafferent responses reach the hippocampus via the somatosensory cortex-enthorinal cortex pathway. Latencies for exafferent and reafferent responses in the somatosensory cortex are significantly shorter than in the hippocampus. In addition, lesions of the somatosensory cortex or downstream pathways to the hippocampal formation (i.e., enthorinal and perirhinal cortices) disrupt sensory processing in the hippocampus. Consistent with these results, we found that peak latencies for twitch-related beta2 oscillations in the cortex preceded peak responses in the hippocampus by ~60 ms, suggesting that sensory feedback from twitches is first processed in S1BF before being conveyed to the hippocampus. This sequential, repetitive activation of cortico-hippocampal circuits provides a unique opportunity for synaptic plasticity and strengthening of connectivity in this network.

**Beta2 oscillations in the cortico-hippocampal system**

Beta2 oscillations (also known as fast beta, slow gamma, or beta/gamma oscillations) are commonly defined as being within the ~ 20-40 Hz frequency band and are present in hippocampal and cortical networks. In the barrel cortex of adult rodents, beta2 oscillations precede exploratory whisker movements but also can be triggered by whisker-related exafference and reafference [208], suggesting that they play a role in sensorimotor integration. In the hippocampus, NMDA-dependent transient beta2 oscillations emerge during touch-guided behavior [209], during exploratory navigation in novel environments [210,211], and during goal-directed behavior in response to reward-related stimuli [212]. Thus, the putative functions of such oscillatory patterns in the hippocampus are diverse in nature and involve the formation of spatial and physical representations of the environment [209,210], novelty detection [211] and hippocampal-related modulation of motivated behavior [212]. Importantly, oscillatory coupling between the adult cortex and hippocampus is also mediated by beta2 oscillations. In the network comprised by the entorhinal cortex (which conveys information from cortical sensory areas to the hippocampal formation) and CA1, beta2 coherent oscillations support functional connectivity during memory encoding and retrieval in a stimulus-guided spatial navigation task [213]. Our coherence results show that in early development, twitch-related sensory processing during AS triggers similar patterns of beta2-dependent cortico-hippocampal connectivity that are associated with complex behavioral and cognitive skills in adulthood.

**Active sleep, acetylcholine, and beta oscillations: a window on developmental plasticity**

During AS, cholinergic inputs from the basal forebrain release acetylcholine (ACh) in cortex and hippocampus [214]. In addition, sensory stimulation is associated with ACh release in both structures [215]. Our finding that beta2 oscillations are enhanced during AS-related twitching is consistent with the convergence of state- and sensory-dependent release of ACh in the cortico-hippocampal system. In the neonatal sensory cortex *in vitro*, beta oscillations can be elicited after bath application of carbachol, a cholinergic agonist. The necessity of cholinergic input for the generation of beta2 oscillations in the hippocampus *in vivo* is still a matter of debate, but ACh release induces beta2 oscillations in hippocampal slices [220]. Because ACh induces synaptic plasticity and coordinates neuronal population activity [216–218], AS and twitching provide a unique neurochemical context for the emergence and strengthening of newly formed connections between distant but functionally related networks in the early postnatal period.

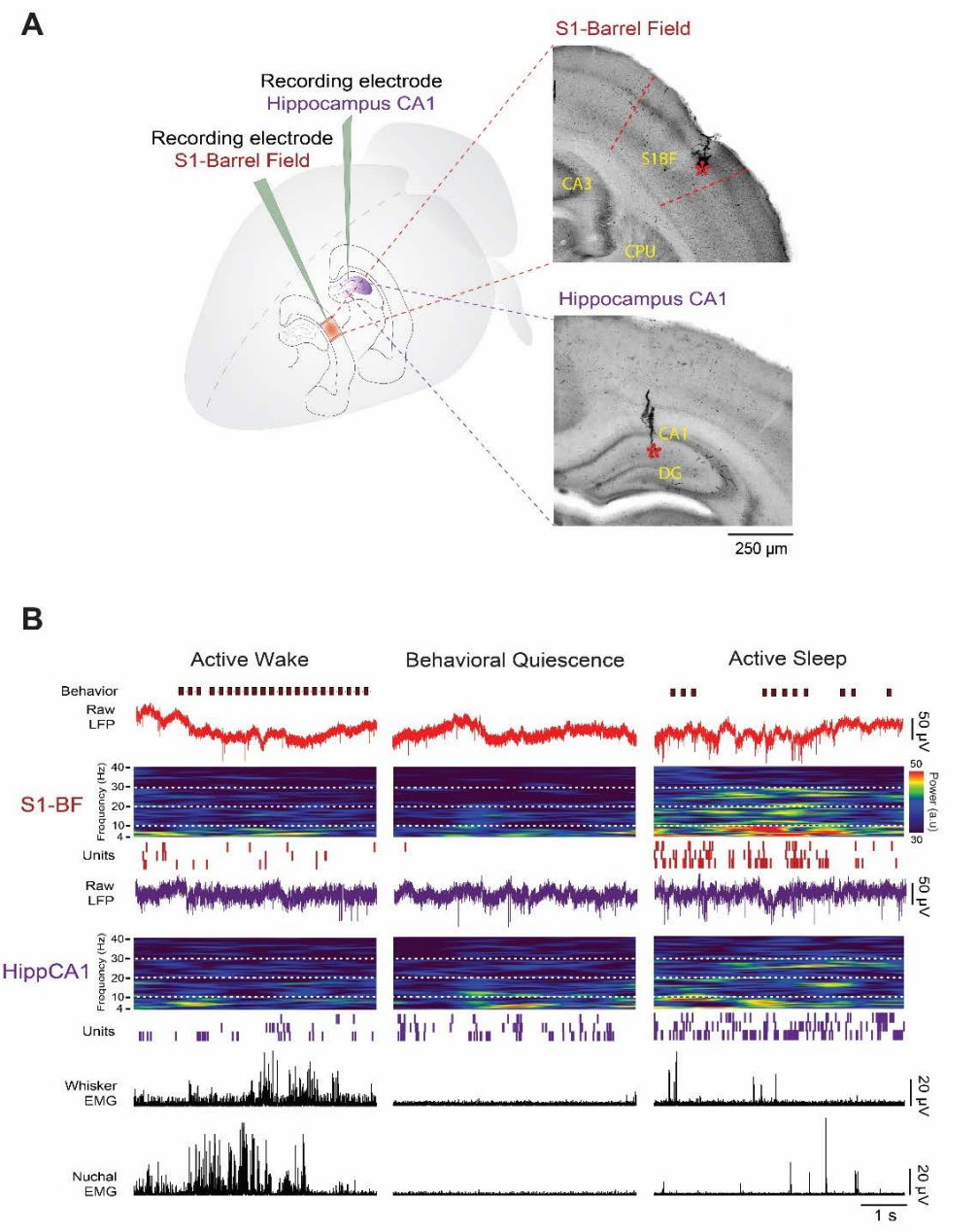


**Figure 17. Dual recordings in S1BF and Hipp CA1 in P8 rats.** (A) Illustration depicting electrode placements in S1BF and Hipp CA1. (B) Representative data from a P8 rat showing sleep and wake behavior, LFP (raw signal and corresponding time-frequency spectrograms) and unit activity in the barrel cortex (S1-BF; red traces) and CA1 region of hippocampus (Hipp CA1; purple traces), and whisker and nuchal EMGs (black traces) across behavioral states.

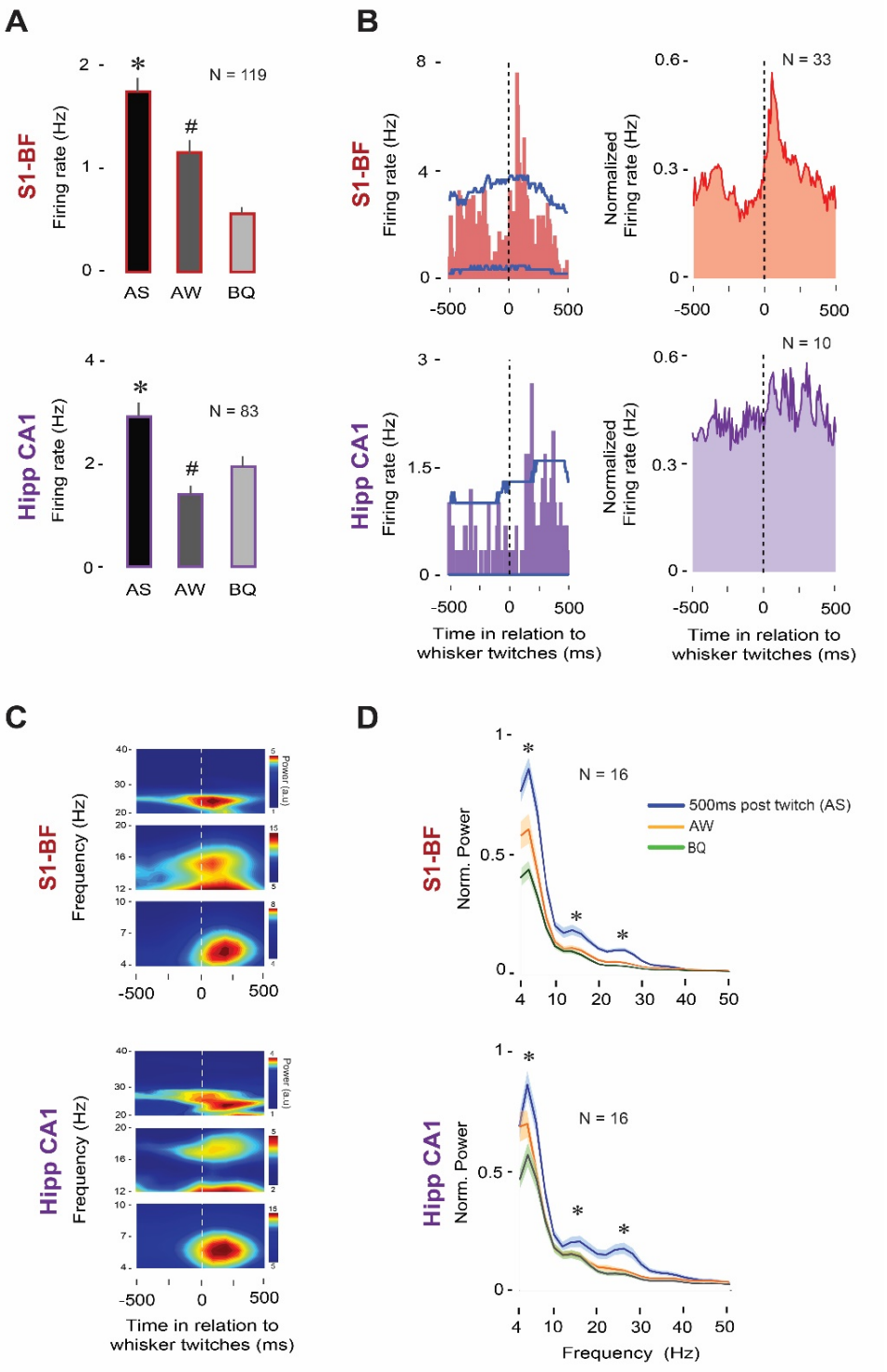


**Figure 18. State- and twitch-dependent neural activity in S1BF and Hipp CA1 at P8.** (A) Mean firing rates across behavioral states for neurons in S1BF (n = 119,

top) and Hipp CA1 (n = 83, bottom). * significant difference from AW and BQ ($p < 0.001$). # significant difference from BQ ($p < 0.001$). (B) Left: Representative perievent histograms (10-ms bins) for spike activity in relation to whisker twitches in the S1BF (top) and Hipp CA1 (bottom) of a P8 rat. Vertical dashed lines denote twitch onset. Upper and lower acceptance bands ($p <0.01$ for each band) are indicated by dashed lines. Right: Perievent histograms for normalized spike activity in relation to whisker twitches averaged across all significant twitch-related units in S1BF (n = 33, top) and Hipp CA1 (n = 10, bottom). (C) Twitch triggered time-frequency spectrograms for a representative P8 rat in S1BF (top) and Hipp CA1 (bottom). (D) Mean normalized power spectra of LFP activity in S1BF (n = 16, top) and Hipp CA1 (n = 16, bottom) after twitches during active sleep (AS, blue; post-twitch window: 500 ms), active wake (AW, orange) and behavioral quiescence (BQ, green). Shaded area indicates $\pm$SEM. * significant difference from AW and BQ, $p < 0.01$.

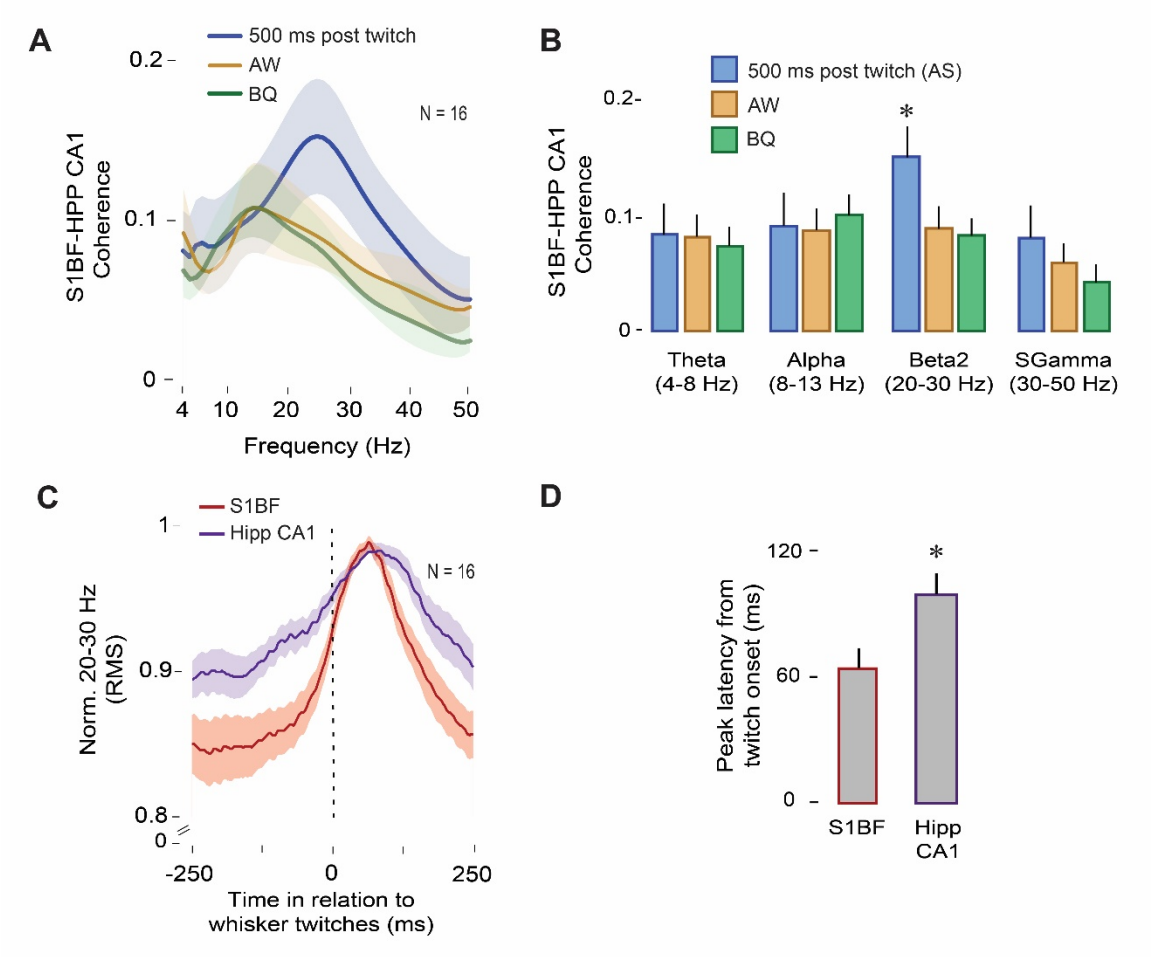


**Figure 19. Twitching during active sleep promotes LFP coherence between S1BF and Hipp CA1**. (A) Mean LFP-LFP coherence spectra between S1BF and Hipp CA1 (16 pups, 16 LFP pairs) after whisker twitches during active sleep (AS; post-twitch window: 500 ms, blue), active wake (AW; orange) and behavioral quiescence (BQ, green). Shaded area indicates SEM. (B) Mean LFP-LFP coherence between S1BF and Hipp CA1 for different frequency bands. * significant difference from other behavioral states, $p < 0.05$. (D) Normalized twitch-triggered LFP signals (20-30 Hz, root mean square) in S1BF (red) and Hipp CA1 (purple) averaged across pups (n = 16). Vertical dashed line indicates whisker twitch onset. Shaded area denotes ±SEM. (E) Mean peak latency from twitch onset from the data shown in (D) for S1 (red) and Hipp CA1 (purple). * significant difference, $p < 0.01$.

# CHAPTER 6: OVERVIEW AND SGNIFICANCE OF RESEARCH

The development of the sensorimotor system relies on early sensory experiences [10–12]. Because sensory feedback from twitching during AS robustly activates neuronal networks across the neuraxis, it has been proposed that twitching contributes to the activity-dependent development of the sensorimotor system [14,79,102]. However, the motor pathways contributing to the production of twitching in early infancy have remained largely unknown. The data presented in Chapter 2 demonstrate that the newborn rat RN is involved in the generation of twitching and processes twitch-related sensory feedback. Thus, we proposed that the RN is an important site for sensorimotor processing in early development. Indeed, the RN is anatomically and functionally connected with a variety of sensorimotor networks, including the spinal cord [40,55], midbrain and brainstem nuclei [37,41], hypothalamus [56], cerebellum [57], somatosensory cortex [58], motor cortex [59], and hippocampus [60]. However, the specific conditions and mechanisms supporting communication between the infant RN and the aforementioned sensorimotor networks have remained unexplored.

In the nervous system of adult and developing animals, functionally related structures establish neuronal communication via synchronized or coupled oscillatory activity [71–75]. In Chapter 3, we show for the first time that neuronal oscillatory activity in the RN is dominated by theta oscillations (~4-7 Hz). By the end of the first postnatal week, RN theta was expressed in brief oscillatory bursts associated with twitching during AS. By the end of the second postnatal week, RN

theta was expressed continuously throughout bouts of AS. At both ages, oscillatory activity in the RN was markedly reduced or suppressed during periods of quiescence or wakefulness. Importantly, the oscillatory dynamics in the developing RN resemble those previously reported in the developing hippocampus [23]. Thus, we next asked whether theta oscillations in the RN and hippocampus are temporally coupled and whether such coupling depends on AS. The results described in Chapter 3 confirm that AS promotes oscillatory coupling between the RN and hippocampus by the end of the second postnatal week. Interestingly, the amplitude of theta oscillations in both structures was enhanced during periods of twitching. This observation inspired the hypothesis (further elaborated in Chapter 4) that sensory feedback from twitches drives early network connectivity at ages when oscillatory activity largely depends on sensory stimulation.

In Chapter 5, we show that sensory feedback from twitches of the whiskers trigger oscillatory synchrony at ~ 20-30 Hz between the barrel cortex and the CA1 area in the hippocampus by the end of the first postnatal week. Importantly, coupled oscillatory activity between cortex and hippocampus was suppressed during periods of wakefulness or behavioral quiescence. This finding supports the hypothesis presented in Chapter 4—that AS and twitching provide a unique context for the emergence and expression of functional connectivity in the sensorimotor system.

Altogether, the findings presented in this dissertation have important methodological and clinical implications. Even though AS is maximally expressed in early life and is relatively prominent in the perinatal period [1–6], investigations

of early functional connectivity have largely ignored how networks interact in this behavioral state. For example, human studies have focused on quiet (non-REM) sleep or on the so-called “resting state.” Moroever, studies using infant animals have explored network interactions under anesthetic conditions that suppress the normal expression of sleep and wake behaviors. If AS in early infancy is indeed a period of heightened neural activity [1,7], one should expect that network interactions during AS are different from those occurring during other behavioral states. The data presented in this dissertation demonstrate that early connectivity in the sensorimotor system is promoted during AS. In light of these results, we argue that a meaningful analysis of functional connectivity in early development must take into account state-dependent differences in network interactions.

Connectivity patterns during sleep also reveal the expression of atypical synchronized oscillatory activity in young and adult individuals diagnosed with neurodevelopmental disorders characterized by sensorimotor deficits, as in autism [187,188]. Thus, analyses of state-dependent connectivity may provide novel insights into the etiology and mechanisms underlying a variety of such disorders and could perhaps also be used as an early marker for atypical development [189].

Finally, the data presented in this dissertation highlight how sensory feedback from twitching is a major source of stimulation to cortical and subcortical structures and facilitates network interactions within the developing sensorimotor system. Consequently, any environmental or pathological condition that results in sleep restriction or deprivation can be conceptualized as a form of sensory deprivation. Because sensory experience plays a fundamental role in the activity-

dependent development of the sensorimotor system [10–12], decreased sleep during sensitive periods of brain development may cause sensorimotor and cognitive deficits later in life. In that regard, decreased sleep is a symptom in a variety of neurodevelopmental sensorimotor disorders [192].

## REFERENCES


1. Roffwarg, H.P., Muzio, J.N., and Dement, W.C. (1966). Ontogenetic development of the human sleep-dream cycle. Science *152*, 604–619.

2. Jouvet-Mounier, D., Astic, L., and Lacote, D. (1970). Ontogenesis of the States of Sleep in Rat, Cat, and Guinea Pig during the First Postnatal Month. Dev. Psychobiol. *2*, 216–239.

3. Blumberg, M.S., and Seelke, A.M.H. (2010). The form and function of infant sleep: From muscle to neocortex. Oxford Univ. Press, 391–423.

4. Kayser, M.S., and Biron, D. (2016). Sleep and development in genetically tractable model organisms. Genetics *203*, 21–33.

5. Sorribes, A. (2013). The ontogeny of sleep–wake cycles in zebrafish: a comparison to humans. Front. Neural Circuits *7*, 178.

6. Raizen, D.M., Zimmerman, J.E., Maycock, M.H., Ta, U.D., You, Y., Sundaram, M. V., and Pack, A.I. (2008). Lethargus is a Caenorhabditis elegans sleep-like state. Nature *451*, 569–572.

7. Marks, G.A., Shaffery, J.P., Oksenberg, A., Speciale, S.G., and Roffwarg, H.P. (1995). A functional role for REM sleep in brain maturation. Behav. Brain Res. *69*, 1–11.

8. Frank, M.G. (2011). Sleep and developmental plasticity: Not just for kids. Prog. Brain Res. *193*, 221–232.

9. Shaffery, J.P., Sinton, C.M., Bissette, G., Roffwarg, H.P., and Marks, G.A. (2002). Rapid eye movement sleep deprivation modifies expression of long-term potentiation in visual cortex of immature rats. Neuroscience *110*, 431–443.

10. Fox, K. (1992). A critical period for experience-dependent synaptic plasticity in rat barrel cortex. J. Neurosci. *12*, 1826–1838.

11. Simons, D.J., and Land, P.W. (1987). Early experience of tactile stimulation influences organization of somatic sensory cortex. Nature *326*, 694–697.

12. Crocker-Buque, A., Brown, S.M., Kind, P.C., Isaac, J.T.R., and Daw, M.I. (2015). Experience-Dependent, Layer-Specific Development of Divergent Thalamocortical Connectivity. Cereb. Cortex *25*, 2255–2266.

13. Akhmetshina, D., Nasretdinov, A., Zakharov, A., Valeeva, G., and Khazipov, R. (2016). The Nature of the Sensory Input to the Neonatal Rat Barrel Cortex. J. Neurosci. *36*, 9922–9932.

14. Blumberg, M. (2010). Beyond dreams: do sleep-related movements contribute to brain development? Front. Neurol. 1:140

15. Inácio, A.R., Nasretdinov, A., Lebedeva, J., and Khazipov, R. (2016). Sensory feedback synchronizes motor and sensory neuronal networks in the neonatal rat spinal cord. Nat. Commun. *7*, 13060.

16. Petersson, P., Waldenström, A., Fåhraeus, C., and Schouenborg, J. (2003). Spontaneous muscle twitches during sleep guide spinal self-organization. Nature *424*, 72–75.

17. Tiriac, A., Uitermarkt, B.D., Fanning, A.S., Sokoloff, G., and Blumberg, M.S. (2012). Rapid whisker movements in sleeping newborn rats. Curr. Biol. *22*, 2075–2080.

18. Tiriac, A., Del Rio-Bermudez, C., Blumberg, M.S. (2014). Self-generated movements with unexpected sensory consequences. Curr. Biol. *24*, 2136–41.

19. Tiriac, A., and Blumberg, M.S. (2016). Gating of reafference in the external cuneate nucleus during self-generated movements in wake but not sleep. Elife *5*, e18749.

20. Khazipov, R., Sirota, A., Leinekugel, X., Holmes, G.L., Ben-Ari, Y., and Buzsaki, G. (2004). Early motor activity drives spindle bursts in the developing somatosensory cortex. Nature *432*, 758–761.

21. McVea, D.A., Mohajerani, M.H., and Murphy, T.H. (2012). Voltage-Sensitive Dye Imaging Reveals Dynamic Spatiotemporal Properties of Cortical Activity after Spontaneous Muscle Twitches in the Newborn Rat. J. Neurosci. *32*, 10982–10994.

22. Akhmetshina, D., Nasretdinov, A., Zakharov, A., Valeeva, G., and Khazipov, R. (2016). The nature of the sensory input to the neonatal rat barrel cortex. J. Neurosci. *36*, 9922–9932.

23. Mohns, E.J., and Blumberg, M.S. (2008). Synchronous bursts of neuronal activity in the developing hippocampus: modulation by active sleep and association with emerging gamma and theta rhythms. J. Neurosci. *28*, 10134–10144.

24. Mohns, E.J., and Blumberg, M.S. (2010). Neocortical Activation of the Hippocampus during Sleep in Infant Rats. J. Neurosci. *30*, 3438–3449.

25. Del Rio-Bermudez, C., Plumeau, A.M., Sattler, N.J., Sokoloff, G., and Blumberg, M.S. (2016). Spontaneous activity and functional connectivity in the developing cerebellorubral system. J. Neurophysiol., *116*, 1316-1327.

26. Sokoloff, G., Plumeau, A.M., Mukherjee, D., and Blumberg, M.S. (2015). Twitch-related and rhythmic activation of the developing cerebellar cortex. J. Neurophysiol. *114*, 1746–1756.

27. Sokoloff, G., Uitermarkt, B.D., and Blumberg, M.S. (2015). REM sleep twitches rouse nascent cerebellar circuits: Implications for sensorimotor development. Dev. Neurobiol. *75*, 1140–1153.

28. Robinson, S.R., Blumberg, M.S., Lane, M.S., and Kreber, L.A. (2000). Spontaneous motor activity in fetal and infant rats is organized into discrete multilimb bouts. Behav. Neurosci. *114*, 328–336.

29. Abel, T., Havekes, R., Saletin, J.M., and Walker, M.P. (2013). Sleep, plasticity and memory from molecules to whole-brain networks. Curr. Biol. *23*.

30. Kreider, J.C., and Blumberg, M.S. (2000). Mesopontine contribution to the expression of active “twitch” sleep in decerebrate week-old rats. Brain Res. *872*, 149–159.

31. Karlsson, K., and Blumberg, M.S. (2005). Active medullary control of atonia in week-old rats. Neuroscience *130*, 275–283.

32. Karlsson, K., Gall, A.J., Mohns, E.J., Seelke, A.M.H., and Blumberg, M.S. (2005). The neural substrates of infant sleep in rats. PLoS Biol. *3*, 0891–0901.

33. Chase, M.H., and Morales, F.R. (1990). The atonia and myoclonia of active (REM) sleep. Annu. Rev. Psychol. *41*, 557–584.

34. Siegel, J.M., Nienhuis, R., Fahringer, H.M., Chiu, C., Dement, W.C., Mignot, E., and Lufkin, R. (1992). Activity of medial mesopontine units during cataplexy and sleep-waking states in the narcoleptic dog. J. Neurosci. *12*, 1640–1646.

35. Leonard, C.S., and Llinás, R. (1994). Serotonergic and cholinergic inhibition of mesopontine cholinergic neurons controlling rem sleep: An in vitro electrophysiological study. Neuroscience *59*, 309–330.

36. Boissard, R., Gervasoni, D., Schmidt, M.H., Barbagli, B., Fort, P., and Luppi, P.H. (2002). The rat ponto-medullary network responsible for paradoxical sleep onset and maintenance: A combined microinjection and functional neuroanatomical study. Eur. J. Neurosci. *16*, 1959–1973.

37. Pompeiano, O., and Satoh, T. (1967). Vestibular influences on the red nucleus during sleep. Pflugers Arch. Gesamte Physiol. Menschen Tiere *298*, 159–162.

38. Gassel, M.M., Marchiafava, P.L., and Pompeiano, O. (1966). Rubrospinal Influences during desynchronized sleep. Nature *209*, 1218–1220.

39. Li, D., and Peever, J. (2014). Pharmacogenetic stimulation of the red nucleus influences muscle tone during rapid eye movement (REM) sleep in mice. Minneapolis: Conference presented at the Annual Meeting of the Associated Professional Sleep Societies, SLEEP,

40. Kuypers, H. (1981). Anatomy of the descending pathways vol II. J. Brookhart and V. Mountcastle, eds. (Bethesda, MD: American Physiological Society).

41. Mileykovskiy, B.Y., Kiyashchenko, L.I., and Siegel, J.M. (2002). Cessation of activity in red nucleus neurons during stimulation of the medial medulla in decerebrate rats. J. Physiol. *545*, 997–1006.

42. Hermer-Vazquez, L., Hermer-Vazquez, R., Moxon, K.A., Kuo, K.H., Viau, V., Zhan, Y., and Chapin, J.K. (2004). Distinct temporal activity patterns in the rat M1 and red nucleus during skilled versus unskilled limb movement. Behav. Brain Res. *150*, 93–107.

43. Muir, G.D., and Whishaw, I.Q. (2000). Red nucleus lesions impair overground locomotion in rats: A kinetic analysis. Eur. J. Neurosci. *12*, 1113–1122.

44. Williams, P.T.J., Kim, S., and Martin, J.H. (2014). Postnatal maturation of the red nucleus motor map depends on rubrospinal connections with forelimb motor pools. J. Neurosci. *34*, 4432–41.

45. Ghez, C. (1975). Input-output relations of the red nucleus in the cat. Brain Res. *98*, 93–108.

46. Morris, R., Vallester, K.K., Newton, S.S., Kearsley, A.P., and Whishaw, I.Q. (2015). The differential contributions of the parvocellular and the magnocellular subdivisions of the red nucleus to skilled reaching in the rat. Neuroscience *295*, 48–57.

47. Del Rio-Bermudez, C., Sokoloff, G., and Blumberg, M.S. (2015). Sensorimotor Processing in the Newborn Rat Red Nucleus during Active Sleep. J. Neurosci. *35*, 8322–32.

48. Pompeiano, O., and Brodal, A. (1957). Experimental demonstration of a somatotopical origin of rubrospinal fibers in the cat. J. Comp. Neurol. *108*, 225–251.

49. Eccles, J.C., Rantucci, T., Scheid, P., and Taborikova, H. (1975). Somatotopic studies on red nucleus: spinal projection level and respective receptive fields. J. Neurophysiol. *38*, 965–980.

50. Larsen, K.D., and Yumiya, H. (1980). The red nucleus of the monkey - Topographic localization of somatosensory input and motor output. Exp. Brain Res. *40*, 393–404.

51. Herter, T.M., Takei, T., Munoz, D.P., and Scott, S.H. (2015). Neurons in red nucleus and primary motor cortex exhibit similar responses to mechanical perturbations applied to the upper-limb during posture. Front. Integr. Neurosci. *9*: 29.

52. Sarrafizadeh, R., Keifer, J., and Houk, J.C. (1996). Somatosensory and movement-related properties of red nucleus: a single unit study in the turtle. Exp Brain Res *108*, 1–17.

53. Liu, Y., Pu, Y., Gao, J.H., Parsons, L.M., Xiong, J., Liotti, M., Bower, J.M., and Fox, P.T. (2000). The human red nucleus and lateral cerebellum in supporting roles for sensory information processing. Hum. Brain Mapp. *10*, 147–159.

54. Bland, B.H., and Oddie, S.D. (2001). Theta band oscillation and synchrony in the hippocampal formation and associated structures: The case for its role in sensorimotor integration. Behav. Brain Res. *127*, 119–136.

55. Paxinos, G. (2015). The Rat Nervous System. Academic Press: Cambridge, MA.

56. Bernays, R.L., Heeb, L., Cuenod, M., and Streit, P. (1988). Afferents to the rat red nucleus studied by means of d-[3H] aspart ate, [3H]choline and non-selective tracers. Neuroscience *26*, 601–619.

57. Flumerfelt, B.A. (1980). An ultrastructural investigation of afferent connections of the red nucleus in the rat. J. Anat. *131*, 621–633.

58. Ebrahimi-Gaillard, A., and Roger, M. (1993). [The corticorubral projection in rats: topographic distribution of fibers arising from areas of the sensorimotor cortex functionally identified by microstimulation]. C R Acad Sci III *316*, 502–507.

59. Giuffrida, R., Volsi, G.L., and Perciavalle, V. (1988). Influences of cerebral cortex and cerebellum on the red nucleus of the rat. Behav. Brain Res. *28*, 109–111.

60. Dypvik, A.T., and Bland, B.H. (2004). Functional connectivity between the red nucleus and the hippocampus supports the role of hippocampal formation in sensorimotor integration. J. Neurophysiol. *92*, 2040–2050.

61. Freeman, J.H., and Steinmetz, A.B. (2011). Neural circuitry and plasticity mechanisms underlying delay eyeblink conditioning. Learn. Mem. *18*, 666–677.

62. Kennedy, P.R. (1990). Corticospinal, rubrospinal and rubro-olivary projections: a unifying hypothesis. Trends Neurosci. *13*, 474–479.

63. Martin, J.H., and Ghez, C. (1988). Red nucleus and motor cortex: Parallel motor systems for the initiation and control of skilled movement. Behav. Brain Res. *28*, 217–223.

64. Khazipov, R., and Luhmann, H.J. (2006). Early patterns of electrical activity in the developing cerebral cortex of humans and rodents. Trends Neurosci. *29*, 414–418.

65. Blanquie, O., Kilb, W., Sinning, A., and Luhmann, H.J. (2017). Homeostatic interplay between electrical activity and neuronal apoptosis in the developing neocortex. Neuroscience, 358, 190-200.

66. Hanganu-Opatz, I.L. (2010). Between molecules and experience: Role of early patterns of coordinated activity for the development of cortical maps and sensory abilities. Brain Res. Rev. *64*, 160–176.

67. McVea, D.A., Murphy, T.H., and Mohajerani, M.H. (2016). Large scale cortical functional networks associated with slow-wave and spindle-burst-related spontaneous activity. Front. Neural Circuits *10*.

68. Yang, J.-W., Reyes-Puerta, V., Kilb, W., and Luhmann, H.J. (2016). Spindle Bursts in Neonatal Rat Cerebral Cortex. Neural Plast. *2016*, 1–11.

69. Lebedeva, J., Zakharov, A., Ogievetsky, E., Minlebaeva, A., Kurbanov, R., Gerasimova, E., Sitdikova, G., and Khazipov, R. (2015). Inhibition of cortical activity and apoptosis caused by ethanol in neonatal rats in vivo. Cereb. Cortex, *27*, 1068-1082

70. Blanquie, O., Yang, J.-W., Kilb, W., Sharopov, S., Sinning, A., and Luhmann, H.J. (2017). Electrical activity controls area-specific expression of neuronal apoptosis in the developing mouse cerebral cortex. Elife *6*, 1–21.

71. Brockmann, M.D., Poschel, B., Cichon, N., and Hanganu-Opatz, I.L. (2011). Coupled oscillations mediate directed interactions between prefrontal cortex and hippocampus of the neonatal rat. Neuron *71*, 332–347.

72. Uhlhaas, P.J., Roux, F., Rodriguez, E., Rotarska-Jagiela, A., and Singer, W. (2010). Neural synchrony and the development of cortical networks. Trends Cogn. Sci. *14*, 72–80.

73. Del Rio-Bermudez, C., Kim, J., Sokoloff, G., and Blumberg, M.S. (2017). Theta oscillations during active sleep synchronize the developing rubro-hippocampal sensorimotor network. Curr. Biol. *27*, 1413–1424.

74. Karalis, N., Dejean, C., Chaudun, F., Khoder, S., Rozeske, R.R., Wurtz, H., Bagur, S., Benchenane, K., Sirota, A., Courtin, J., *et al.* (2016). 4-Hz oscillations synchronize prefrontal-amygdala circuits during fear behavior. Nat. Neurosci. *19*, 605–12.

75. Buzsáki, G., and Draguhn, A. (2004). Neuronal oscillations in cortical networks. Science *304*, 1926–9.

76. Wolpert, D.M., Ghahramani, Z., and Jordan, M.I. (1995). An internal model for sensorimotor integration. Science *269*, 1880–1882.

77. Berthier, N.E., Rosenstein, M.T., and Barto, A.G. (2005). Approximate optimal control as a model for motor learning. Psychol. Rev. *112*, 329–346.

78. Robinson, S.R., Kleven, G.A., and Brumley, M.R. (2008). Prenatal development of interlimb motor learning in the rat fetus. Infancy *13*, 204–228.

79. Blumberg, M.S., Marques, H.G., and Iida, F. (2013). Twitching in sensorimotor development from sleeping rats to robots. Curr. Biol. *23*, R532–R537.

80. Padel, Y., and Jeneskog, T. (1981). Inhibition of rubro-spinal cells by somesthetic afferent activity. Neurosci. Lett. *21*, 177–182.

81. Tiriac, A., Del Rio-Bermudez, C., and Blumberg, M.S. (2014). Self-generated movements with “unexpected” sensory consequences. Curr. Biol. *24*, 2136–2141.

82. Seelke, A.M.H., and Blumberg, M.S. (2008). The microstructure of active and quiet sleep as cortical delta activity emerges in infant rats. Sleep *31*, 691–9.

83. Harrison, M.T., and Geman, S. (2009). A rate and history-preserving resampling algorithm for neural spike trains. Neural Comuptation *21*, 1244–1258.

84. Amarasingham, A., Harrison, M.T., Hatsopoulos, N.G., and Geman, S. (2012). Conditional modeling and the jitter method of spike re-sampling. J Neurophysiol *107*, 517–531.

85. Ciranna, L., Licata, F., Li Volsi, G., and Santangelo, F. (2003). Role of GABAA and GABAB receptors in GABA-induced inhibition of rat red nucleus neurons. Neurosci. Lett. *341*, 221–224.

86. Sato, K., Zhang, J.H., Saika, T., Sato, M., Tada, K., and Tohyama, M. (1991). Localization of glycine receptor alpha 1 subunit mRNA-containing neurons in the rat brain: an analysis using in situ hybridization histochemistry. Neuroscience *43*, 381–95.

87. Altmann, H., ten Brugencate, G., Sonhof, U., and Steinberg, R. (1973). Action of γ-aminobutyric acid and glycine on red nucleus neurons. Pflug Arch Eur J Phy *342*, 283–288.

88. Jiang, M.C., Alheid, G.F., Nunzi, M.G., and Houk, J.C. (2002). Cerebellar input to magnocellular neurons in the red nucleus of the mouse: Synaptic analysis in horizontal brain slices incorporating cerebello-rubral pathways. Neuroscience *110*, 105–121.

89. Brooks, P.L., and Peever, J.H. (2012). Identification of the transmitter and receptor mechanisms responsible for REM sleep paralysis. J. Neurosci. *32*, 9785–95.

90. Lisman, J.E. (1997). Bursts as a unit of neural information: Making unreliable synapses reliable. Trends Neurosci. *20*, 38–43.

91. Cohen, J. (1988). Statistical power analysis for the behavioral sciences. Stat. Power Anal. Behav. Sci. *2nd* edition. Academic Press: Cambrigde (MA).

92. Peever, J., Luppi, P.H., and Montplaisir, J. (2014). Breakdown in REM sleep circuitry underlies REM sleep behavior disorder. Trends Neurosci. *37*, 279–288.

93. Stecina, K., Slawinska, U., and Jankowska, E. (2008). Ipsilateral actions from the feline red nucleus on hindlimb motoneurones. J. Physiol. *586*, 5865–5884.

94. Holstege, G., and Tan, J. (1988). Projections from the red nucleus and surrounding areas to the brainstem and spinal cord in the cat. An HRP and autoradiographical tracing study. Behav. Brain Res. *28*, 33–57.

95. Appelberg, B. (1962). The effect of electrical stimulation in nucleus ruber on the response to stretch in primary and secondary muscle spindle merents. Acta Physiol. Scand. *56*, 140–151.

96. Padel, Y., Bourbonnais, D., and Sybirska, E. (1986). A new pathway from primary afferents to the red nucleus. Neurosci. Lett. *64*, 75–80.

97. Naus, C., Flumerfelt, B.A., and Hrycyshyn, A.W. (1985). An anterograde HRP-WGA study of aberrant corticorubral projections following neonatal lesions of the rat sensorimotor cortex. Exp. Brain Res. *59*, 365–371.

98. Keifer, J., and Lustig, D.G. (1999). Comparison of cortically and subcortically controlled motor systems. II. Distribution of anterogradely labeled terminal boutons on intracellularly filled rubrospinal neurons in rat and turtle. J. Comp. Neurol. *416*, 101–111.

99. Pong, M., Horn, K.M., and Gibson, A.R. (2002). Spinal projections of the cat parvicellular red nucleus. J. Neurophysiol. *87*, 453–468.

100. Kennedy, P.R., and Humphrey, D.R. (1987). The compensatory role of the parvocellular division of the red nucleus in operantly conditioned rats. Neurosci. Res. *5*, 39–62.

101. Ahissar, E. (2003). Closed-loop neuronal computations: focus on vibrissa somatosensation in rat. Cereb. Cortex *13*, 53–62.

102. Blumberg, M.S. (2015). Developing sensorimotor systems in our sleep. Curr. Dir. Psychol. Sci. *24*, 32–37.

103. Kayser, M.S., and Biron, D. (2016). Sleep and development in genetically tractable model organisms. Genetics *203*, 21–33.

104. Khazipov, R., Sirota, A., Leinekugel, X., Holmes, G.L., Ben-Ari, Y., and Buzsáki, G. (2004). Early motor activity drives spindle bursts in the developing somatosensory cortex. Nature *432*, 758–61.

105. Tiriac, A., Sokoloff, G., and Blumberg, M.S. (2015). Myoclonic twitching and sleep-dependent plasticity in the developing sensorimotor system. Curr. Sleep Med. Reports *1*, 74–79.

106. Nioche, C., Cabanis, E. a, and Habas, C. (2009). Functional connectivity of the human red nucleus in the brain resting state at 3T. AJNR. Am. J. Neuroradiol. *30*, 396–403.

107. Ryou, J.W., Cho, S.Y., and Kim, H.T. (1998). Lesion of the cerebellar interpositus nucleus or the red nucleus affects classically conditioned neuronal activity in the hippocampus. Prog. Neuro-Psychopharmacology Biol. Psychiatry *22*, 169–185.

108. Bird, C.M., and Burgess, N. (2008). The hippocampus and memory: insights from spatial processing. Nat. Rev. Neurosci. *9*, 182–194.

109. Bast, T. (2007). Toward an integrative perspective on hippocampal function: from the rapid encoding of experience to adaptive behavior. Rev. Neurosci. *18*, 253–281.

110. Vanderwolf, C.H. (2001). The hippocampus as an olfacto-motor mechanism: Were the classical anatomists right after all? In Behav Brain Res. *127*, 25–47.

111. Fujisawa, S., and Buzsáki, G. (2011). A 4 Hz Oscillation Adaptively Synchronizes Prefrontal, VTA, and Hippocampal Activities. Neuron *72*, 153–165.

112. Ekstrom, A.D., Caplan, J.B., Ho, E., Shattuck, K., Fried, I., and Kahana, M.J. (2005). Human hippocampal theta activity during virtual navigation. Hippocampus *15*, 881–889.

113. Grion, N., Akrami, A., Zuo, Y., Stella, F., and Diamond, M.E. (2016). Coherence between rat sensorimotor system and hippocampus is enhanced during tactile discrimination. PLoS Biol. *14*.

114. Allen, T.A., Narayanan, N.S., Kholodar-Smith, D.B., Zhao, Y., Laubach, M., and Brown, T.H. (2008). Imaging the spread of reversible brain inactivations using fluorescent muscimol. J. Neurosci. Methods *171*, 30–38.

115. Blumberg, M.S., Sokoloff, G., Tiriac, A., and Del Rio-Bermudez, C. (2015). A valuable and promising method for recording brain activity in behaving newborn rodents. Dev. Psychobiol. *57*, 506–517.

116. Cohen, X.M. (2014). Analyzing Neural Time Series Data. MIT Press, Cambridge (MA).

117. Cui, J., Xu, L., Bressler, S.L., Ding, M., and Liang, H. (2008). BSMART: A Matlab/C toolbox for analysis of multichannel neural time series. Neural Networks *21*, 1094–1104.

118. Brovelli, A., Ding, M., Ledberg, A., Chen, Y., Nakamura, R., and Bressler, S.L. (2004). Beta oscillations in a large-scale sensorimotor cortical network: directional influences revealed by Granger causality. Proc. Natl. Acad. Sci. U. S. A. *101*, 9849–54.

119. Le Van Quyen, M., Foucher, J., Lachaux, J., Rodriguez, E., Lutz, a, Martinerie, J., and Varela, F.J. (2001). Comparison of Hilbert transform and wavelet methods for the analysis of neuronal synchrony. J. Neurosci. Methods *111*, 83–98.

120. Kim, J., Delcasso, S., and Lee, I. (2011). Neural Correlates of Object-in-Place Learning in Hippocampus and Prefrontal Cortex. J. Neurosci. *31*, 16991–17006.

121. Kim, J., Goldsberry, M. E., Harmon, T. C., Freeman, J.H. (2016). Developmental changes in hippocampal ca1 single neuron firing and theta activity during associative learning. PLoS One *11*, e0164781.

122. Nokia, M.S., Penttonen, M., Korhonen, T., and Wikgren, J. (2008). Hippocampal theta (3-8Hz) activity during classical eyeblink conditioning in rabbits. Neurobiol. Learn. Mem. *90*, 62–70.

123. Wikgren, J., Nokia, M.S., and Penttonen, M. (2010). Hippocampo-cerebellar theta band phase synchrony in rabbits. Neuroscience *165*, 1538–1545.

124. Montgomery, S.M., Sirota, A., and Buzsáki, G. (2008). Theta and gamma coordination of hippocampal networks during waking and rapid eye movement sleep. J. Neurosci. *28*, 6731–6741.

125. Wills, T.J., Cacucci, F., Burgess, N., and O'Keefe, J. (2010). Development of the hippocampal cognitive map in preweanling rats. Science *328*, 1573–1576.

126. Granger, C.W.J. (1969). Investigating Causal Relations by Econometric Models and Cross-spectral Methods. Econometrica *37*, 424–438.

127. De Zeeuw, C.I., Hoogenraad, C.C., Koekkoek, S.K.E., Ruigrok, T.J.H., Galjart, N., and Simpson, J.I. (1998). Microcircuitry and function of the inferior olive. Trends Neurosci. *21*, 391–400.

128. Vertes, R.P., and Kocsis, B. (1997). Brainstem-diencephalo-septohippocampal systems controlling the theta rhythm of the hippocampus. Neuroscience *81*, 893–926.

129. Allen, C.N., and Crawford, I.L. (1984). GABAergic agents on the medial septal nucleus affect hippocampal theta rhythm and acetylcholine utilization. Brain Res. *322*, 261–267.

130. Torres, F., and Anderson, C. (1985). The normal EEG of the human newborn. J. Clin. Neurophysiol. *2*, 89–103.

131. Vanhatalo, S., and Kaila, K. (2006). Development of neonatal EEG activity: From phenomenology to physiology. Semin. Fetal Neonatal Med. *11*, 471–478.

132. Danglot, L., Triller, A., and Marty, S. (2006). The development of hippocampal interneurons in rodents. Hippocampus *16*, 1032–1060.

133. Bender, R., Plaschke, M., Naumann, T., Wahle, P., and Frotscher, M. (1996). Development of cholinergic and GABAergic neurons in the rat medial septum: Different onset of choline acetyltransferase and glutamate decarboxylase mRNA expression. J. Comp. Neurol. *372*, 204–214.

134. de Lecea, L., del Río, J. a, and Soriano, E. (1995). Developmental expression of parvalbumin mRNA in the cerebral cortex and hippocampus of the rat. Brain Res. Mol. Brain Res. *32*, 1–13.

135. Buzsáki, G., Lai-Wo S., L., and Vanderwolf, C.H. (1983). Cellular bases of hippocampal EEG in the behaving rat. Brain Res. Rev. *6*, 139–171.

136. Amilhon, B., Huh, C.Y.L., Dé, F., Manseau, R., Ducharme, G., Nichol, H., Adamantidis, A., and Williams, S. (2015). Parvalbumin Interneurons of Hippocampus Tune Population Activity at Theta Frequency. Neuron *86*, 1277–1289.

137. Ciranna, L., Licata, F., Li Volsi, G., and Santangelo, F. (2000). Neurotransmitter-mediated control of neuronal firing in the red nucleus of the rat: reciprocal modulation between noradrenaline and GABA. Exp. Neurol. *163*, 253–63.

138. Hontanilla, B., Parent, A., and Giménez-Amaya, J.M. (1995). Heterogeneous distribution of neurons containing calbindin D-28k and/or parvalbumin in the rat red nucleus. Brain Res. *696*, 121–126.

139. Fu, Y. S., Tseng, G. F., Ying, H.-S. (1994). The Postnatal Development of the Gaba a /benzodiazepine Receptor in the Rat Red Nucleus. J. Recept. Res. *14*, 267–280.

140. Ricardo, J.A. (1981). Efferent connections of the subthalamic region in the rat. II. The zona incerta. Brain Res. *214*, 43–60.

141. Staiger, J.F., and Wouterlood, F.G. (1990). Efferent projections from the lateral septal nucleus to the anterior hypothalamus in the rat: A study combining Phaseolus vulgaris-leucoagglutinin tracing with vasopressin immunocytochemistry. Cell Tissue Res. *261*, 17–23.

142. Buzsáki, G. (2006). Rhythms of the Brain. Oxford University Press: Oxford, UK.

143. Bland, B.H. (1986). The physiology and pharmacology of hippocampal formation theta rhythms. Prog. Neurobiol. *26*, 1–54.

144. Robinson, T.E., Kramis, R.C., and Vanderwolf, C.H. (1977). Two types of cerebral activation during active sleep: relations to behavior. Brain Res. *124*, 544–549.

145. Bland, S.K., and Bland, B.H. (1986). Medial septal modulation of hippocampal theta cell discharges. Brain Res. *375*, 102–116.

146. Tiriac, A., and Blumberg, M.S. (2016). The Case of the Disappearing Spindle Burst. Neural Plast. *2016*.

147. Rathelot, J.A., and Padel, Y. (1997). Ascending spinal influences on rubrospinal cells in the cat. Exp. Brain Res. *116*, 326–340.

148. Christian, K.M., and Thompson, R.F. (2003). Neural substrates of eyeblink conditioning: acquisition and retention. Learn. Mem. (Cold Spring Harb. NY) *10*, 427–455.

149. Hoffmann, L.C., and Berry, S.D. (2009). Cerebellar theta oscillations are synchronized during hippocampal theta-contingent trace conditioning. Proc. Natl. Acad. Sci. U. S. A. *106*, 21371–6.

150. Bender, F., Gorbati, M., Cadavieco, M.C., Denisova, N., Gao, X., Holman, C., Korotkova, T., and Ponomarenko, A. (2015). Theta oscillations regulate the speed of locomotion via a hippocampus to lateral septum pathway. Nat. Commun. *6*, 8521.

151. Power, J.D., Fair, D.A., Schlaggar, B.L., and Petersen, S.E. (2010). The Development of Human Functional Brain Networks. Neuron *67*, 735–748.

152. Popa, D., Duvarci, S., Popescu, A.T., Léna, C., and Paré, D. (2010). Coherent amygdalocortical theta promotes fear memory consolidation during paradoxical sleep. Proc. Natl. Acad. Sci. U. S. A. *107*, 6516–9.

153. Boyce, R., Glasgow, S.D., Williams, S., and Adamantidis, A.R. (2016). Causal evidence for the role of REM sleep theta rhythm in contextual memory consolidation. Science. *352*, 812–816.

154. Altman, J., and Sudarshan, K. (1975). Postnatal development of locomotion in the laboratory rat. Anim. Behav. *23*, 896–920.

155. Whitfield-Gabrieli, A.S., Thermenos, H.W., Milanovic, S., Tsuang, M.T., Faraone, S. V, Mccarley, R.W., Shenton, M.E., Green, A.I., Nieto-, A., Laviolette, P., *et al.* (2013). Hyperactivity and hyperconnectivity of the default Hyperactivity in schizophrenia and in first-degree network relatives with schizophrenia of persons. Proc. Natl. Acad. Sci. U. S. A *106*, 1279–1284.

156. Kennedy, D.P., Redcay, E., and Courchesne, E. (2006). Failing to deactivate: resting functional abnormalities in autism. Proc. Natl. Acad. Sci. U. S. A. *103*, 8275–8280.

157. Uddin, L.Q., Kelly, A.M.C., Biswal, B.B., Margulies, D.S., Shehzad, Z., Shaw, D., Ghaffari, M., Rotrosen, J., Adler, L.A., Castellanos, F.X., *et al.* (2008). Network homogeneity reveals decreased integrity of default-mode network in ADHD. J. Neurosci. Methods *169*, 249–254.

158. Vanvuchelen, M., Roeyers, H., and De Weerdt, W. (2007). Nature of motor imitation problems in school-aged boys with autism: a motor or a cognitive problem? Autism *11*, 225–240.

159. Hannant, P., Cassidy, S., Tavassoli, T., and Mann, F. (2016). Sensorimotor difficulties are associated with the severity of autism spectrum conditions. Front. Integr. Neurosci. *10*, 1–14.

160. Wang, S.S.H., Kloth, A.D., and Badura, A. (2014). The Cerebellum, Sensitive Periods, and Autism. Neuron *83*, 518–532.

161. Takarae, Y., Minshew, N.J., Luna, B., and Sweeney, J.A. (2007). Atypical involvement of frontostriatal systems during sensorimotor control in autism. Psychiatry Res. *156*, 117–127.

162. Kikuchi, M., Yoshimura, Y., Hiraishi, H., Munesue, T., Hashimoto, T., Tsubokawa, T., Takahashi, T., Suzuki, M., Higashida, H., and Minabe, Y. (2015). Reduced long-range functional connectivity in young children with autism spectrum disorder. Soc. Cogn. Affect. Neurosci. *10*, 248–254.

163. Hartung, H., Cichon, N., De Feo, V., Riemann, S., Schildt, S., Lindemann, C., Mulert, C., Gogos, J.A., and Hanganu-Opatz, I.L. (2016). From shortage to surge: a developmental switch in hippocampal-prefrontal coupling in a gene-environment model of neuropsychiatric disorders. Cereb. Cortex *26*, 4265–4281.

164. Yang, J.-W., Hanganu-Opatz, I.L., Sun, J.-J., and Luhmann, H.J. (2009). Three patterns of oscillatory activity differentially synchronize developing neocortical networks in vivo. J. Neurosci. *29*, 9011–9025.

165. Vanhatalo, S., and Kaila, K. (2006). Development of neonatal EEG activity: from phenomenology to physiology. Semin. Fetal Neonatal Med. *11*, 471–478.

166. Bitzenhofer, S.H., Ahlbeck, J., Wolff, A., Wiegert, J.S., Gee, C.E., Oertner, T.G., and Hanganu-Opatz, I.L. (2017). Layer-specific optogenetic activation of pyramidal neurons causes beta–gamma entrainment of neonatal networks. Nat. Commun. *8*, 14563.

167. Luhmann, H.J., and Khazipov, R. (2017). Neuronal activity patterns in the developing barrel cortex. Neuroscience *1*, 256-267.

168. Leinekugel, X., Khazipov, R., Cannon, R., Hirase, H., Ben-Ari, Y., and Buzsáki, G. (2002). Correlated bursts of activity in the neonatal hippocampus in vivo. Science *296*, 2049–52.

169. An, S., Kilb, W., and Luhmann, H.J. (2014). Sensory-evoked and spontaneous gamma and spindle bursts in neonatal rat motor cortex. J. Neurosci. *34*, 10870–10883.

170. Buhl, D.L., and Buzsáki, G. (2005). Developmental emergence of hippocampal fast-field “ripple” oscillations in the behaving rat pups. Neuroscience *134*, 1423–1430.

171. Bitzenhofer, S.H., Ahlbeck, J., Wolff, A., Wiegert, J.S., Gee, C.E., Oertner, T.G., and Hanganu-Opatz, I.L. (2017). Layer-specific optogenetic activation of pyramidal neurons causes beta–gamma entrainment of neonatal networks. Nat. Commun. *8*, 14563.

172. Kilb, W., Kirischuk, S., and Luhmann, H.J. (2011). Electrical activity patterns and the functional maturation of the neocortex. Eur. J. Neurosci. *34*, 1677–1686.

173. Lahtinen, H., Palva, J.M., Sumanen, S., Voipio, J., Kaila, K., and Taira, T. (2002). Postnatal development of rat hippocampal gamma rhythm in vivo. J. Neurophysiol. *88*, 1469–1474.

174. Suchkov, D., Sharipzyanova, L., and Minlebaev, M. (2018). Horizontal synchronization of neuronal activity in the barrel cortex of the neonatal rat by spindle-burst oscillations. Front. Cell. Neurosci. *12*, 5.

175. Meier, P., Finch, A., and Evan, G. (2000). Apoptosis in development. Nature *407*, 796–801.

176. Benders, M.J., Palmu, K., Menache, C., Borradori-Tolsa, C., Lazeyras, F., Sizonenko, S., Dubois, J., Vanhatalo, S., and Hüppi, P.S. (2015). Early brain activity relates to subsequent brain growth in premature infants. Cereb. Cortex *25*, 3014–3024.

177. Wikstro, S., Iyer, K.K., Roberts, J.A., Hellstro, L., Pupp, I.H., Ley, D., Vanhatalo, S., and Breakspear, M. (2015). Cortical burst dynamics predict clinical outcome early in extremely preterm infants. Brain, 2206–2218.

178. Diamond, M.E., von Heimendahl, M., Knutsen, P.M., Kleinfeld, D., and Ahissar, E. (2008). “Where” and “what” in the whisker sensorimotor system. Nat. Rev. Neurosci. *9*, 601–612.

179. Erzurumlu, R.S., and Gaspar, P. (2012). Development and critical period plasticity of the barrel cortex. Eur. J. Neurosci. *35*, 1540–53.

180. McVea, D.A., Murphy, T.H., and Mohajerani, M.H. (2016). Large scale cortical functional networks associated with slow-wave and spindle-burst-related spontaneous activity. Front. Neural Circuits *10*.

181. Blanquie, O., Yang, J.-W., Kilb, W., Sharopov, S., Sinning, A., and Luhmann, H.J. (2017). Electrical activity controls area-specific expression of neuronal apoptosis in the developing mouse cerebral cortex. Elife *6*, 1–21.

182. Blumberg, M.S., Coleman, C.M., Sokoloff, G., Weiner, J.A., Fritszch, B., and McMurray, B. (2015). Development of twitching in sleeping infant mice depends on sensory experience. Curr. Biol. *25*, 656–662.

183. Del Rio-Bermudez, C., Kim, J., Sokoloff, G., and Blumberg, M.S. (2017). Myoclonic twitches during active sleep drive coordinated activity in the newborn rat cortico-hippocampal network. In Neuroscience Meeting Planner (Washington, DC: Society for Neuroscience).

184. Hartung, H., Cichon, N., De Feo, V., Riemann, S., Schildt, S., Lindemann, C., Mulert, C., Gogos, J.A., and Hanganu-Opatz, I.L. (2016). From shortage to surge: a developmental switch in hippocampal-prefrontal coupling in a gene-environment model of neuropsychiatric disorders. Cereb. Cortex *26*, 4265–4281.

185. Watanabe, T., Kan, S., Koike, T., Misaki, M., Konishi, S., Miyauchi, S., Miyahsita, Y., and Masuda, N. (2014). Network-dependent modulation of brain activity during sleep. Neuroimage *98*, 1–10.

186. Vijayan, S., Lepage, K.Q., Kopell, N.J., and Cash, S.S. (2017). Frontal beta-theta network during REM sleep. Elife *6*, 1–19.

187. Leveille, C., Barbeau, E.B., Bolduc, C., Limoges, E., Berthiaume, C., Chevrier, E., Mottron, L., and Godbout, R. (2010). Enhanced connectivity between visual cortex and other regions of the brain in autism: A REM sleep EEG coherence study. Autism Res. *3*, 280–285.

188. Daoust, A.M., Limoges, É., Bolduc, C., Mottron, L., and Godbout, R. (2004). EEG spectral analysis of wakefulness and REM sleep in high functioning autistic spectrum disorders. Clin. Neurophysiol. *115*, 1368–1373.

189. Kurth, S., Riedner, B.A., Dean, D.C., Muircheartaigh, J.O., Huber, R., Jenni, O.G., Deoni, S.C.L., and Lebourgeois, M.K. Traveling slow oscillations during sleep : a marker of brain connectivity in childhood. 10–12.

190. Li, W., Ma, L., Yang, G., and Gan, W.-B. (2017). REM sleep selectively prunes and maintains new synapses in development and learning. Nat. Neurosci. *20*, 427-437

191. Sei, H., Saitoh, D., Yamamoto, K., Morita, K., and Morita, Y. (2000). Differential effect of short-term REM sleep deprivation on NGF and BDNF protein levels in the rat brain. Brain Res. *877*, 387–390.

192. Picchioni, D., Reith, R., Nadel, J., and Smith, C. (2014). Sleep, plasticity and the pathophysiology of neurodevelopmental disorders: the potential roles of protein synthesis and other cellular processes. Brain Sci. *4*, 150–201.

193. Bitzenhofer, S.H., Ahlbeck, J., and Hanganu-Opatz, I.L. (2017). Methodological approach for optogenetic manipulation of neonatal neuronal networks. Front. Cell. Neurosci. *11*, 1–13.

194. Murata, Y., and Colonnese, M.T. (2016). An excitatory cortical feedback loop gates retinal wave transmission in rodent thalamus. Elife *5*.

195. Milh, M., Kaminska, A., Huon, C., Lapillonne, A., Ben-Ari, Y., and Khazipov, R. (2007). Rapid cortical oscillations and early motor activity in premature human neonate. Cereb. Cortex *17*, 1582–1594.

196. An, S., Kilb, W., and Luhmann, H.J. (2014). Sensory-evoked and spontaneous gamma and spindle bursts in neonatal rat motor cortex. J. Neurosci. *34*, 10870–10883.

197. Del Rio-Bermudez, C., and Blumberg, M.S. (2018). Active sleep promotes functional connectivity in developing sensorimotor networks. BioEssays *40*, 1700234

198. McVea, D.A., Mohajerani, M.H., and Murphy, T.H. (2012). Voltage-sensitive dye imaging reveals dynamic spatiotemporal properties of cortical activity after spontaneous muscle twitches in the newborn Rat. J. Neurosci. *32*, 10982–10994.

199. Seelke, A.M.H., Dooley, J.C., and Krubitzer, L.A. (2012). The emergence of somatotopic maps of the body in s1 in rats: The correspondence between functional and anatomical organization. PLoS One *7*.

200. Singer, W. (1993). Synchronization of cortical activity and its putative role in information processing and learning. Annu. Rev. Physiol. *55*, 349–374.

201. Preston, A.R., and Eichenbaum, H. (2013). Interplay of hippocampus and prefrontal cortex in memory. Curr. Biol. *23:* R764–R773.

202. Whitlock, J.R., Sutherland, R.J., Witter, M.P., Moser, M.-B., and Moser, E.I. (2008). Navigating from hippocampus to parietal cortex. Proc. Natl. Acad. Sci. *105*, 14755–14762.

203. Chiba, A.A., Kesner, R.P., and Reynolds, A.M. (1994). Memory for spatial location as a function of temporal lag in rats: role of hippocampus and medial prefrontal cortex. Behav Neural Biol *61*, 123–131.

204. Chersi, F., and Burgess, N. (2015). The cognitive architecture of spatial navigation: hippocampal and striatal contributions. Neuron *88*, 64–77.

205. Sofroniew, N.J., Vlasov, Y.A., Hires, S.A., Freeman, J., and Svoboda, K. (2015). Neural coding in barrel cortex during whisker-guided locomotion. Elife *4*.

206. Pereira, A., Ribeiro, S., Wiest, M., Moore, L.C., Pantoja, J., Lin, S.-C., and Nicolelis, M.A.L. (2007). Processing of tactile information by the hippocampus. Proc. Natl. Acad. Sci. *104*, 18286–18291.

207. Bellistri, E., Aguilar, J., Brotons-Mas, J.R., Foffani, G., and De la Prida, L.M. (2013). Basic properties of somatosensory-evoked responses in the dorsal hippocampus of the rat. J. Physiol. *591*, 2667–2686.

208. Hamada, Y., Miyashita, E., and Tanaka, H. (1999). Gamma-band oscillations in the “barrel cortex” precede rat’s exploratory whisking. Neuroscience *88*, 667–671.

209. Itskov, P.M., Vinnik, E., and Diamond, M.E. (2011). Hippocampal representation of touch-guided behavior in rats: Persistent and independent traces of stimulus and reward location. PLoS One *6*.

210. Berke, J.D., Hetrick, V., Breck, J., and Greene, R.W. (2008). Transient 23-30 Hz oscillations in mouse hippocampus during exploration of novel environments. Hippocampus *18*, 519–529.

211. França, A.S.C., do Nascimento, G.C., Lopes-dos-Santos, V., Muratori, L., Ribeiro, S., Lobão-Soares, B., and Tort, A.B.L. (2014). Beta2 oscillations (23-30 Hz) in the mouse hippocampus during novel object recognition. Eur. J. Neurosci. *40*, 3693–3703.

212. Lansink, C.S., Meijer, G.T., Lankelma, J. V., Vinck, M.A., Jackson, J.C., and Pennartz, C.M.A. (2016). Reward expectancy strengthens ca1 theta and beta band synchronization and hippocampal-ventral striatal coupling. J. Neurosci. *36*, 10598–10610.

213. Igarashi, K.M., Lu, L., Colgin, L.L., Moser, M.B., and Moser, E.I. (2014). Coordination of entorhinal-hippocampal ensemble activity during associative learning. Nature *510*, 143–147.

214. Marrosu, F., Portas, C., Mascia, M.S., Casu, M.A., Fà, M., Giagheddu, M., Imperato, A., and Gessa, G.L. (1995). Microdialysis measurement of cortical and hippocampal acetylcholine release during sleep-wake cycle in freely moving cats. Brain Res. *671*, 329–332.

215. Dudar, J.D., Whishaw, I.Q., and Szerb, J.C. (1979). Release of acetylcholine from the hippocampus of freely moving rats during sensory stimulation and running. Neuropharmacology *18*, 673–678.

216. Picciotto, M.R., Higley, M.J., and Mineur, Y.S. (2012). Acetylcholine as a neuromodulator: cholinergic signaling shapes nervous system function and behavior. Neuron *76*, 116–129.

217. McKay, B.E., Placzek, A.N., and Dani, J.A. (2007). Regulation of synaptic transmission and plasticity by neuronal nicotinic acetylcholine receptors. Biochem. Pharmacol. *74*, 1120–1133.

218. Colgin, L.L., Kubota, D., and Lynch, G. (2003). Cholinergic plasticity in the hippocampus. Proc. Natl. Acad. Sci. U. S. A. *100*, 2872–7.

219. Chen, G., Rasch, M.J., Wang, R., and Zhang, X.H. (2015). Experience-dependent emergence of beta and gamma band oscillations in the primary visual cortex during the critical period. Sci. Rep. *5*.

220. Shimono, K., Brucher, F., Granger, R., Lynch, G., and Taketani, M. (2000). Origins and distribution of cholinergically induced beta rhythms in hippocampal slices. J. Neurosci. *20*, 8462–8473.